Effect of the Morin transition on the Seebeck coefficient in single crystals of doped hematite
by Roger Irvin Staab

A thesis submitted to the Graduate Faculty in partial fulfillment of the requirements for the degree of
DOCTOR OF PHILOSOPHY in Electrical Engineering
Montana State University
© Copyright by Roger Irvin Staab (1971)

Abstract:
The Seebeck coefficient was measured in single crystals of Mg- and Ti-doped hematite in the temperature range 215-300°K, with samples oriented along the [111] direction and in the (111) plane. The following observations were made: 1) The orientation dependence of the Seebeck coefficient at TM for the Mg-doped samples is consistent with double exchange, which involves thermally activated hopping between lattice sites. For Ti-doped samples, there is an anomalous effect for transport within the (111) plane which is explained by a contribution due to impurity conduction superimposed on the normal double-exchange results.

2) A dependence of the magnitude of the Seebeck coefficient on sample length is seen, which is not predicted unless phonon drag is introduced. Phonon drag also provides an explanation for the observed slopes in the Seebeck data, where the magnitude increased for decreasing temperature in the Ti-doped samples but decreased with decreasing temperature for the Mg-doped samples.

3) A memory effect is observed in which the change in the Seebeck coefficient at TM for transport in the [111] direction is altered by an applied magnetic field (~1500 gauss), and this altered form is repeated after the magnetic field is removed. This is attributed to a domain structure above TM where the weak ferromagnetic moment exists in hematite.

EFFECT OF THE MORIN TRANSITION ON THE SEEBECK COEFFICIENT IN SINGLE CRYSTALS OF DOPED HEMATITE

by

ROGER IRVIN STAAB

A thesis submitted to the Graduate Faculty in partial fulfillment of the requirements for the degree

of

DOCTOR OF PHILOSOPHY

in

Electrical Engineering

Approved:

Head, Major Department

Chairman, Examining Committee

Graduate Dean

MONTANA STATE UNIVERSITY
Bozeman, Montana

June, 1971

ACKNOWLEDGMENTS

I would like to express my sincere appreciation to my advisor, Dr. John Hanton, for originally suggesting the problem, and for his helpful comments on the methods and presentation.

I am indebted to Dr. John Hermanson for his many helpful discussions on the aspects of solid state theory. My fellow graduate students, Mr. Robert Parker and Mr. Don Worsencroft, offered very beneficial assistance through discussions and suggestions. In addition, my gratitude is expressed to Dr. Calvin Ransom for providing the single crystals from which the samples were obtained for this work.

I would also like to thank the National Aeronautics and Space Administration for making a three-year fellowship available to me.

A special thanks is conveyed to my wife, Charlotte, who provided the needed moral support throughout my graduate work.

TABLE OF CONTENTS

Chapter		Page
	Preface	x
I	INTRODUCTION	1
	A. Crystal Structure	1
	B. Magnetic Structure	1
	C. Basic Electrical Properties	8
	D. Possible Conduction Mechanisms	9
II	THEORETICAL ASPECTS	17
	A. Band Theory	17
	B. Narrow Bands: The Polaron	21
	1. Large polarons	23
	2. Large-polaron transport	24
	a. Boltzmann equation: weak coupling ($\alpha < 1$)	24
	b. Boltzmann equation: strong coupling ($\alpha > > 1$)	26
	c. Density matrix	26
	d. Seebeck coefficient	27
	3. Large versus small polarons	27
	4. Small polarons	29
	5. Small-polaron transport	35
	a. Hopping mobility	35
	b. Band mobility	38
	c. Methods other than the Boltzmann equation	38
	d. Seebeck coefficient	39
	6. Estimate for T_t	44
	C. Impurity Conduction	46
	D. Effect of Magnetic Order	49
	1. Effect on hopping probability	50
	2. Double exchange in hematite	51

Chapter		Page
III	THE EXPERIMENT	56
IV	THE EXPERIMENTAL RESULTS	64
	A. Presentation of the Results	64
	B. Discussion of the Results	82
V	CONCLUSIONS	111
	APPENDIX I	115
	APPENDIX II	120
	BIBLIOGRAPHY	125

LIST OF FIGURES

Figure		Page
1	Crystal Structure of α-Fe_2O_3	2
2	Magnetic Structure of α-Fe_2O_3	3
3	Two-Sublattice Model for Magnetization in Hematite	4
4	Approximate Energy Band Scheme for α-Fe_2O_3	11
5	Shape and Orientations of the Two Samples	57
6	Construction of the Heat Blocks	58
7	Circuit for Measuring Seebeck Voltage	62
8	Thermocouple Circuit for Measuring Ambient Temperature and Temperature Difference	62
9	Seebeck Coefficient versus 1/T for Mg-Doped Sample Along [111] Direction	66
10	Seebeck Coefficient versus 1/T for Mg-Doped Sample in (111) Plane	67
11	Seebeck Coefficient versus 1/T for Ti-Doped Sample Along [111] Direction	68
12	Seebeck Coefficient versus 1/T for Ti-Doped Sample in (111) Plane	69
13	Seebeck Coefficient versus 1/T for Fresh Mg-Doped Sample Along [111] Direction	71
14	Seebeck Coefficient versus 1/T for Fresh Mg-Doped Sample in (111) Plane	72
15	Seebeck Coefficient versus 1/T for Fresh Ti-Doped Sample in (111) Plane	73

Figure		Page
16	Mg-Doped Sample Along [111] Direction with Applied Magnetic Field	76
17	Mg-Doped Sample Along [111] Direction after Removal of Applied Magnetic Field	77
18	Mg-Doped Sample Along [111] Direction after Removal of Applied Reverse Magnetic Field	78
19	Ti-Doped Sample in (111) Plane Before and After Applying and Removing Magnetic Field	80
20	Ti-Doped Sample Along [111] Direction with Applied Magnetic Field	81
21	Mg-Doped Sample in (111) Plane with Applied Magnetic Field	83
22	Mg-Doped Sample Along [111] Direction after Heating to T_N	84
23	Mg-Doped Sample in (111) Plane after Heating to T_N	85
24	Ti-Doped Sample Along [111] Direction after Heating to T_N	86
25	Ti-Doped Sample in (111) Plane after Heating to T_N	87
26	Iron Placement and Spin Structure for $T < T_M$	93
27	Iron Placement and Spin Structure for $T > T_M$	94
28	Two Types of 180-Degree Domain Walls	107

Figure Page

A-1 122

A-2 122

A-3 123

A-4 123

A-5 124

A-6 124

ABSTRACT

The Seebeck coefficient was measured in single crystals of Mg- and Ti-doped hematite in the temperature range 215-300°K, with samples oriented along the [111] direction and in the (111) plane. The following observations were made:

1) The orientation dependence of the Seebeck coefficient at T_M for the Mg-doped samples is consistent with double exchange, which involves thermally activated hopping between lattice sites. For Ti-doped samples, there is an anomalous effect for transport within the (111) plane which is explained by a contribution due to impurity conduction superimposed on the normal double-exchange results.

2) A dependence of the magnitude of the Seebeck coefficient on sample length is seen, which is not predicted unless phonon drag is introduced. Phonon drag also provides an explanation for the observed slopes in the Seebeck data, where the magnitude increased for decreasing temperature in the Ti-doped samples but decreased with decreasing temperature for the Mg-doped samples.

3) A memory effect is observed in which the change in the Seebeck coefficient at T_M for transport in the [111] direction is altered by an applied magnetic field ($\sim$1500 gauss), and this altered form is repeated after the magnetic field is removed. This is attributed to a domain structure above T_M where the weak ferromagnetic moment exists in hematite.

PREFACE

A problem which has generated considerable interest is understanding the transport mechanism in oxides of the 3-d transition metals. Since the 3-d band in these materials is only partially filled, metallic properties would be expected. Instead, in pure samples, these materials appear to be insulators, and under non-stoichiometric conditions, they become semiconductors. There has also been observed an anomalous Hall effect in these materials.

In attempting to explain these effects, much of the attention has been focused on nickel oxide (NiO), along with a little work on the alpha phase of iron oxide or hematite (α-Fe_2O_3). Since these and other 3-d oxides are antiferromagnetic, some researchers have speculated that the magnetic state may be a strong influencing factor on the transport processes, but this idea has been touched upon only lightly in previous research. In this regard, hematite is interesting because it undergoes a low-temperature magnetic phase transition in which the sublattice magnetization orientations change. Thus, a study of the transport properties around this phase transition could lead to a better understanding of the effect of the magnetic state on charge transport.

Previous research has also led to a disagreement between proponents of two different conduction models, the hopping model and the

band model. There is general agreement that at sufficiently low temperatures, transport is governed by impurity conduction, but there is disagreement over the higher-temperature region. Also, most of the previous research (especially that on hematite) has been done on polycrystalline samples in which grain-boundary effects are significant at temperatures near and below room temperature, so even the low-temperature conclusions are at times speculative.

This dissertation discusses measurements of the Seebeck coefficient in single crystals of doped hematite in an attempt to understand the transport mechanism. The crystals were synthetically grown so that the concentration and types of impurities were controlled, and, because they were single crystals, grain-boundary effects were not a problem. Crystal dopings were chosen to provide data on both n- and p-type impurities. The Seebeck effect was studied because it results from a temperature gradient applied across the sample, and no external magnetic fields are necessary (as in the Hall effect). This leaves the magnetic state of the sample undisturbed except for thermal fluctuations.

The historical background of the problem is given in the introductory chapter. Important aspects of the pertinent theoretical developments are presented in more detail in Chapter II.

Chapter III is devoted to the methods used to obtain the experimental results, and these results are presented and discussed in Chapter IV.

Finally, conclusions of this work are presented in Chapter V.

CHAPTER I

INTRODUCTION

A. Crystal Structure

Hematite (α-Fe_2O_3) crystallizes in the trigonal structure (space group D_{3d}^6) with a rhombohedral unit cell containing two molecules and thus four iron atoms.[1] There are six oxygen atoms around each iron atom and four iron atoms around each oxygen. The iron and oxygen atoms go into alternating layers perpendicular to the trigonal axis, with the iron atoms lying along this axis. Figure 1 gives a schematic representation of the iron and oxygen placement in the crystal structure.

B. Magnetic Structure

Hematite is antiferromagnetic with a Néel temperature $T_N \simeq 675°C$.[2] The relative orientation of the four magnetic ions in the unit cell is +--+ along the trigonal axis (figure 2). If the model of alternating layers of iron and oxygen ions is adopted, then each neighboring pair of cation sublattices is coupled antiferromagnetically (figure 3).[3]

A macroscopic understanding of antiferromagnetism can be obtained from the concept of the Weiss molecular field. It is assumed that the field seen by an ion at a site in sublattice A is

$$\bar{H}_{MA} = -N_{AA}\bar{M}_A - N_{AB}\bar{M}_B \quad ,$$

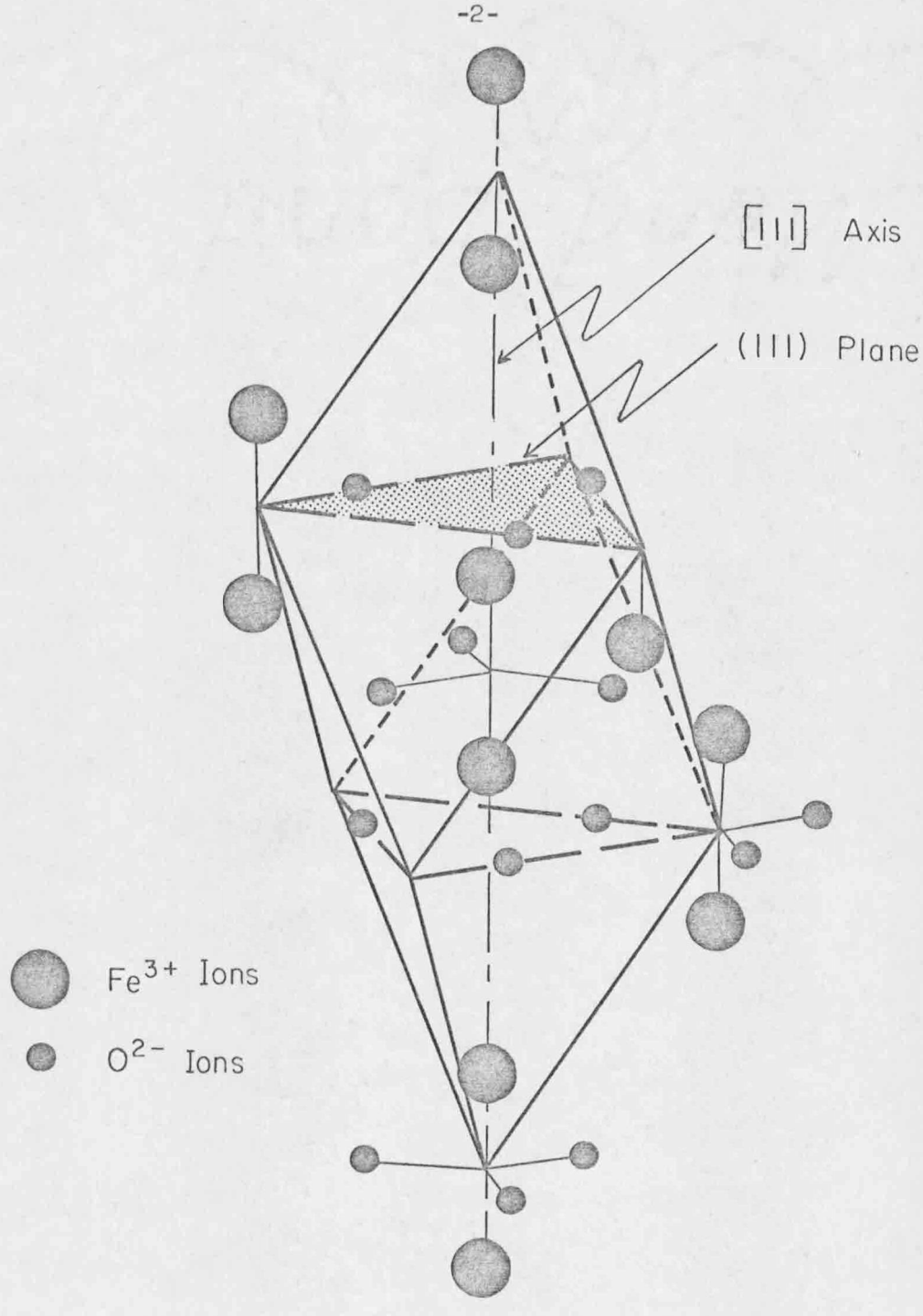


Figure 1. Crystal Structure of α-Fe_2O_3.

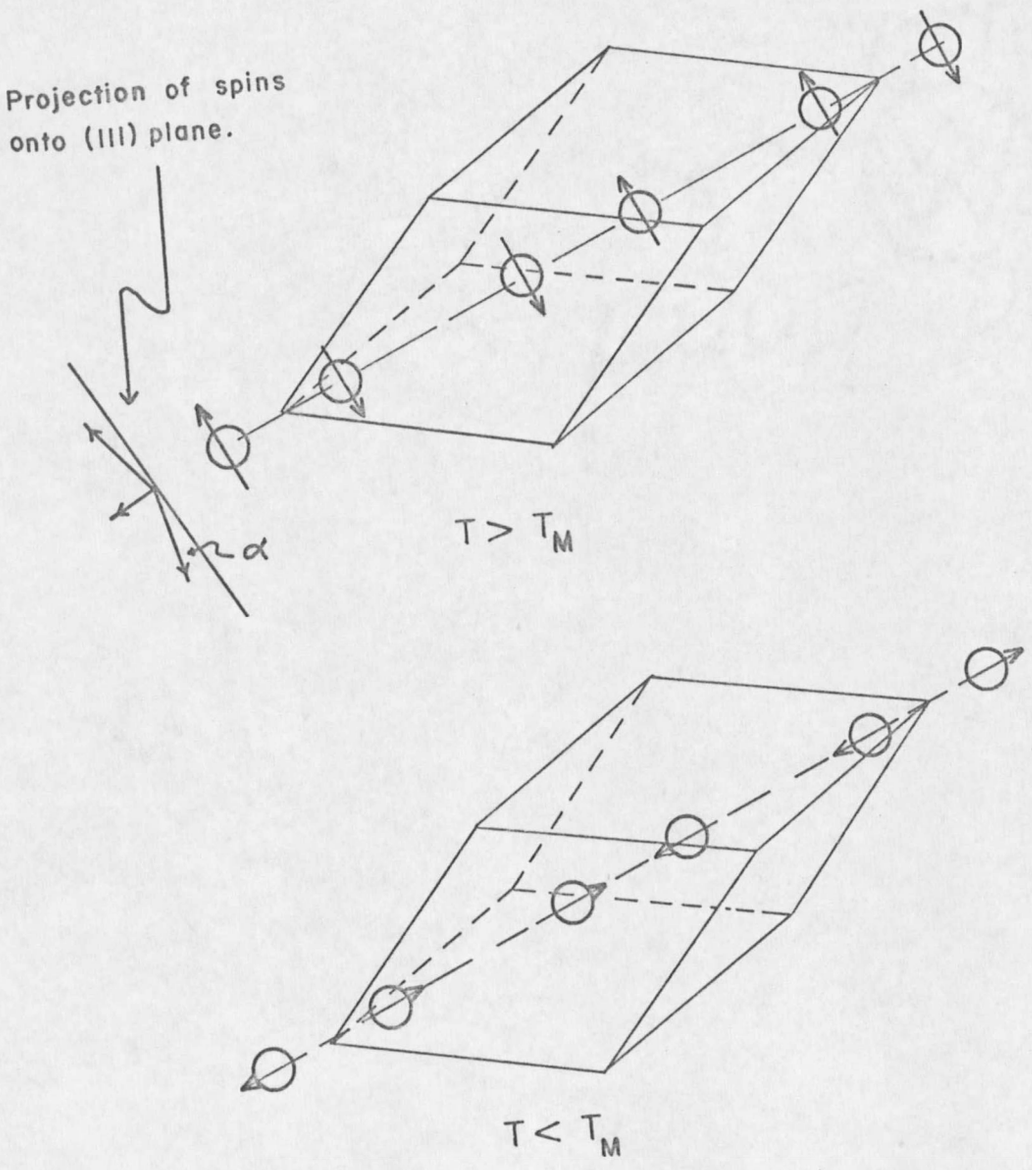


Figure 2. Magnetic Structure of α-Fe_2O_3. Arrows represent magnetization directions of iron ions.

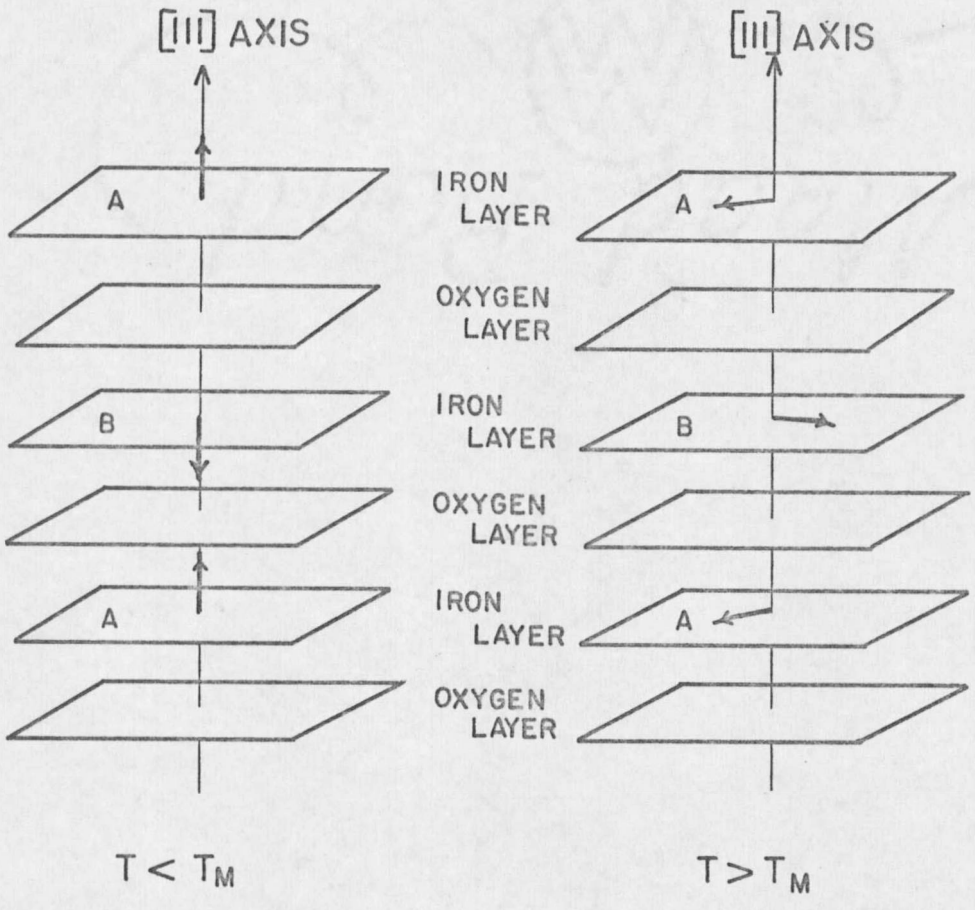
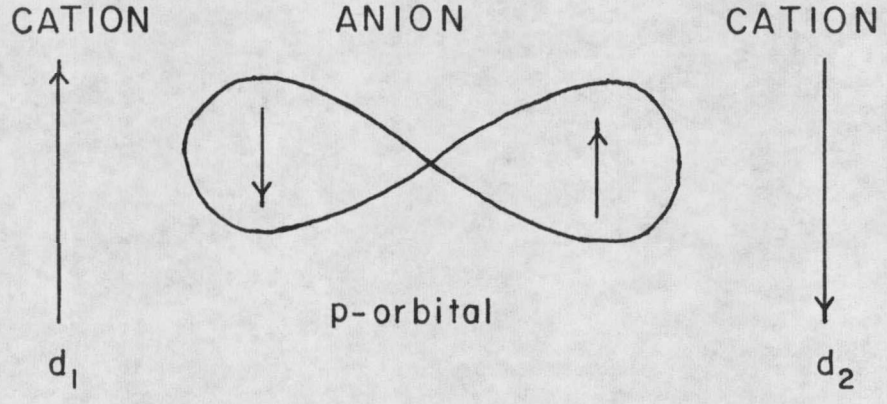


Figure 3. Two-Sublattice Model for Magnetization in Hematite.

where $\bar{M}_A$ and $\bar{M}_B$ are the sublattice magnetizations. N_{AB} would be positive for antiferromagnetic nearest-neighbor interactions. N_{AA} is the constant for intra-sublattice interactions due to exchange.

It is difficult to imagine a direct exchange interaction taking place over the large distances due to the intermediate oxygen layer in hematite. Thus, for a microscopic description, Anderson[4] developed a model for superexchange in which the extent of the d-orbitals of the iron ions is effectively lengthened by intermediate interactions with the p-orbitals of the oxygen ions. This model results in antiferromagnetic coupling of neighboring cations, but no net transfer of charge. Since the exchange takes place through the intermediate p-orbitals, the interaction is strongest for 180 degree coupling, where iron 3d-orbitals are located at opposite extremities of the dumbbell-shaped p-orbital.



In addition to the high temperature transition (T_N) to paramagnetism, a low temperature transition known as the Morin transition [5] (T_M) has been observed at which the orientation of the antiferromagnetic sublattice magnetizations shifts direction. Above T_M, the magnetization is in the basal (111) plane and a weak ferromagnetic moment is also observed in this plane. Below T_M, the sublattice magnetizations are along the trigonal $\left[111\right]$ axis and cancel.

In early studies, a weak ferromagnetic moment was observed both above and below the Morin transition. Many studies have been made in an attempt to explain its origin. Néel[6] attributed it to a defect in stoichiometry. Li[7] and Jacobs and Bean [8] felt it was due to unbalanced domain walls. It was later determined that the weak moment below T_M was due to impurities, since the moment did not appear in synthetic crystals in which the impurities were controlled. [9] For the remaining moment above T_M, Dzialoshinski offered an explanation based on thermodynamic and symmetry arguments.[10] The theory allows a term of the form

$$\bar{D} \cdot (\bar{S}_1 \times \bar{S}_2)$$

to appear, where $\bar{S}_1$ and $\bar{S}_2$ are the spins in the two sublattices and $\bar{D}$ is a constant vector which is parallel to the trigonal axis in hematite. Below T_M, even if the spins in the two sublattices were

not antiparallel, the cross product $\bar{S}_1 \times \bar{S}_2$ would yield a vector perpendicular to $\bar{D}$ and the dot product would be zero. Above T_M, the cross product yields a vector parallel to $\bar{D}$, and the magnitude of the vector is $|\bar{S}_1||\bar{S}_2| \sin \theta_{12}$. Thus, the dot product is non-zero if the spins are slightly canted. If the term is negative, the energy is reduced if canting is present. However, $\bar{D}$ cannot be calculated from this theory. Moriya[11] was able to explain the canted spin arrangement by considering the effect of anisotropic superexchange including an explicit treatment of spin-orbit coupling. He recognized that the term $\bar{D} \cdot (\bar{S}_1 \times \bar{S}_2)$ had the form of an antisymmetric term of a general expression for spin-spin interaction (note that interchanging $\bar{S}_1$ and $\bar{S}_2$ changes the sign of the term). Upon including spin-orbit coupling in Anderson's[4] superexchange theory, he found the basis functions were no longer eigenfunctions of S_Z, but now they were mixtures of spin-up and spin-down states. His result for the energy of the system included the former isotropic superexchange and dipolar interaction terms, plus a term of the form $\bar{D} \cdot (\bar{S}_1 \times \bar{S}_2)$.

Thus, it appears that hematite is antiferromagnetic with the spins slightly canted from antiparallel orientation in the basal plane above the Morin transition. The temperature at which this transition takes place can be depressed by doping the crystal,

[5,12,13,14] but only rhodium doping has raised it.[15] In a pure sample, $T_M \simeq -10°C$.[16]

One magnetic structure factor which is still a point of question is the basal plane anisotropy. The trigonal structure would indicate a three-fold symmetry but some researchers have not observed this in synthetic single crystals[17,18] while others have observed a six-fold anisotropy when conducting magnetic resonance studies.[19, 20,21]

C. Basic Electrical Properties

Hematite is generally considered to be an oxide semiconductor in which carriers arise because of oxygen deficiency, resulting in Fe^{2+} ions.[22] Morin[23] was one of the first researchers to report the findings of a study of electrical properties, in which he investigated polycrystalline samples with stoichiometric deviations and titanium impurities. His results indicated semiconductor behavior.

In a later paper, Morin[24] reported the following results on pure and titanium-doped samples:

1) no normal Hall effect was seen,

2) intrinsic samples could be made n- or p-type without changing conductivity (σ),

3) unusually low values of mobility (μ) were found by applying band theory expressions to experimental results,

4) impurity concentration from electrical results strongly disagreed with chemical analysis.

Basically, his explanation was to postulate a "hopping" conduction in the narrow 3d band. This will be considered further in part D of this chapter.

Gardner, et.al.[25,22] studied the effect of doping on conductivity and carrier sign in polycrystalline samples. They found that the doped samples showed a linear $\log_{10} \sigma$ versus T curve. The pure samples showed three distinct activation regions: $T < 450°C$, $450°C < T < 800°C$, $T > 800°C$. This was explained by postulating that carriers arise by oxygen loss at high temperature and by intrinsic electron transitions resulting in 2p holes. In studying carrier sign, it was found that Mg or Ni doping led to p-type samples while Mn or Cr doping led to n-type samples. This can be understood by looking at the normal valence states of these ions. Iron in hematite has a normal valence of +3. Mg and Ni are ordinarily +2, while Mn is +7 and Cr is +6. Thus, substitution of Mg for Fe results in an electron deficiency in the bonding, while Cr or Mn result in electron excesses.

D. Possible Conduction Mechanisms

To understand what mechanisms are available for the conduction process in hematite, one must first look at the electronic states

for this crystal. A characteristic of hematite as well as other transition metal oxides is a partially filled 3d band, but apparently the 3d states do not show appreciable overlap in the wide spacing of the oxide compound, resulting in either a narrow band or isolated levels. In addition, there is a filled 2p band due to the oxygen ions and an empty 4s band of the iron ions. Finally, there are the impurity states (donors or acceptors) due to doping. An approximate energy-band diagram is given in figure 4.

In order to get charge transport in the 3d levels, one of two types of motion is likely: hopping or polaron motion. Both involve localization of a carrier with the main differences being the degree of localization and the localization mechanism. In the hopping model, the carrier is localized at its host ion and must overcome an activation barrier to move to a neighboring ion. In the polaron model, the carrier is localized by a polarization cloud set up around the carrier by its charge.[56] In order for it to move, the carrier must drag this polarization cloud with it. Only in the case of extremely localized polarons do these two models appear the same. Hopping motion involves thermal fluctuations of the lattic potential with an associated activation energy, while polaron motion results from a finite probability that the particle can exist beyond the potential barrier.[26] This distinction is confusing at times in the literature and will be discussed more in Chapter II.

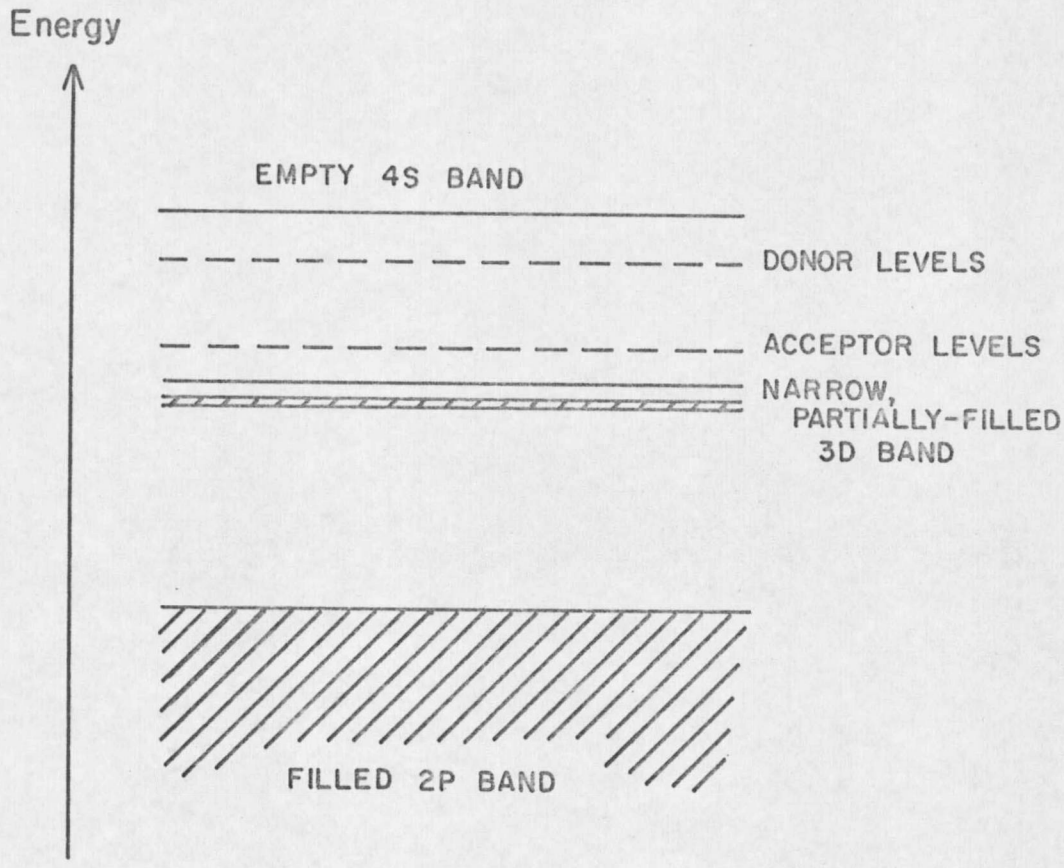


Figure 4. Approximate Energy Band Scheme for α-Fe_2O_3. The placements of the 3d levels and of the acceptor and donor levels are for schematic purposes only. Dashes represent localized or nearly localized levels.

Early experimental results supporting the hopping picture were reported by Morin.[23,24] With this model he was able to explain the low mobilities and apparent activation energies which he had observed. This was also supported by Gardner, et.al.[25] and by Heikes and Johnston.[27]

The absence of a normal Hall voltage reported by Morin[24] also supported a hopping model,[28] but more recent researchers have reported seeing an anomalous Hall voltage.[29,30] A trend away from the hopping model began to appear in the reporting of results (mainly on NiO). Bosman and Crevecoeur[29] found a mobility with no activation energy, and they were able to explain the temperature dependence of the conductivity in terms of the variation of carrier concentrations with temperature. Van Daal and Bosman[30] felt that the anomalous Hall results could be explained by a normal contribution plus an interaction with the magnetization induced in the sample due to the applied field. Their low-temperature results for Hall mobility questioned the validity of applying the small polaron model. The Hall mobility showed a decrease with increasing temperature. However, Austin et.al.[31] concluded that the magnitude and temperature dependence of the mobility suggested small-polaron motion rather than hopping. Their results were explained in terms of polaron conduction in the 3d levels and inter-acceptor hopping in the im-

purity states. Aiken and Jordan[32] found evidence for small-polaron hopping between acceptors. Finally, Acket and Volger[33] observed an apparent magnetostriction in α-Fe_2O_3 which would result in distortion of the lattice as temperature was varied. If hopping was present, then the lattice distortion should have caused a change in the activation energy, but this was not seen. Also, no anisotropy in the conductivity was seen, but hopping transport in magnetically ordered lattices requires particular relations between the initial and final ionic spin states (see Chapter II.D), which would seemingly produce an anisotropy.

In contrast with these results, Firsov[34] found theoretically that Hall mobility and drift mobility could differ significantly for certain temperatures, with a possible increase in Hall mobility at high temperatures. He felt there was not enough experimental evidence to rule out small-polaron motion. Emin and Holstein[35] treated the Hall effect adiabatically, resulting in the former expression for drift mobility but a change in the Hall mobility, allowing a decreasing function of temperature. (The essential meaning of the term adiabatic as used here is that the condition $J > \hbar\omega_o$ is satisfied, where J is the exchange integral. Equivalently, $1/\omega_o > \hbar/J$, where $1/\omega_o$ is related to the relaxation time of the ionic motion and $\hbar/J$ is the time required for the ad-

justment of the electronic wave function to the ionic displacement.)[26] Their conclusion was that small-polaron motion does not require an activated Hall mobility. Bransky and Tallan[36] have recently found evidence of an activation energy in the mobility in NiO, and they conclude that thermally-activated hopping fits their results. Hopping is still seen in low-temperature impurity conduction (as mentioned in the preceding paragraph), but its effect is believed to be pronounced below ~ 140°K in NiO[29] and ~ 200°K in α-Fe_2O_3.[37] Impurity conduction is discussed further in Chapter II.C.

What is the source of these discrepancies? One possibility is the state of the theories themselves. The band structure of the crystal could be determined by the electrical properties if the transport mechanism was known. The band structure has been calculated for NiO using an approximation method,[38,39] which is also the case in the development of the polaron theory. Thus, the basic equations and quantities of the two theories are in doubt.

Another defect in previous research has been the use of polycrystalline samples in which grain boundaries can significantly affect the results. Some researchers have claimed the elimination of grain boundary effects[40] while other authors feel that all previous data which were not taken on single crystals should be set aside as questionable.[28]

Another problem is possible misuse of band theory equations on localized problems. Frohlich[41] stated that many transport formulae break down under conditions of localization and lead to an extremely small mean free path. Platzman[42] pointed out that the Boltzmann equation generally holds for weak coupling to phonons. He has used a density-matrix approach for polaron transport. Efros[43] has studied the relations between the kinetic coefficients in low mobility semiconductors and has derived thermoelectric relations from small-polaron considerations.

It is quite likely that a mixture of transport mechanisms is the real situation, in which case it would be difficult to find the correct combination of models which would explain the anomalous results obtained to date.

Until now, a possibly very important factor has been completely ignored--these are magnetic crystals. The effect of the magnetic state on electrical properties has been briefly mentioned[30] with regard to experimental results, but has received very few detailed discussions.[26,28,44] Methfessel and Mattis[28] state that "the very existence of magnetism in a solid is tantamount to the breakdown of the conventional electron energy-band picture." The reasoning is that band pictures are generally built on one electron approximations in which electron-electron interactions

have been ignored, while electron-electron spin interactions are fundamental to magnetic ordering.

In a doctoral thesis, Ransom[44] attempted to relate the magnetic state to the electrical properties (specifically the Hall effect) of Mg-doped hematite single crystals. His results pointed to an orientation dependence of the electrical properties which could be explained by introducing Zener's double exchange.[45] Since double exchange depends on the ability of the carrier to localize itself at an ionic site and interact with the ion's spin, Ransom chose the hopping model. This was also based on the appearance of an activation energy for the mobility.

CHAPTER II

THEORETICAL ASPECTS

A. Band Theory[46]

To look at the electronic properties of a solid, one generally looks at its band structure. The bands of allowed energy result from the overlap of isolated atomic wave functions when the atoms are brought close together in a crystal structure. The degree of overlap determines the "width" of the band or the number of allowed states. Thus, band structure is a property of all solids, but the width of the bands may vary considerably from one solid to another.

The theoretical derivation of the band structure for a given solid is quite complicated, and so many simplifying models have been developed. One of the most commonly used models is the nearly-free-electron model, so named because one electron is considered moving in a background potential composed of effects from the lattice and from other electrons. Other effects, such as spin-spin interactions, are ignored or treated as small perturbations. The usual Hamiltonian for this type of system is made up of the lattice Hamiltonian and the Hamiltonian for the electron moving in a periodic potential, plus small perturbing terms.

Another approach is the so-called tight-binding approximation (see Appendix I), in which one builds the system on the basis of the

wave functions for the purely atomic case. This method is particularly effective if the carriers are nearly isolated around individual ions and thus are not free. The total wave function is a sum of atomic wave functions located on the individual ions, and the resulting function must be a solution of the Schroedinger equation for the crystal. Again, only a background potential due to the lattice is seen, and spin-spin interactions are ignored.

The model naturally becomes more cumbersome when interaction terms become large because the perturbation method is no longer appropriate. As the particle undergoes interactions such as collisions with lattice phonons, its motion is disturbed from the normal free-particle motion. This is accounted for by assigning an effective mass to the particle. Thus, as the interactions become stronger, the particle begins to look heavier or lighter, depending on whether the interactions tend to increase or decrease the bandwidth. This mass can be defined as

$$\frac{1}{m^*_{ij}} = \frac{1}{\hbar^2} \frac{d^2 E_k}{dk_i dk_j} \quad ,$$

where $\hbar$ is Planck's constant, k_i and k_j are the wave vectors in the i^{th} and j^{th} directions, E_k is the energy as a function of k, and m^*_{ij} is an element of the effective mass tensor, which denotes that the

effective mass can differ for different crystallographic directions.

An important development in analyzing electronic properties of solids has been the formulation of the Boltzmann transport equation. It has a statistical basis and the usual solution relies on the definition of a relaxation time between collisions. Once the equation has been set up, its solution yields a distribution function, $f(\bar{k}, \bar{r}, t)$, where $\bar{k}$ is the wave vector for the distribution, which describes the assembly of conducting particles, $\bar{r}$ is the position vector, and t is time. This distribution function can then be used to determine the electronic properties of a solid.[47] It is from this basis that many existing transport coefficients have been evaluated.

One approach to solving the Boltzmann equation is the relaxation time approximation in which it is assumed that

$$-\left.\frac{\partial f}{\partial t}\right|_{\text{collisions}} = \frac{f - f_o}{\tau} ,$$

where f and f_o are the nonequilibrium and equilibrium distribution functions, respectively. When the relaxation time (τ) has been defined, the mobility can be found from the expression

$$\mu = \frac{e}{m^*} \langle \tau \rangle$$

where $\langle\ \rangle$ denotes the statistical average, and μ, e, and m^* are the mobility, electronic charge, and effective mass, respectively.

An important result of charge transport is seen if a temperature gradient is set up across a sample. A net drift of charge carriers occurs from the hot end to the cold end, and this drift continues until an electric field is set up to balance the flow of carriers. This is known as the Seebeck effect, and the proportionality constant relating the electric field to the temperature gradient is the Seebeck coefficient (S).

The Seebeck coefficient for spherical bands can be found from the Pisarenko formula.[48] Assuming that $\tau = \tau_o e^q$, then for an n-type semiconductor in the extrinsic region, one has

$$S = \frac{k}{e}\left[\frac{5}{2} + q + \ln \frac{2(2\pi m^* kT/h^2)^{3/2}}{N_D}\right],$$

where N_D is the donor concentration. This relation is valid only for temperatures at which a relaxation time exists (see section B.2.a of this chapter). A similar result is found for a p-type semiconductor. If mixed conduction is present, then[49]

$$S = \frac{\Sigma_i S_i \sigma_i}{\Sigma_i \sigma_i},$$

where S_i and σ_i are the Seebeck coefficient and conductivity,

respectively, for the i^{th} type of carrier. The sign of S_i is that of the carrier involved.

B. Narrow Bands: The Polaron

When the atoms are brought together to form the crystal structure, some wave functions may show strong overlap, while others, especially those of the core electrons, may overlap only slightly. Thus, in a given crystal one may see a range of bandwidths, possibly from wide bands to localized levels, in which no overlap occurs. The electrons in narrow bands are most likely to be found near the ionic sites, which increases the interaction probability between an ion and the electron.

As its band of allowed states becomes narrower, the electron interacts more strongly with the ionic sites nearest it, and the presence of the electronic charge actually distorts the normal charge configuration of the surrounding lattice, resulting in a potential well around the electron. This electron with its surrounding polarization cloud is known as the polaron. Although this is still a band-type problem, it must be treated differently. Now the electron-lattice interaction term cannot be treated as a perturbation but must be incorporated in the zeroth-order Hamiltonian.

$$H = H_{electron} + H_{phonon} + H_{interaction}.$$

$H_{interaction}$ is generally assumed to be linear in the ionic displacement coordinates from equilibrium.[50] This is a simplifying assumption based on a Taylor's series expansion of the energy of the electron due to the presence of the ions:

$$E(x_n) = E(x_o) + \left.\frac{\partial E}{\partial x_n}\right|_{x_n=x_o} (x_n - x_o) + \frac{1}{2}\left.\frac{\partial^2 E}{\partial x_n^2}\right|_{x_n=x_o} (x_n - x_o)^2 + \ldots \quad (8)$$

If the displacements x_n are small, only the linear term $C(x_n - x_o)$ need be retained, and higher order terms can be neglected. Note that the term $E(x_o)$ is the electronic energy due to the ions fixed at their equilibrium positions. This term is generally incorporated into the term $H_{electron}$.

This problem can be further broken down depending on the extent of this polarization. If the polarization extends over many lattice parameters, then a dielectric-continuum model can be used. This is the large-polaron case. Alternatively, if the polarization does not extend over more than one lattice parameter, a model using localized states is more appropriate. This is the small-polaron case.

Treatments of the large and small polarons have been developed by Holstein[50] and others.[51,26] A review of their results follows.

1. Large polarons.

Fröhlich[51] has derived a large-polaron Hamiltonian based on the dielectric-continuum model (see preceding paragraphs), and this Hamiltonian has served as the starting point for many treatments of the large polaron.[51,52,53] Fröhlich's result is:

$$H = \sum_n \left[-\frac{\hbar^2}{2M} \frac{\partial^2}{\partial x_n^2} + \frac{1}{2} M\omega_o^2 x_n^2 \right] + p^2/2m^* + e\Phi(\bar{r}).$$

The first term represents the energy of the phonon field, where M is the ionic mass and ω_o is the phonon frequency. The second term represents the band energy due to the presence of the electron in the periodic lattice. The effective mass, m^*, accounts for the periodic lattice potential. Finally, the third term denotes the interaction between the electron and the phonon field through a macroscopic polarization potential Φ. Φ depends on a dimensionless constant α which has been termed the coupling constant, indicating the strength of the interaction.

This Hamiltonian has been applied with approximation techniques to the cases of weak ($\alpha < 1$)[51], intermediate ($1 < \alpha < 5$)[52,53], and strong ($\alpha > 5$)[26] coupling with the general results that the rest energy of the system is lowered and a new effective mass m^{**} is found which depends on α and increases in some manner as α increases.[26] For all $\alpha \neq 0$, $m^{**} > m^*$. The resulting eigenstates

remain Bloch-like, so the system retains its band nature, but the band is narrowed as the increased effective mass shows.

2. Large-polaron transport

There are two fundamentally different temperature regions in evaluating polaron mobility. At low temperatures, only a few optical phonons are excited, and so scattering is due primarily to impurities and acoustic phonons. At high temperatures, optical-phonon scattering dominates.

Of the methods used to calculate large-polaron mobility, two approaches have been reviewed by Appel.[26] The first method assumes the validity of the Boltzmann equation, while the second method involves the use of the density matrix. Emphasis is placed here on the Boltzmann results.

a. Boltzmann equation: weak coupling ($\alpha<1$). Although the strong electron-lattice interaction in the polaron case makes defining a relaxation time questionable, at sufficiently high temperatures, $kT >> h\omega_o$, where ω_o is the optical Einstein frequency, which says that the polaron's initial energy ($\sim kT$) is large compared with the energy change due to a collision. That this is a necessary condition for a relaxation time to exist can be seen from the following argument: At high temperatures, the lattice is highly

excited and the carrier gains or loses energy through many collisions with the lattice phonons. At low temperatures, the lattice is not highly excited, and, whereas it is still possible for the carrier to give energy to the lattice, it is difficult for the lattice to give energy to the carrier, since the lattice has little energy to transfer. Thus, there is a tendency toward unbalanced absorption of energy by the lattice.[54]

The high temperature approach is thus one of deriving a relaxation time and using it to calculate μ via the formula

$$\mu = (e/m^{**})\langle\tau\rangle .$$

This leads to

$$\mu \propto z^{1/2} ,$$

where $z = \hbar\omega_o/k_B T << 1$.

At lower temperatures, the relaxation-time approach must be abandoned, and a variation principle can be used.[26] This consists of assuming a trial wave function containing a variable parameter. The resulting energy is then minimized by varying this parameter. The result is more general than the previous solution, and reduces to the relaxation-time solution at high temperatures. At low temperatures, it looks like $e^z - 1$. The presence of a term of this

type can be understood by noting that mobility is proportional to the time between collisions which in turn is proportional to $1/\Gamma$, where Γ is the transition probability. The transition probability depends on the number of phonons, and if Bose statistics are assumed, this introduces a term $1/(e^z - 1)$.

b. Boltzmann equation: strong coupling ($\alpha >> 1$). Pekar[55] has developed expressions for the mobility in the strong-coupling case. His results are

$$\mu \alpha e^z ,$$

valid at low temperatures, and

$$\mu \alpha z^{-1/2} ,$$

valid at high temperatures.

c. Density matrix. Use of the Boltzmann equation is limited when dealing with polarons since it is not valid under conditions of very strong coupling or interference among successive scattering processes. This has led to treatments employing the density matrix. This method still involves a perturbation treatment, and its application to strong coupling has been questioned.[51] The results of various authors show some disagreement, and a summary of these results may be found in the article by Appel.[26]

d. Seebeck coefficient. To this author's knowledge, a general development of transport coefficients outside the Boltzmann-equation approach has not been done, so the Seebeck coefficient for polarons has been adapted from the standard band result. Thus,[37]

$$S = \frac{k}{e}\left[C + \ln \frac{2(2\pi m^{**} kT/h^2)^{3/2}}{n}\right]$$

for an n-type semiconductor, where C is related to the heat of transfer due to the carrier motion, and n is the carrier concentration. Since

$$n = 2(2\pi m^{**} kT/h^2)^{3/2} \exp(-E_F/kT) ,$$

then

$$eST = CkT + E_F .$$

3. Large versus small polarons.

As mentioned at the start of this section, a polaron can be classified as large or small if its polarization cloud extends over many lattice spacings or a single lattice spacing, respectively. This can lead to some differences of fundamental importance. Since the large polaron extends over many lattice spacings, the polaron "sees" a background effect due to superposing the effects of many individual ions, and a dielectric continuum model is appropriate.

On the other hand, the small polaron "sees" individual ionic sites, and the atomicity of the lattice must be taken into account, generally through the tight-binding method.

The size of the polaron can be estimated from the Feynman polaron radius, r_f.[26] This is obtained from a model in which an electron with effective mass m^* is bound harmonically to a "particle" with mass $M = m^{**} - m^*$. The characteristic frequency of this system becomes $\nu = (K/\mu)^{1/2}$, where K is the force constant and $\mu^{-1} = M^{-1} + m^{*-1}$. Then $r_f = (3\mu\nu/2)^{1/2}$.

An important consequence of the small-polaron concept is the possibility that the polarization due to the small polaron may become localized to such a degree that m^{**} gets very large and trapping occurs. This would result in a change in the transport mechanism from narrow-band tunneling to thermally-activated hopping from one isolated site to another.

Another consequence can be seen in the magnetic aspects. The large polaron will experience exchange interactions with the ionic spins, but again the result will be a superposition of exchange terms from several ions, resulting in at least partial cancellation of individual ionic effects. The small polaron will interact strongly with the spin of the one ion nearest it and should see an intra-atomic exchange interaction. In the extreme case of trapping near

an ionic site, the spin of the polaron would have to take on a particular value according to Hund's rule.

4. Small polarons.

A derivation of small-polaron eigenvalues and eigenstates has been given by Holstein.[50] In a previous paper,[56] he had developed what he called the molecular-crystal model for polaron motion. It is a one-dimensional model incorporating the following assumptions:

1) each lattice site consists of a diatomic molecule having a single vibrational degree of freedom, denoted by the displacement, x_n, from equilibrium (introducing a lattice with a basis is equivalent to considering optical phonons),

2) the tight-binding approach is used to represent the single excess electron in this crystal,

3) the "local" electronic energy, E_n, depends linearly on x_n (this term introduces interactions between the electron and the lattice).

For sufficiently small electronic overlap between sites, this overlap can be treated as a perturbation on the system described above.

Holstein's result for tight binding (see Appendix I) was:

$$\left[i\hbar \frac{\partial}{\partial t} - \sum_m \left(-\frac{\hbar^2}{2M} \frac{\partial^2}{\partial x_m^2} + \frac{1}{2} M\omega_o^2 x_m^2 \right) - E(x_n) - W(x_1, \ldots, x_n) \right] x\, a_n(x_1, \ldots, x_n) = \sum_{\pm} J(x_n, x_{n\pm1})\, a_{n\pm1}(x_1, \ldots, x_n) \quad ,$$

where M is the ionic mass. $E(x_n)$ is the energy due to the system of the electron and an isolated molecule, $W_n(x_1, \ldots, x_n)$ is the effect on $E(x_n)$ of the other molecules in the crystal, and J is the electronic overlap integral which depends on the inter-nuclear coordinates of the neighboring sites n and $n \pm 1$ (the sum on the J terms is only over nearest neighbors).

Holstein then made the following assumptions:

1) The intermolecular energies $W_n(x_1, \ldots, x_n)$ can be neglected,

2) all the overlap integrals are equal (regardless of ionic displacements) to a constant, -J,

3) $E(x_n) = -Ax_n$.

With these simplifications, his result became

$$i\hbar \frac{\partial\, a_n(x_1, \ldots, x_n)}{\partial t} = \left[\sum_{m=1}^{n} \left(-\frac{\hbar^2}{2M} \frac{\partial^2}{\partial x_m^2} + \frac{1}{2} M\omega_o^2 x_m^2 \right) - Ax_n \right] a_n - J\left[a_{n+1} + a_{n-1} \right].$$

Holstein pointed out that if the displacements (x_n) were all fixed at the same value, this equation reduced to the usual tight-binding result for single Bloch electrons.

This equation was based on the Einstein model for phonon dispersion, in which the optical modes were considered to have the same frequency, ω_o. In order to introduce dispersion, a coupling term of the form

$$\frac{1}{2} M\omega_1^2 \, x_m \, x_{m+1}$$

had to be introduced. (Holstein showed that this was a necessary term in order to have meaningful transition probabilities for cases in which phonons were emitted or absorbed.) A transformation to normal coordinates, in which the displacements were transformed into normal vibrational modes of the lattice, led to the following result:

$$i\hbar \frac{\partial a_n(\ldots q_k \ldots)}{\partial t}$$

$$= \sum_k \left[\left(- \frac{\hbar^2}{2M} \frac{\partial^2}{\partial q_k^2} + \frac{1}{2} M\omega_k^2 q_k^2 \right) - \left(\frac{2}{N}\right)^{1/2} A q_k \sin\left(kn + \frac{\pi}{4}\right) \right]$$

$$x \, a_n(\ldots q_k \ldots) - J \left[a_{n+1} + a_{n-1} \right] ,$$

where

$$\omega_k^2 = \omega_o^2 + \omega_1^2 \cos k.$$

This problem can now be solved in zeroth order by setting $J = 0$. The perturbation $J \neq 0$ is then applied to the unperturbed wave functions with standard perturbation theory. The mathematical details and the eigenfunction and eigenvalue solutions can be found in Holstein's paper[50] and will not be reproduced here. However, the pertinent results can be summarized.

The allowed transitions due to the calculated matrix elements have been divided into two categories: diagonal and nondiagonal transitions, corresponding to the respective matrix elements. In diagonal transitions, the vibration quantum numbers remain the same before and after the transition ($N_k = N_{k'}$). In nondiagonal transitions, some of the quantum numbers change by one or two units, which means that the vibrational state of the system has been changed by the absorption or emission of a phonon(s).

At $T = 0°K$, all the vibration quantum numbers are zero. Energy conservation requires that large-amplitude transitions must be diagonal. Since all the N_k are zero, nondiagonal transitions would require that some of the N_k increase but none can decrease; thus, there would be a net increase of phonon energy in the lattice. An

important result of this situation is that the eigenstates constitute a "polaron-band" with half-width

$$\Delta E = 2Je^{-S} \quad ,$$

where

$$S = \frac{1}{\pi}\int_0^{\pi} (A^2/2M\omega_k^2\hbar\omega_k)(1-\cos k)dk.$$

This bandwidth is generally $\sim 10^{-2}$ - 10^{-4} times the original electronic bandwidth 2J.

If one continues to ignore nondiagonal transitions for the moment and the temperature is allowed to increase to a nonzero value, a similar result is obtained for the band half-width,

$$\Delta E = 2Je^{-S(\ldots N_k \ldots)} \quad ,$$

where now

$$S(\ldots N_k \ldots) = \frac{1}{\pi}\int_0^{\pi} (A^2/2M\omega_k^2\hbar\omega_k)(1-\cos k) \cdot (1 + 2N_k)dk$$

and some of the N_k can be non-zero (excited vibrational states). The bandwidth is thus an exponentially decreasing function of temperature.

Holstein has then argued that for nondiagonal transitions, the transition probability will include factors like N_k due to phonon absorptions. At low temperatures, the lowest-order phonon-absorption processes dominate, and these are shown to go to zero as $T \rightarrow 0$. This is taken as confirmation that diagonal processes dominate at low temperatures.

As the temperature increases still further, the mean lifetime of a polaron-band state decreases since the transition rate (Γ) for a particular transition increases due to the increase in the N_k involved (stimulated emission). At the same time, the polaron bandwidth (W) has decreased. This implies that it is possible to reach a temperature at which the polaron-band picture breaks down. The lifetime Γ^{-1} of a band state becomes less than the time $\hbar W^{-1}$ required for the polaron to traverse a lattice spacing. Holstein attributed this to a reversal of the importance of diagonal and nondiagonal transitions, and he pointed out the need for returning to the localized polaron states rather than their plane-wave combinations for the zeroth-order states of the system. This temperature has been denoted T_t and will be considered further in section B.6 of this chapter.

With the breakdown of the band picture at high T, the normal tunneling transitions can no longer take place. There is no signifi-

cant overlap of wavefunctions centered at two adjacent sites, so the transitions take place by thermally activated hopping. The polaron is raised to an excited state due to thermal phonons in the lattice, and from this excited state, it can make a transition to a nearby site, emitting phonons after the transition is complete.

5. Small-polaron transport.

Bosman and Van Daal[37] have summarized the results for small-polaron mobility in the band and hopping regions. As in the case of the large polaron, one again has to worry about the strong interaction between the charge carrier and the lattice and the resulting doubt concerning the validity of the Boltzmann equation for this problem. Most of the calculations of the mobility have been based on the Boltzmann equation. A review of these results is presented here, and comments on other methods appear in the subsequent section 5.c.

a. Hopping mobility. Bosman and Van Daal[37] have made an estimate of the upper limit for hopping mobility. The result is

$$\mu < \frac{1}{4\pi} \frac{ea^2}{\hbar} \frac{\hbar\omega_o}{kT} .$$

With $h\omega_o \simeq kT$ and suitable parameters ($a \simeq 3A$), this becomes

$$\mu < 0.1 \text{ cm}^2/\text{volt-second}.$$

The hopping mobility has been derived for the cases of adiabatic[35] and non-adiabatic[37] processes. As was noted in section D of Chapter I, for adiabatic processes, $J > h\,\omega_o$, and the electronic wave function is able to adapt to the ionic motion. For non-adiabatic processes, the wave function does not adapt quickly enough to follow the ionic motion.

The non-adiabatic mobility was derived under the assumptions of J small enough to be considered a perturbation and of no dispersion in the optical vibration spectrum. The following result was obtained (approximated for high temperatures $T > \frac{1}{2}\,\theta_D$ (see section B.6)):

$$\mu = \left(\frac{\pi}{2}\right)^{1/2} \frac{ea^2}{\hbar} \left(\frac{J}{\hbar\,\omega_o}\right)^2 \frac{1}{\gamma^{1/2}} \left(\frac{\hbar\,\omega_o}{kT}\right)^{3/2} \exp\left[-\frac{1}{2}\,\gamma\,\hbar\,\omega_o/kT\right],$$

or

$$\mu \propto \frac{1}{T^{3/2}} \exp\,(-U/kT),$$

where

$$U = \frac{1}{2}\,\gamma\,\hbar\,\omega_o$$

and

$$\gamma \simeq \frac{1.25}{\pi} \left(\frac{1}{\epsilon_{\text{optical}}} - \frac{1}{\epsilon_{\text{static}}}\right) \frac{e^2}{\hbar\,\omega_o a}$$

is the electron-lattice coupling constant.

Holstein[50] investigated the conditions for which this mobility expression was valid. He found that in order for small polarons to exist, the condition

$$2J < E_b$$

should hold (a result of decreasing the total energy by polaron formation) where 2J is half the bandwidth and E_b is the maximum polaron binding energy:

$$E_b = \gamma \hbar \omega_o .$$

Also, the treatment of J as a perturbation required

$$J < \hbar \omega_o .$$

This was noted as being the borderline condition for considering non-adiabatic processes.

For the adiabatic case, in which $J > \hbar \omega_o$, the result

$$\mu = \frac{3}{4\pi} \frac{ea^2}{\hbar} \frac{\hbar \omega_o}{kT} \exp\left[-(U-J)/kT\right]$$

was obtained. It was pointed out above that J had to be less than U for the small polaron to exist, so an upper limit of $J < 1/3U$ was chosen for a one-dimensional crystal. In three dimensions, this becomes $J < U$.

b. Band mobility. Holstein[50] found that the low-temperature region was governed by typical band motion in a narrow band with exponentially decreasing bandwidth. His result for mobility in the non-adiabatic case was

$$\mu = \frac{1}{\pi^{1/2}} \frac{ea^2}{\hbar} \frac{\hbar\omega_o}{kT} \left(\gamma \operatorname{csch} \frac{1}{2} \frac{\hbar\omega_o}{kT}\right)^{1/2} \exp\left(-2\gamma \operatorname{csch} \frac{1}{2} \frac{\hbar\omega_o}{kT}\right) .$$

These mobility expressions can be summarized qualitatively by noting that hopping motion results in an exponentially increasing function of temperature characterized by an activation energy, whereas band motion results in a decreasing function of temperature.

c. Methods other than the Boltzmann equation. Two methods have been mentioned by Appel[26] which have been applied to the small-polaron problem in an attempt to overcome the shortcomings of the Boltzmann equation under conditions of strong and extended interactions. These are the density-matrix approach and the Kubo response-function approach.

The first of these consists of setting up the problem in terms of the quantum mechanical density matrix. The results tend to support the previous results based on the Boltzmann equation. In particular, Friedman[57] found that

$$\mu = \mu_{\text{hopping}} + \mu_{\text{band}}$$

when he applied the density-matrix method to the Holstein Hamiltonian.

The Kubo response-function approach[58] has also tended to support the results based on the Boltzmann equation, and reference is made to Appel[26] for a summary of the use of this method.

d. Seebeck coefficient. In the discussion of the thermoelectric effect for both wide bands and large polarons, the derivation of the expression for the thermoelectric power has been ignored. The Pisarenko formula is a standard result for semiconductors under the assumption of spherical bands, and its form and applicability was accepted without question. At this point, it might be well to briefly review the derivation of the general Seebeck coefficient, since one must fall back on the general form to handle the two cases encountered in small polarons.

Ziman[59] has used the distribution function f_k (the solution to the Boltzmann equation) to solve for electric current density and heat current density, using the formulae

$$\bar{J} = \int e \, \bar{v}_k \, f_k \, \overline{dk}$$

and

$$\bar{U} = \int f_k \left\{ \epsilon(\bar{k}) - \eta \right\} \bar{v}_k \, \overline{dk} \, .$$

The first equation represents the vector sum over all k of the total number of current density elements with wave vector k. The second equation is the same type except there is now an energy flux instead of a charge flux. Heat is defined as internal energy minus free energy, hence the $\epsilon(\bar{k}) - \eta$ term, in which η is the chemical potential.

When the form for f_k is substituted into these equations, the results are

$$\bar{J} = e^2 \bar{K}_0 \cdot \bar{E} + \frac{e}{T} \bar{K}_1 \cdot (-\nabla T)$$

and

$$\bar{U} = e\bar{K}_1 \cdot \bar{E} + \frac{1}{T} \bar{K}_2 \cdot (-\nabla T) ,$$

where the K_i are in general tensors, and $\bar{E}$ and ∇T are the electric field and temperature gradient, respectively. If the electric field, current, and temperature gradient are all in the same direction, then

$$J_x = e^2 K_0 E_x - \frac{e}{T} K_1 \frac{dT}{dx} .$$

If $J_x = 0$, then

$$E_x = \frac{1}{e^2} \frac{K_1}{K_0} \frac{e}{T} \frac{dT}{dx} .$$

The quantity $\frac{1}{e^2}\frac{K_1}{K_0}\frac{e}{T}$ is the Seebeck coefficient. Actually, the quantity $\bar{E}$ in the expression for $\bar{J}$ contained a term $-\frac{1}{e}\nabla\eta$ which represented the change of the chemical potential due to the addition of a temperature gradient. This has the effect of adding a term to the Seebeck coefficient of the form

$$\frac{1}{T}\frac{\eta}{e} .$$

Thus,

$$S = \frac{k}{e}\left[\frac{\eta}{kT} + \frac{1}{kT}\frac{K_1}{K_0}\right] .$$

It is the evaluation of K_1 and K_0 which is necessary for each problem.

For low temperatures at which small-polaron band conduction takes place, Appel[26] has referenced a paper by Madelung[60] in which K_1 and K_0 were calculated using a relaxation time for the interaction with the lattice. The solution is a variation of the Pisarenko formula

$$S = \frac{k}{e}\left(\frac{\eta}{kT} - A\right) ,$$

where A results from transfer of kinetic energy. $A \simeq 1 - 2$ and depends on the distribution function and functional dependence of scattering on energy.

This can be rewritten for a nondegenerate semiconductor by using the relations

$$\frac{\eta}{kT} = \log \frac{N_c}{n} ,$$

$$N_c = 2(2\pi\, m^{**} kT/h^2)^{3/2}$$

and by rewriting m^{**} as

$$m^{**} = m^{*}/Y(T) ,$$

where $Y(T)$ is an oscillator overlap integral and reflects the temperature-dependent bandwidth of small polarons. The result is

$$S = \frac{k}{e}\left\{\log\left[\frac{2(2\pi\, m^{*}\, kT)^{3/2}}{h^3 n}\right] + \frac{3}{2}\log Y(T) - A\right\} .$$

The temperature dependence of $Y(T)$ leads to a stronger temperature dependence for this case than in wide-band semiconductors.

At high temperatures where hopping occurs, all polaron states are at energy $-E_b$ ($E_0 = 0$), and in this reference system, $\eta \rightarrow \eta + E_b$. Thus,

$$S = \frac{k}{e}\left[\frac{\eta + E_b}{kT} + \frac{1}{kT}\,\frac{K_1}{K_0}\right] .$$

Appel[26] has referenced work by Schotte[61] in which he calculated K_1 and K_0 to lowest existing order in J, based on Holstein's Hamiltonian. The result for S is

$$S = \frac{k}{e} \ln \frac{N}{n} ,$$

where the effective density of states N_c has been replaced by N, the density of cations in the crystal. Bosman and Van Daal[37] obtained a similar result, but theirs still included the term due to transfer of kinetic energy. They redefined this term as

$$A = \frac{\beta U}{kT}$$

where U is the activation energy for hopping and β is a constant, and it was noted that values for β of 0.05, 0.1 - 0.4, and zero have been reported.

Very little has been done outside of the Boltzmann approach in determining the form of the Seebeck coefficient. Platzmann[42] has used the density-matrix approach, and his results support those obtained with the Boltzmann equation in the limit of well-defined collisions. Kadanoff and Baym[62] have applied Green's function techniques to general transport and claim to have overcome the limitation of the Boltzmann equation regarding length of time in a

collision. To this author's knowledge, the only useful expressions for the Seebeck coefficient are the ones already described, which are based on the Boltzmann equation.

6. Estimate for T_t.

The temperature at which the transition occurs from band transport to hopping has been estimated by Holstein[50] to be $\frac{1}{2}\Theta_D$ where Θ_D is the optical Debye temperature. Bosman and Van Daal[37] have argued that this may be considered to be an upper limit. A summary of arguments is given herein which indicates that this transition can be depressed well below $\frac{1}{2}\Theta_D$. Numerical calculations by deWit[63] indicated that a small amount of dispersion ($\sim$10%) in the optical spectrum could depress T_t to about $\frac{1}{4}\Theta_D$. Lang and Firsov[64] identified an extra scattering process through virtual transitions to a neighboring site and back again, which could be expected to lower T_t. The presence of impurities could disturb the fluctuations of the lattice, causing the bandwidth to be exceeded by fluctuations of lattice energy at a lower temperature.[65] These points have led Bosman and Van Daal[37] to conclude that T_t is most likely depressed to $\frac{1}{4}\Theta_D$ or lower, and that the very occurrence of small-polaron band behavior is not certain.

Not much has been done on estimates of the Debye temperature of transition-metal oxides, especially in the optical branch. Bosman and Van Daal[37] estimated T_t for NiO to be about $\frac{1}{4}\,\Theta_D$ = 200°K, but they did not explain how they arrived at this number.

For hematite, a calculation was made for the acoustical Debye temperature from a published curve of specific heat.[66] The T^3 law for low temperatures was used (Debye model for specific heat) and the result was Θ = 570°K. This would lead to $T_t \simeq \frac{1}{4} \times 570 = 142.5$°K. However, since the optical branch of the phonon spectrum is at higher energies than the acoustical branch, the optical Debye temperature is likely higher than this value. It is difficult to say how much higher, but it is possible that the value Θ_D = 800°K used for NiO is also appropriate for hematite. This results in

$$T_t \simeq 200°K.$$

Unfortunately, no experimental evidence has been found to verify this estimate.

C. Impurity Conduction.

At sufficiently high temperatures in a doped semiconductor, the impurities are ionized and the resulting holes or electrons are available for transport processes. One must also consider the situation at low temperatures at which the impurities are not ionized. Two possible results exist. Either an impurity band is formed or hopping can occur between impurity sites.

If the impurity concentration is large, the impurity sites may be close enough in the crystal lattice to allow for overlap of the wave functions for the outer, loosely-bound states. This results in a band of allowed states for the non-ionized electron (or hole) with the impurity states acting as effective lattice sites. If the sample is doped only with n-type (or p-type) impurities, then the resulting impurity band will be full; i.e., all states are occupied. However, if a small percentage of impurity of the opposite sign is present (partial compensation), then some of the majority impurities (those of greater concentration) will be compensated by these minority impurities and an unfilled band results.

As the impurity concentration is decreased, the distance between adjacent impurity sites increases rapidly and becomes many lattice spacings. The probability of wave-function overlap diminishes with increasing distance, and the impurity band eventually

breaks down. Since these non-ionized impurity states occupy the same energy level but are at far-removed lattice sites, thermally activated hopping can provide the transport mechanism. In an analogous manner to small-polaron hopping, an impurity state can be excited by interacting with a phonon. This excited state produces an admixture of the original impurity-state wave function with a higher energy wave function, which can have a finite probability of overlap with an adjacent impurity state which is empty. The overlap allows the carrier to transfer to the second impurity state.

That this is significant at low temperatures is seen from the fact that the impurities are not ionized at these low temperatures. It is energetically favorable since less energy has to be obtained from lattice phonons for this impurity conduction (either bandlike or hopping) than for ionizing the impurities.

Many authors[33,32,31] have mentioned impurity conduction at low temperatures, but Bosman and Van Daal[37] have reported experimental evidence of its influence on the Seebeck coefficient in polycrystalline samples of NiO and Fe_2O_3. Its presence is determined by a deviation of plots of Seebeck coefficient versus 1/T from plots of log resistivity versus 1/T. With the combination of n-type semiconduction and impurity conduction, and recalling that

$$S = \frac{\Sigma_i S_i \sigma_i}{\Sigma_i \sigma_i} ,$$

their analysis of the Seebeck coefficient yields:

$$S = -\frac{k}{e}\left\{ \frac{\sigma_n}{\sigma_{tot}}\left(\frac{E_F}{kT} + A\right) - \frac{\sigma_{imp}}{\sigma_{tot}}\left(\frac{E_D - E_F}{kT}\right)\right\} ,$$

where the heat of transfer has been neglected for impurity conduction, and where

$$\sigma_{tot} = \sigma_n + \sigma_{imp} .$$

Thus, at low temperatures where impurity conduction becomes important, a turn-around point in the slope of S versus 1/T is expected. This turn-around is seen at 160°K for NiO and about 125°K for Fe_2O_3, although the deviation between the log resistivity and S plots for Fe_2O_3 seems to be pronounced up to temperatures ~300°K. These results were for dopings of 0.1 atomic percent Nb or Zr in Fe_2O_3. It was noted that the impurity band transport would not be likely for dopings of less than 5 atomic percent.

The results reported by Bosman and Van Daal[37] for Fe_2O_3 were on ceramic samples. They were unable to get low-temperature DC results, so AC results were reported, which they felt were representative of the true bulk properties.

It might be noted that if the impurities do not assume a net spin in the magnetically ordered crystal, then a magnetic ordering factor would not be present in the inter-impurity hopping. However, if the impurities did assume net non-zero spins, their spins would align into the antiferromagnetic ordering of the lattice and a magnetic ordering term could result in the hopping mobility. For the impurities used in the present work, Mg has a $2p^6 3s^2$ closed shell configuration, while Ti has $3p^6 3d^2 4s^2$. Both of these atoms show an even number of electrons, although the 3d shell in Ti is unfilled so these two 3d electrons could align their spins parallel. The Mg impurity would ordinarily not have a net spin. However, due to the strong interactions when these impurities are placed in a magnetically ordered lattice, the outer electrons could very well be excited to other states and net spins could result.

D. Effect of Magnetic Order.

Generally, the effect of the charge carrier's spin has been neglected in band treatments of semiconductors. This is ordinarily a good assumption since the velocity of a carrier in the vicinity of the ionic cores or of other electrons is high enough that the exchange interaction between the spin of the carrier and the spin of the ion or other electron is small compared with other terms.

When the bands become narrow, the velocity of the carrier is diminished and it becomes more localized in nature. This can result in stronger exchange interactions with the ionic cores and, in the limit of complete localization of the carrier, Hund's rule must be satisfied for the spin of the carrier relative to the ionic spin. This rule requires that if the shell is less than half filled, the next spin goes in parallel to the existing ones, while it goes in antiparallel to the majority if the shell is more than half filled. Following this argument, then, spin-induced exchange interactions are most likely to be important in situations where transport occurs by thermally activated hopping.

1. Effect on hopping probability.

Heikes[67] and Appel[68] have suggested that for hopping between two cations n and n', a spin transfer must likewise occur. This spin transfer is unaffected by the mechanism of the transfer process; i.e., thermally activated hopping does not alter spin, so that the ability of the carrier to satisfy Hund's rule at each ionic site depends on the relative spin orientations of the two sites. This introduces a phase factor in the expression for the transition probability which is maximum when the ionic spins are parallel and is zero when they are antiparallel. Since at finite temperatures spin fluctuations disturb the parallel or antiparallel

alignment of spins in magnetically ordered systems, these spin fluctuations determine the form of this phase factor.

Haubenreisser[69] noted that this model was similar to Zener's[45] double exchange. Consider the system $Fe^{2+}O^{2-}Fe^{3+}$. This is equivalent to $Fe^{3+}O^{2-}Fe^{2+}$ and the transition between these two configurations can be accomplished via a two-step process in which an electron transfers from the oxygen to the Fe^{3+} ion, and then an electron transfers from the Fe^{2+} to the oxygen to re-establish the stable O^{2-} configuration. This type of process results in ferromagnetic coupling between the two cations.[2]

2. Double exchange in hematite.

Ransom[44] has considered the possible role of double exchange in hematite. He noted that intra-atomic exchange would take place at each localized site, but in transferring from site A to site B, the energy matrix $\langle B \mid H_T \mid A \rangle$ must account for the possibility that the two states may be based on different coordinate systems. He chose to transform the transfer matrix elements by using the rotation operator $R_u(\theta) = e^{iJ_u\theta}$ for rotation about an axis u by an angle θ, where J_u is the u component of angular momentum.

The eigenstates of the transfer system consisted of the two sites i and j each having possible spin states spin-up (α) or spin-down (β). The four possibilities were designated $|d_i\alpha\rangle$, $|d_i\beta\rangle$, $|d_j\alpha'\rangle$, $|d_j\beta'\rangle$.

The rotation operator was rewritten using the Pauli spin matrices[70], with the result

$$R_u(\theta) = 1 \cos\frac{\theta}{2} - i\,\sigma_u \sin\frac{\theta}{2} \quad ,$$

where σ_u is the Pauli spin matrix for the axis u. Following Ransom's development, the rotation axis was chosen as the y axis, so

$$\sigma_u = \sigma_y = \begin{pmatrix} 0 & -i \\ i & 0 \end{pmatrix}$$

Now

$$R_u(\theta) = \begin{bmatrix} \cos\frac{\theta}{2} & -\sin\frac{\theta}{2} \\ \sin\frac{\theta}{2} & \cos\frac{\theta}{2} \end{bmatrix}.$$

But

$$\begin{pmatrix} \alpha \\ \beta \end{pmatrix} = R_u(\theta) \begin{pmatrix} \alpha' \\ \beta' \end{pmatrix},$$

and so

$$\alpha = \alpha' \cos\frac{\Theta}{2} - \beta' \sin\frac{\Theta}{2}$$

$$\beta = \alpha' \sin\frac{\Theta}{2} + \beta' \cos\frac{\Theta}{2} \quad .$$

The resulting energy matrix for this system is

$$\begin{array}{c} \\ d_i\alpha \\ d_i\beta \\ d_j\alpha' \\ d_j\beta' \end{array} \begin{array}{c} \begin{array}{cccc} d_i\alpha & d_i\beta & d_j\alpha' & d_j\beta' \end{array} \\ \begin{bmatrix} a & 0 & A\cos\frac{\Theta}{2} & -A\sin\frac{\Theta}{2} \\ 0 & b & A\sin\frac{\Theta}{2} & A\cos\frac{\Theta}{2} \\ A\cos\frac{\Theta}{2} & A\sin\frac{\Theta}{2} & a & 0 \\ -A\sin\frac{\Theta}{2} & A\cos\frac{\Theta}{2} & 0 & b \end{bmatrix} \end{array} .$$

The off-diagonal elements lead to probabilities for transitions from site i to site j.

The application of this result to hematite will be considered for $T < T_M$ and $T > T_M$ in the two cases of transport in the (111) plane and along the [111] axis.

(111) plane. For transport below T_M, the spins are aligned, and thus $\Theta = 0$. The matrix becomes

$$\begin{bmatrix} a & 0 & A & 0 \\ 0 & b & 0 & A \\ A & 0 & a & 0 \\ 0 & A & 0 & b \end{bmatrix} .$$

For $T > T_M$, the spins have changed orientation but are still parallel, so $\Theta = 0$ and the matrix is unchanged.

[111] direction. Below T_M, spins on adjacent ions are antiparallel, and $\Theta = \pi$. The matrix becomes

$$\begin{bmatrix} a & 0 & 0 & -A \\ 0 & b & A & 0 \\ 0 & A & a & 0 \\ -A & 0 & 0 & b \end{bmatrix} .$$

Above T_M, the spins are essentially antiparallel but slightly canted. The angle $\Theta = \pi - 2\alpha$, where α is the canting angle. The matrix becomes

$$\begin{bmatrix} a & 0 & A \sin\alpha & -A \cos\alpha \\ 0 & b & A \cos\alpha & A \sin\alpha \\ A \sin\alpha & A \cos\alpha & a & 0 \\ -A \cos\alpha & A \sin\alpha & 0 & b \end{bmatrix} .$$

For transport in the (111) plane, the transition at T_M should have no effect on the transition probabilities, whereas a change is expected at T_M for transport along the [111] axis, provided this interaction term is important in hematite.

Another consequence of this type of exchange is an expected anisotropy in the transport properties due to the number of available states to which hopping can occur. All states have parallel spin within a (111) plane so there are many possible sites to which hopping can occur within the plane. Along the [111] axis, it is more difficult to find a satisfactory destination for hopping, and thus the mobility is expected to be less along the [111] axis than in the (111) plane if double exchange is important.

CHAPTER III

THE EXPERIMENT

The doped single crystals of hematite were provided by a previous researcher.[71] Samples were oriented and cut from Mg-, Ti-, Ni-, Cu-, and V-doped crystals following the method outlined by Besser.[72] Two samples with approximate dimensions 0.05" x 0.05" x 0.12" were made for each doping with the long dimension parallel to and perpendicular to the [111] axis, respectively (figure 5).

Dopant	Atomic Percent
Mg	0.5
Ti	0.05
Ni	0.125
Cu	0.125
V	1.0

Electrical contact to the samples was made by painting on a silver layer (Englehard #16 flexible silver coating) and firing it at 300°C for ten minutes. This method was chosen after a trial-and-error process failed to produce anything better. The contacts were not ohmic at low current levels, but attempts with indium-alloy solders, vacuum deposition of silver, aluminum, and magnesium, and variations on the firing schedule all produced higher-impedance contacts. The cleaning sequence for each sample was polishing with

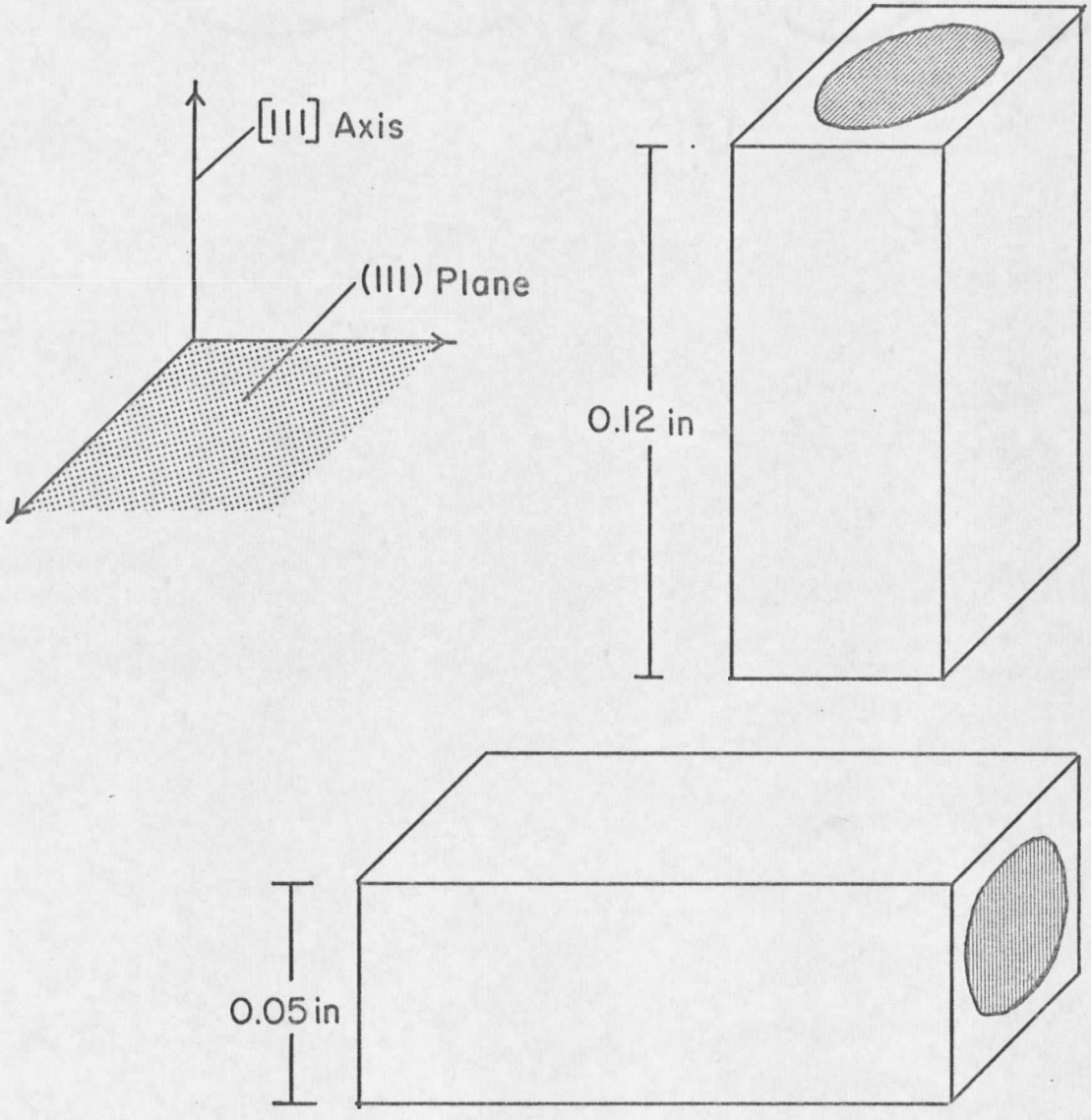


Figure 5. Shape and Orientations of the Two Samples.

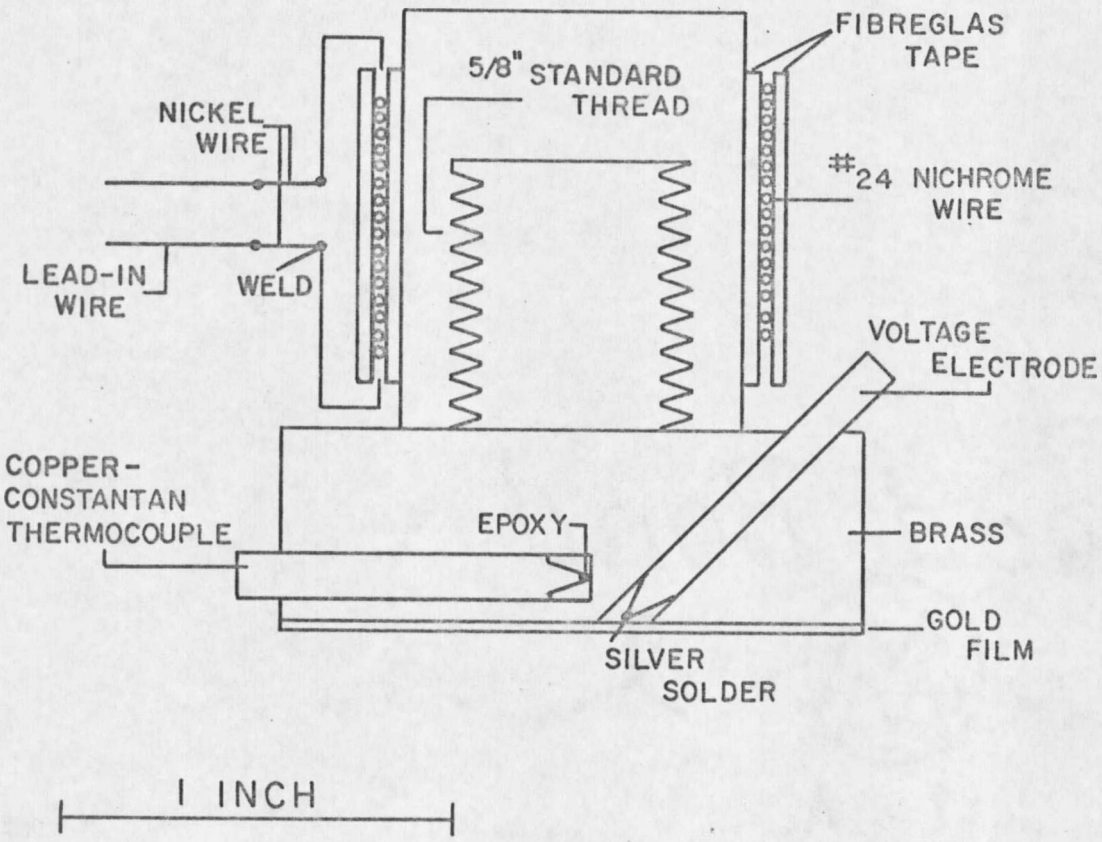


Figure 6. Construction of the Heat Blocks.

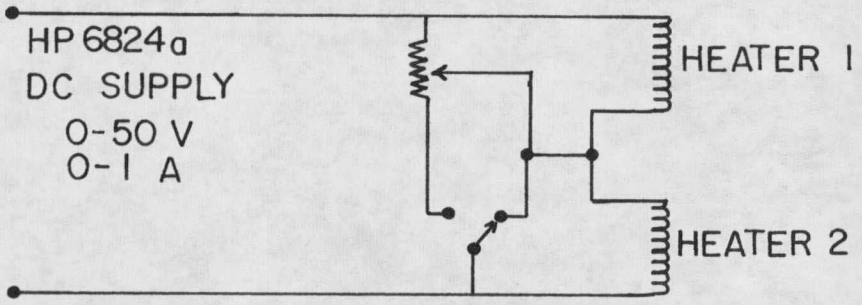
fine emery paper followed by nitric-acid and deionized-water baths. The overall sample impedance at room temperature was about 10KΩ.

Brass blocks were made which served as both sample holder and heaters.[73] The heater wires of #24 nichrome were insulated from the blocks with fiberglas tape and then more tape was wrapped around the heater assembly to electrically insulate the system from the block holders. To attach lead-in wire to the nichrome, short pieces of nickel wire were silver-soldered to the nichrome, and the lead-in wires were then soldered to the nickel.

Copper-constantan thermocouples were silver-soldered into the block faces, which were then machined and mirror polished, and finally a gold film was evaporated onto the finished faces. Originally, it was planned to use the thermocouples for both the electrical and thermal measurements, but voltage interactions between these two circuits forced isolating them electrically from each other. The old leads were left for the voltage measurement, while the thermocouples were set in with an epoxy (Eccobond 285; Emerson & Cuming) which exhibited high thermal conductivity but low electrical conductivity (figure 6).

The heater control circuit was designed to enable block one to be heated to establish the temperature difference, and then provide a balance between the two heaters to maintain a reasonably

constant difference as the run was taken. The following circuit was used:



The heaters were supplied with DC currents ranging from 0.1-1 amp to the series connection.

The Seebeck voltage was measured between the copper wires of the original thermocouples. The large sample impedance caused a modification in the circuit, since with ordinary meter input impedances the voltage drop at the contacts was not negligible with signals on the order of one millivolt. It was felt that a high-input-impedance device would remedy this, but an operational-amplifier circuit with input impedance equal to 10^9 ohms led to two problems: the noise level was increased and the resulting lower current led to an effectively higher impedance due to the contacts. A check showed that this circuit still gave lower readings than nulled readings, in which no current was flowing. The final choice

was a HP 419a null voltmeter which was used on internal battery supply. The amplifier output (signal proportional to meter deflection) was fed to the Y axis of a HP 135a Moseley X-Y recorder. The voltmeter ground was connected to the recorder ground, which in turn went to electrical ground through the line cord (figure 7).

The thermocouples were run through ice reference baths housed in a metal box with all leads shielded. The circuit diagram is shown in figure 8, and with this circuit one can determine the ambient temperature and temperature difference.

Since the noise problem was very critical, R-F filters were placed in the heater supply circuit, and the ground system was connected to a water pipe with 14-gauge wire to provide a better ground. (This was not necessary after the system was moved to another building with a better electrical ground.) Care was taken to avoid any ground loops in the system.

A normal run consisted of cooling the blocks and sample down to the lowest temperature in a refrigeration chamber and then allowing the blocks to warm gradually while providing enough current to maintain a preset temperature difference. When room temperature was reached, enough current was supplied to the heaters to maintain a reasonable heating rate. A complete run took about four hours.

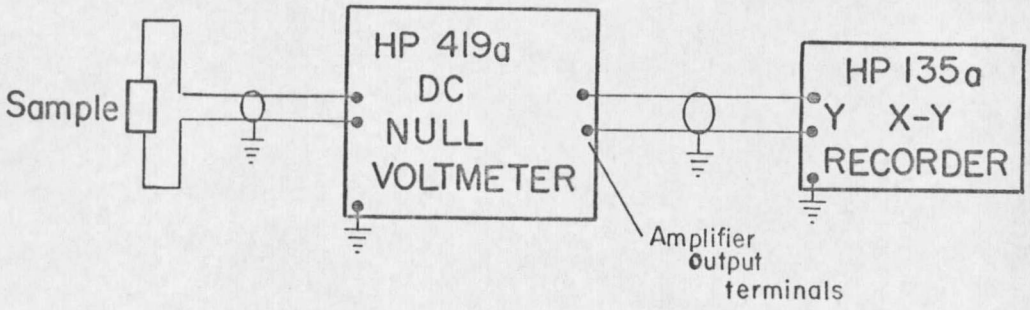


Figure 7. Circuit for Measuring Seebeck Voltage.

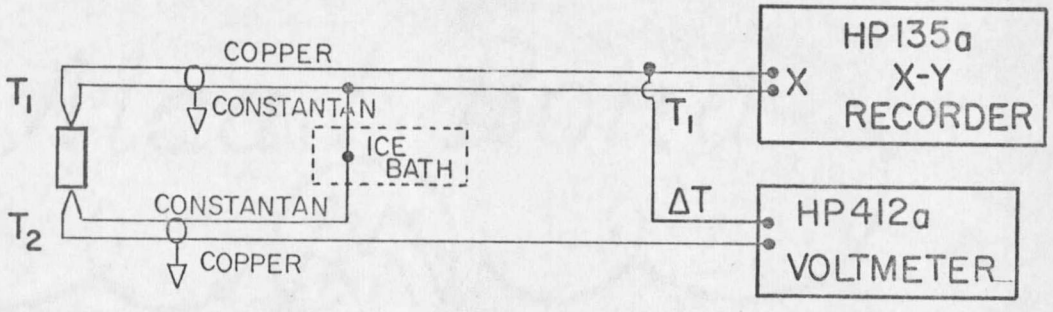


Figure 8. Thermocouple Circuit for Measuring Ambient Temperature and Temperature Difference.

It was found that moisture in the refrigeration chamber could lead to noisy readings at the low-temperature points, so a desiccant consisting of calcium chloride crystals in a wire screen box was placed in the chamber.

CHAPTER IV

RESULTS

A. Presentation of Experimental Results.

In this section, the results of measurements of the Seebeck coefficient for the various samples are reported. It should be noted at this time that results are reported only for Ti- and Mg-doped samples. The samples doped with Ni, Cu, and V were found to exhibit extremely high impedance (10^{12} Ω cm) with voltage levels up to 100 volts across the sample. This was true regardless of the type of contact applied, and since many methods had led to satisfactory (though not ohmic) contacts, the high impedance was suspected to be a bulk property. A paramagnetic-resonance check was made on the vanadium-doped sample, but no vanadium lines were seen.(74) If the vanadium appeared in the lattice in its expected valence state of +5, then the ion would be non-magnetic, which could explain the absence of the line. However, there is still a possibility that the vanadium ion could assume a net spin due to the interactions with the magnetically ordered spins of the antiferromagnetic lattice. Since this questionable magnetic state of the impurity makes the meaning of the paramagnetic-resonance results uncertain, scraps of the crystals doped with Ni, Cu, and V were checked by emission spectroscopy, and no lines due to these impurities were seen.(75) It was concluded that the doping had not been effective in the Cu-, Ni-, and V-doped samples, so these were not pursued further.

Data for Seebeck coefficient versus 1/T in Mg- and Ti-doped samples are reported in figures 9-12. The primary region of interest is the temperature range 240-270°K, which should include the Morin transition for the types and amounts of dopants being investigated. In some of the early runs, temperatures up to and above 100°C were considered, but nothing significant was seen in the Seebeck coefficient at temperatures above room temperature. Since a considerable amount of time was necessary to extend the results above room temperature, the temperature range was restricted to temperatures below room temperature.

The data on Mg-doped samples show a marked difference at $T \simeq 260°K$ for the two orientations. A sharp six percent rise in the Seebeck coefficient with increasing temperature is seen along the $[111]$ direction over a temperature range of about 2.5 degrees, while no effect is seen in the (111) plane. In addition, the magnitude of the coefficient in the (111) orientation is only about 58% of the magnitude for the $[111]$ orientation.

In the Ti-doped samples, a drop is seen with increasing temperature for the Seebeck coefficient in the $[111]$ orientation. This drop is gradual, taking place over a range of fifteen degrees, centered about $T \simeq 248°K$. There is also a repeatable fluctuation region for the (111) orientation, taking place over a range of seventeen

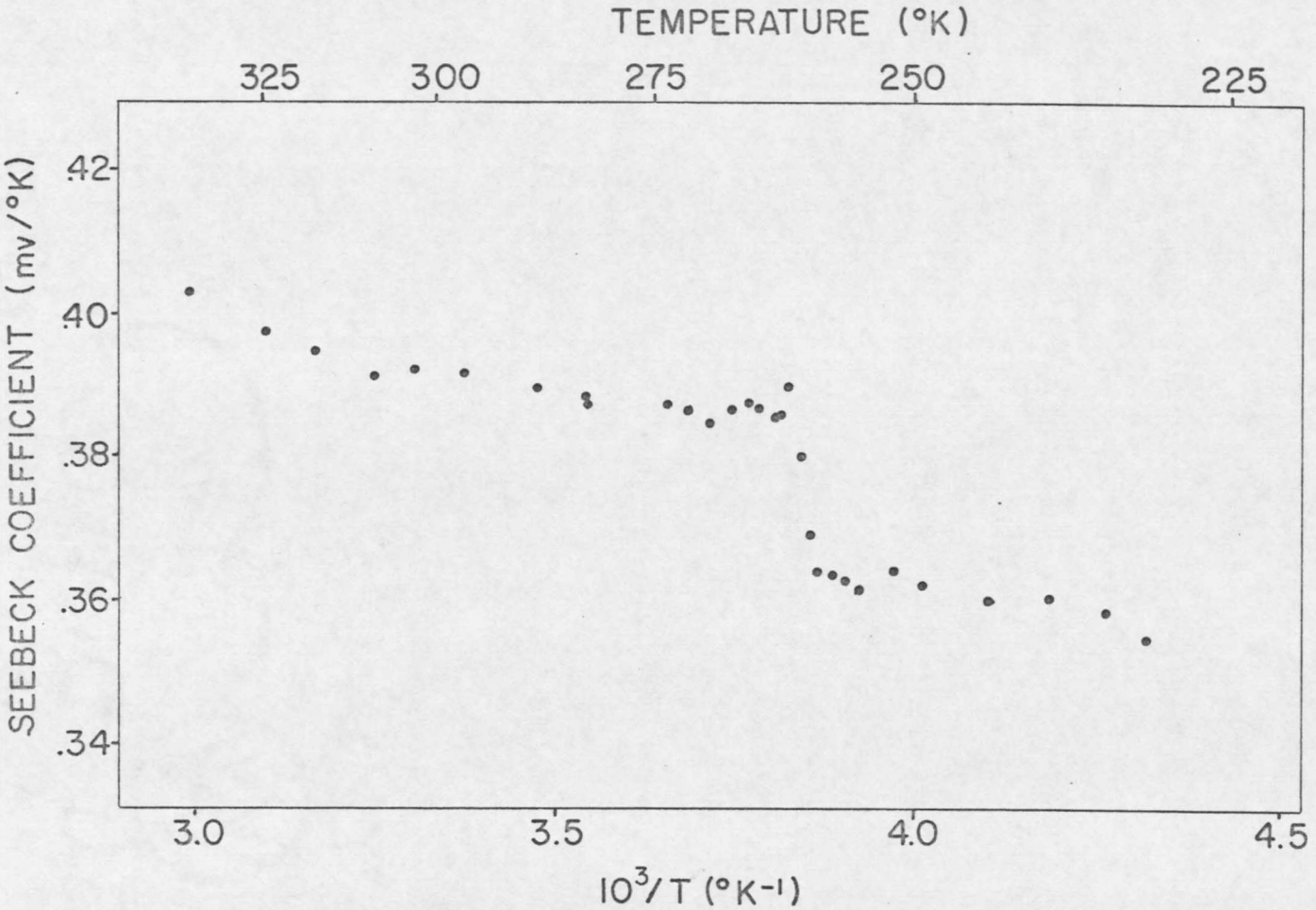


Figure 9. Seebeck Coefficient versus 1/T for Mg-Doped Sample Along [111] Direction.

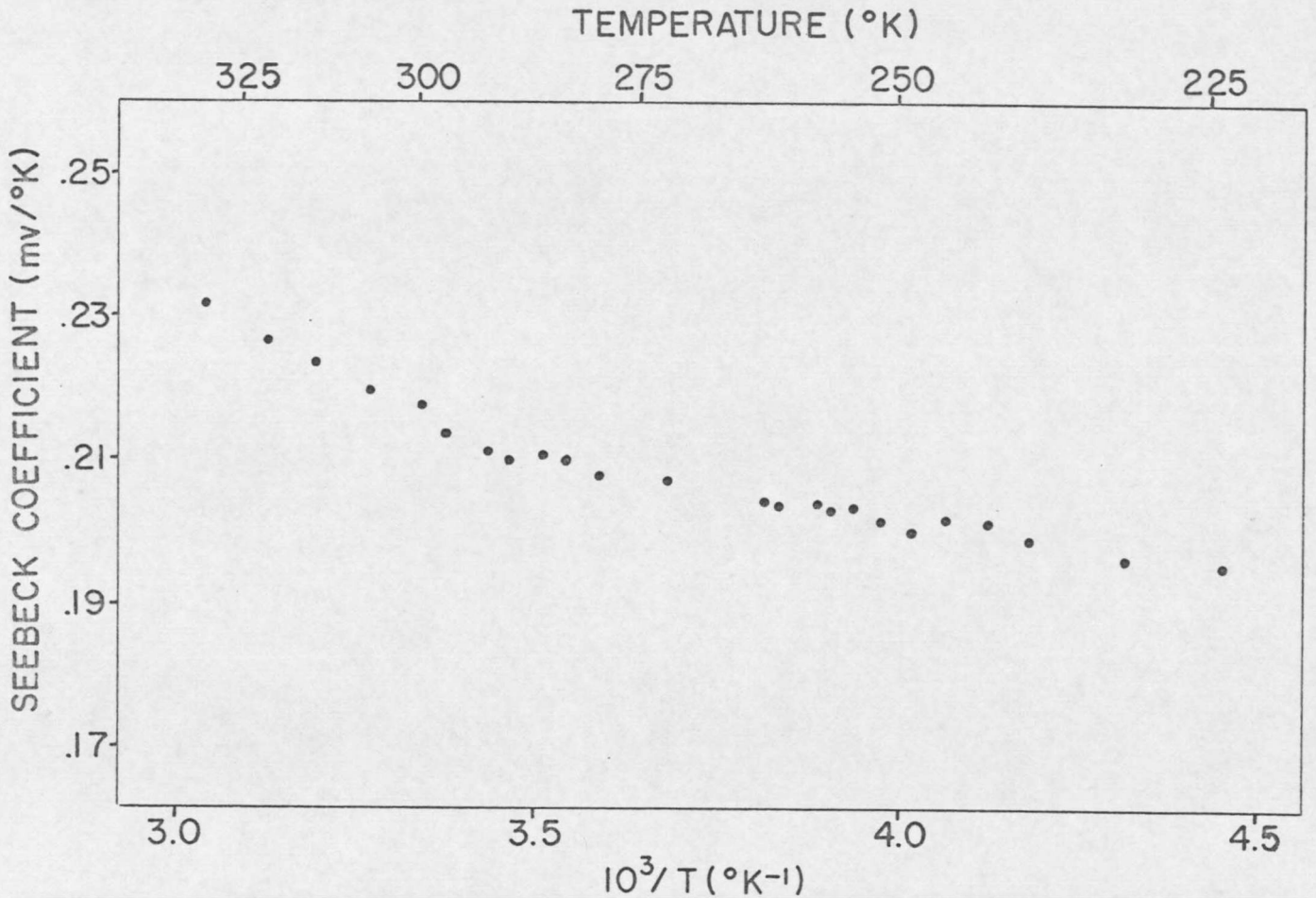


Figure 10. Seebeck Coefficient versus 1/T for Mg-Doped Sample in (111) Plane.

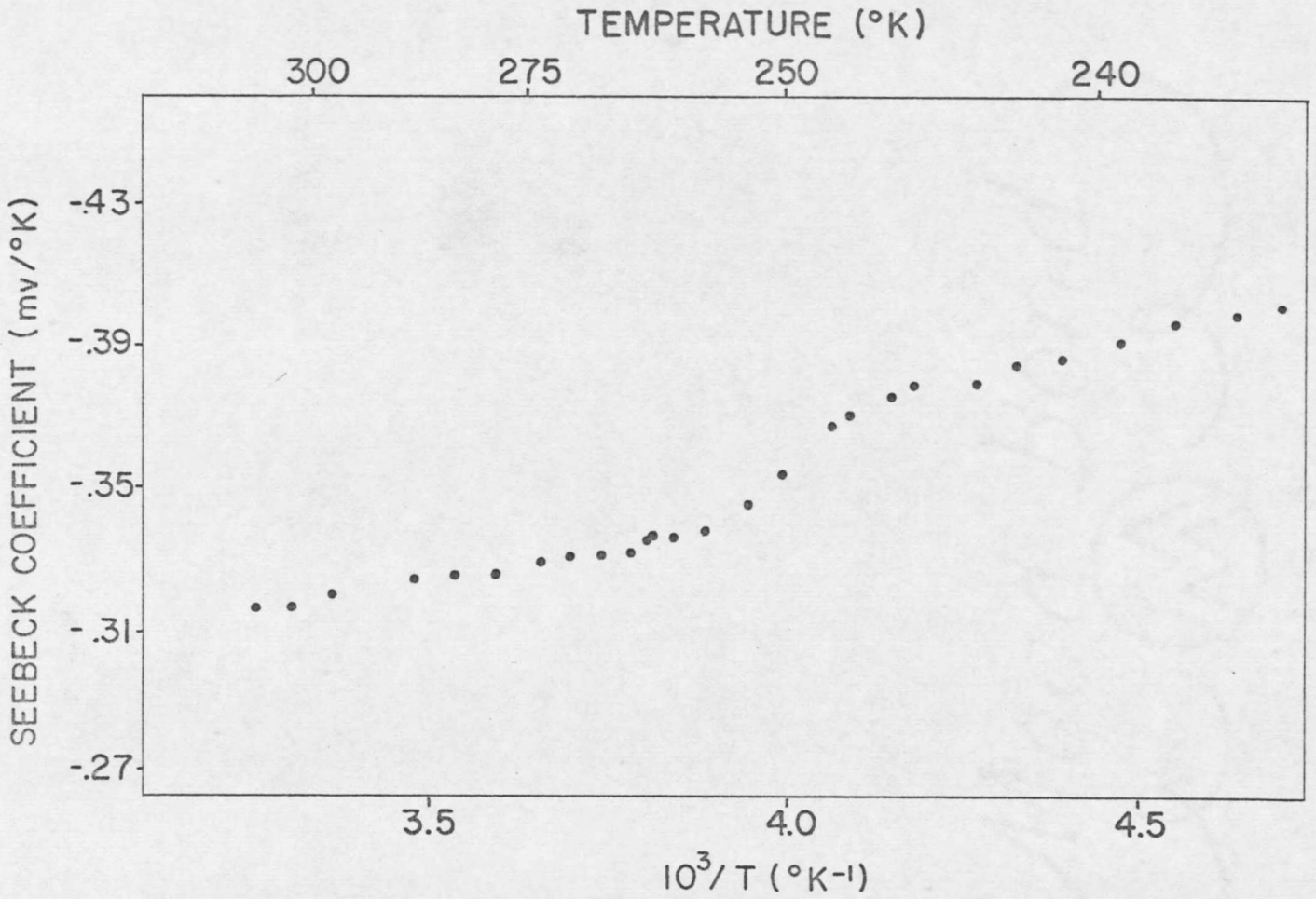


Figure 11. Seebeck Coefficient versus 1/T for Ti-Doped Sample Along [111] Direction.

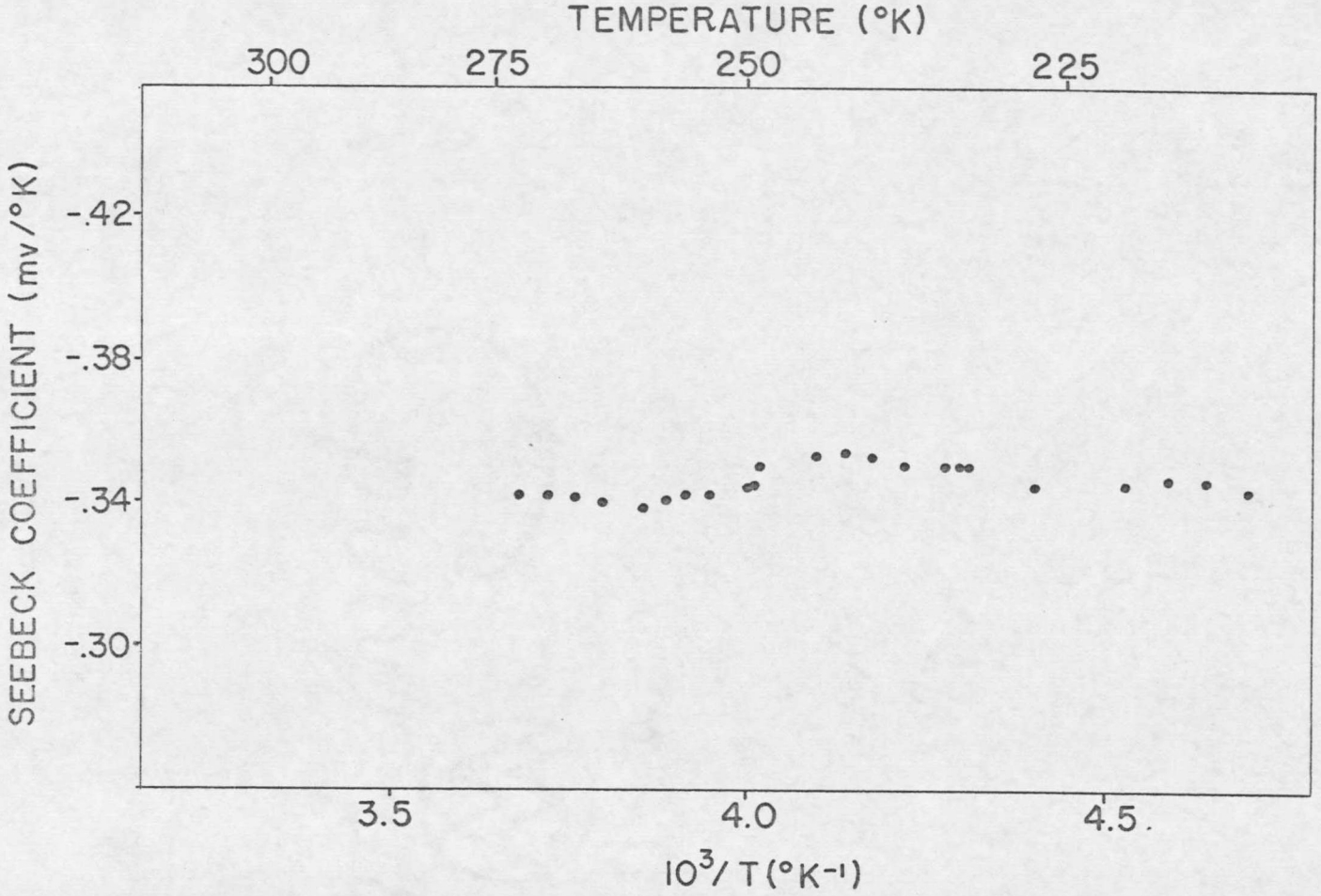


Figure 12. Seebeck Coefficient versus 1/T for Ti-Doped Sample in (111) Plane.

degrees, centered about T ≃ 253°K. However, the percentage magnitude change due to this fluctuation is about five percent, compared with ten percent for the [111] orientation. The magnitude of the Seebeck coefficient is roughly the same for the two orientations, although the plots for the two have slightly different slopes.

To check the repeatability of these results, fresh crystals were aligned and Mg- and Ti-doped samples similar to the previous ones were made. The results of Seebeck-coefficient measurement in these new crystals verified the previous results at the temperatures where fluctuations were seen (figures 13, 14, 15), but differences in magnitude of the Seebeck coefficient between old and new samples were seen. These differences are tabulated below.

Orientation	Dopant	Difference
[111]	Mg	25%
(111)	Mg	44%
(111)	Ti	25%

The previously small magnitude for the (111) orientation in the Mg-doped samples is now much larger, and the difference between magnitudes for the [111] and (111) orientations in the new Mg-doped samples is reduced to 20%.

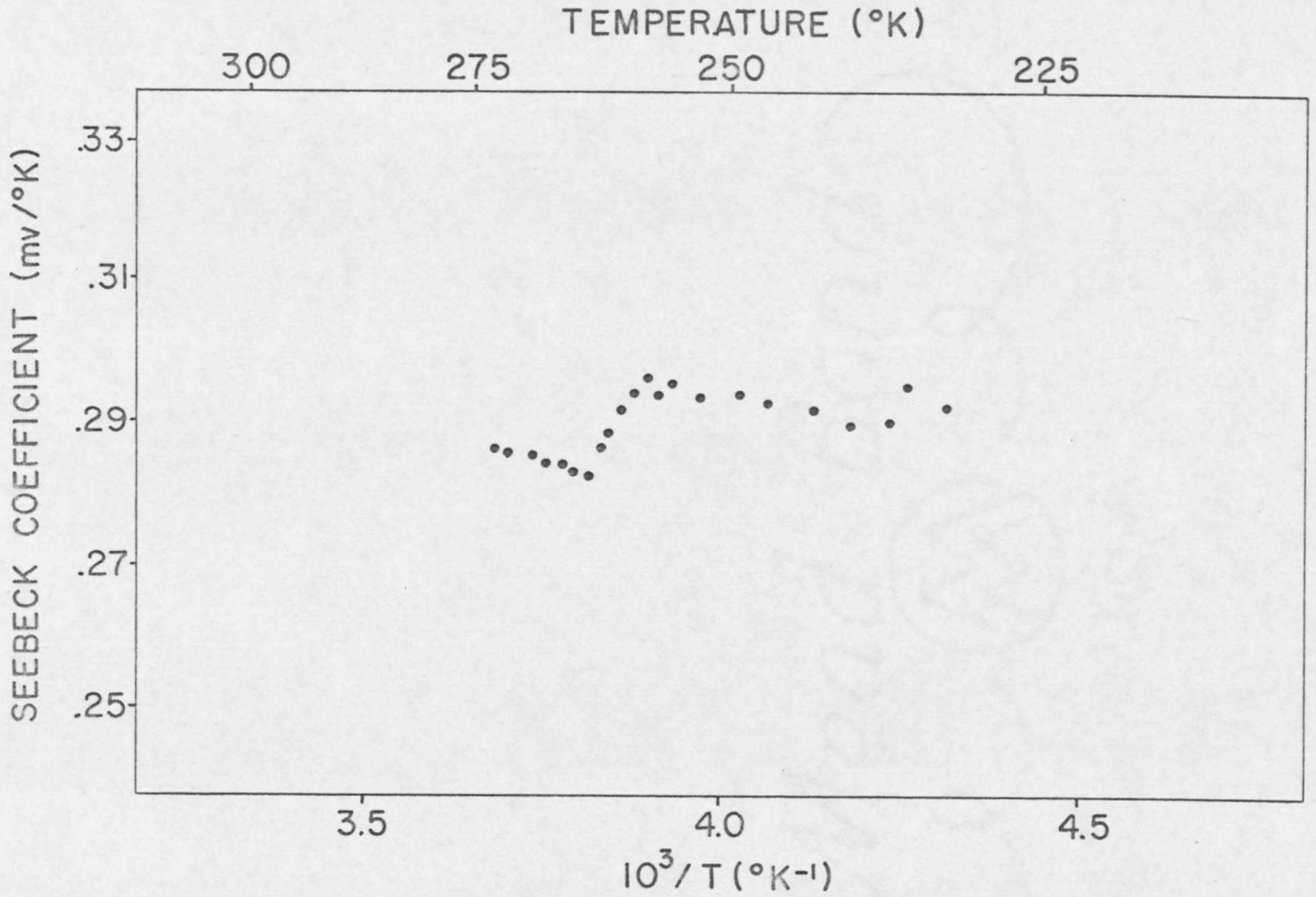


Figure 13. Seebeck Coefficient versus 1/T for Fresh Mg-Doped Sample Along [111] Direction.

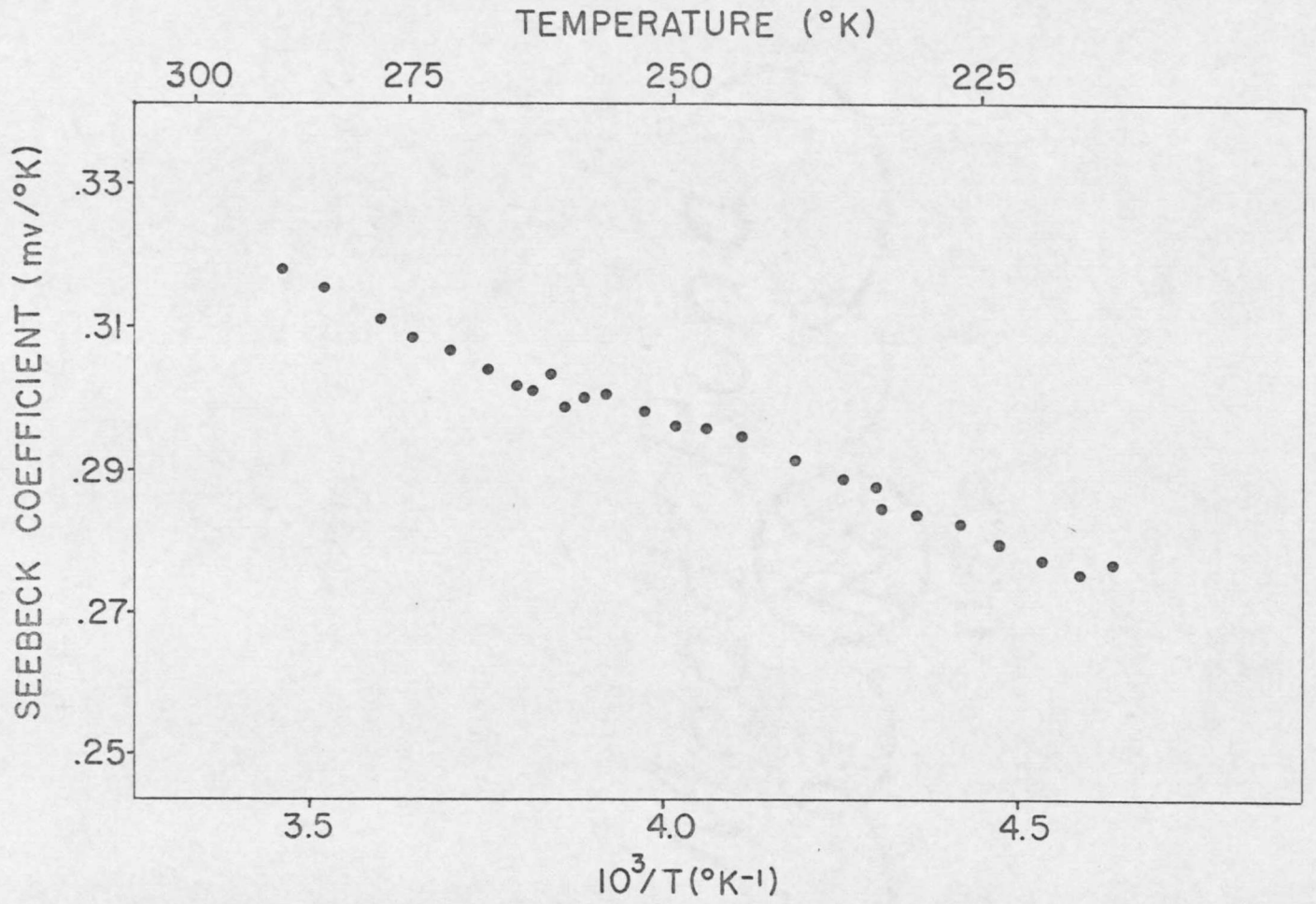


Figure 14. Seebeck Coefficient versus 1/T for Fresh Mg-Doped Sample in (111) Plane.

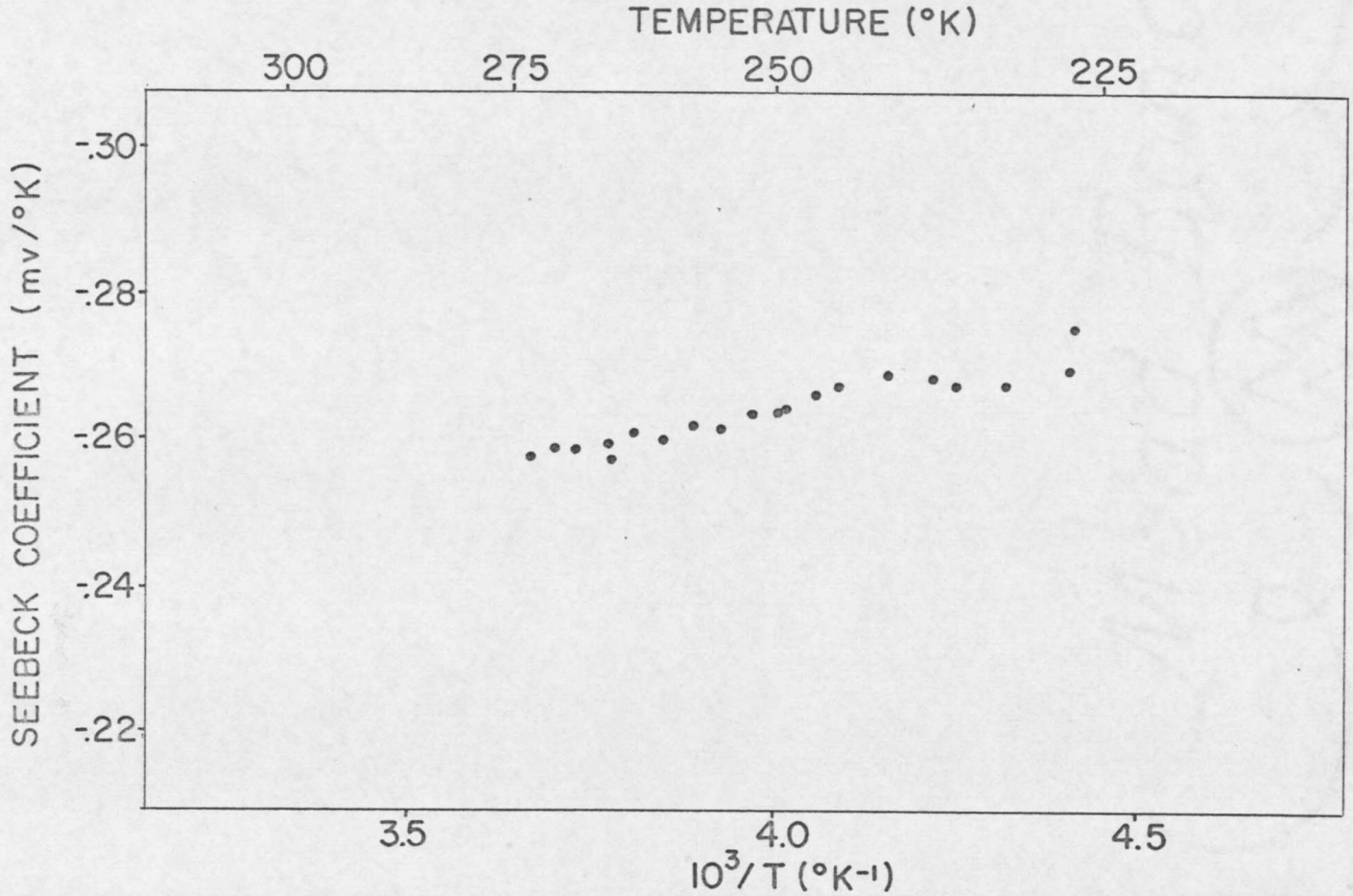


Figure 15. Seebeck Coefficient versus 1/T for Fresh Ti-Doped Sample in (111) Plane.

The lengths of the samples varied somewhat because of problems in cutting the samples from small crystals. The lengths are tabulated below:

Sample Data	Sample Length
Figure 9	0.126 inches
Figure 10	0.073
Figure 11	0.103
Figure 12	0.117
Figure 13	0.086
Figure 14	0.125
Figure 15	0.094

Although differences in magnitudes for two different samples with the same doping and orientation were seen, the repeatability of the results for any given sample was found to be within a few percent, except for occasional problems due to a poorly dried cooling chamber. This could be detected by an ice deposit around the chamber port.

It was also found that the silver contacts could be removed with nitric acid and deionized water and, provided new contacts were applied which exhibited decent electrical properties, the previous results on the Seebeck coefficient of the sample were repeatable, again within a few percent.

Note: Hereafter the abbreviated notation which will be used is $[111]$ for the sample oriented along the $[111]$ direction and (111) for the sample oriented in the (111) plane.

The temperature at which the sharp rise in the magnitude of the Seebeck coefficient was seen in the $[111]$ Mg-doped sample was suspected to be the Morin transition temperature. To check this, a DC magnetic field (~1500 gauss) was applied, with the expected result that the transition temperature was lowered, as reported by Ransom.[44] This is seen in figure 16. It was difficult to detect a shift in the Ti-doped samples because of the broad transition.

An interesting sidelight was observed upon applying the B field in the opposite direction; instead of a drop in magnitude at the transition temperature, a rise was observed (figure 16). This could be switched back and forth by reversing the direction of the magnetic field, without altering the magnitude of the Seebeck coefficient significantly. It was also discovered that after the magnetic field was removed, memory of its last direction was retained. Data are presented in figure 17 for the Seebeck coefficient after the magnetic field of figure 16 had been removed, while the data of figure 18 resulted from removal of the reverse field of figure 16. The run could be taken many times after the field had been removed, and the memory was retained.

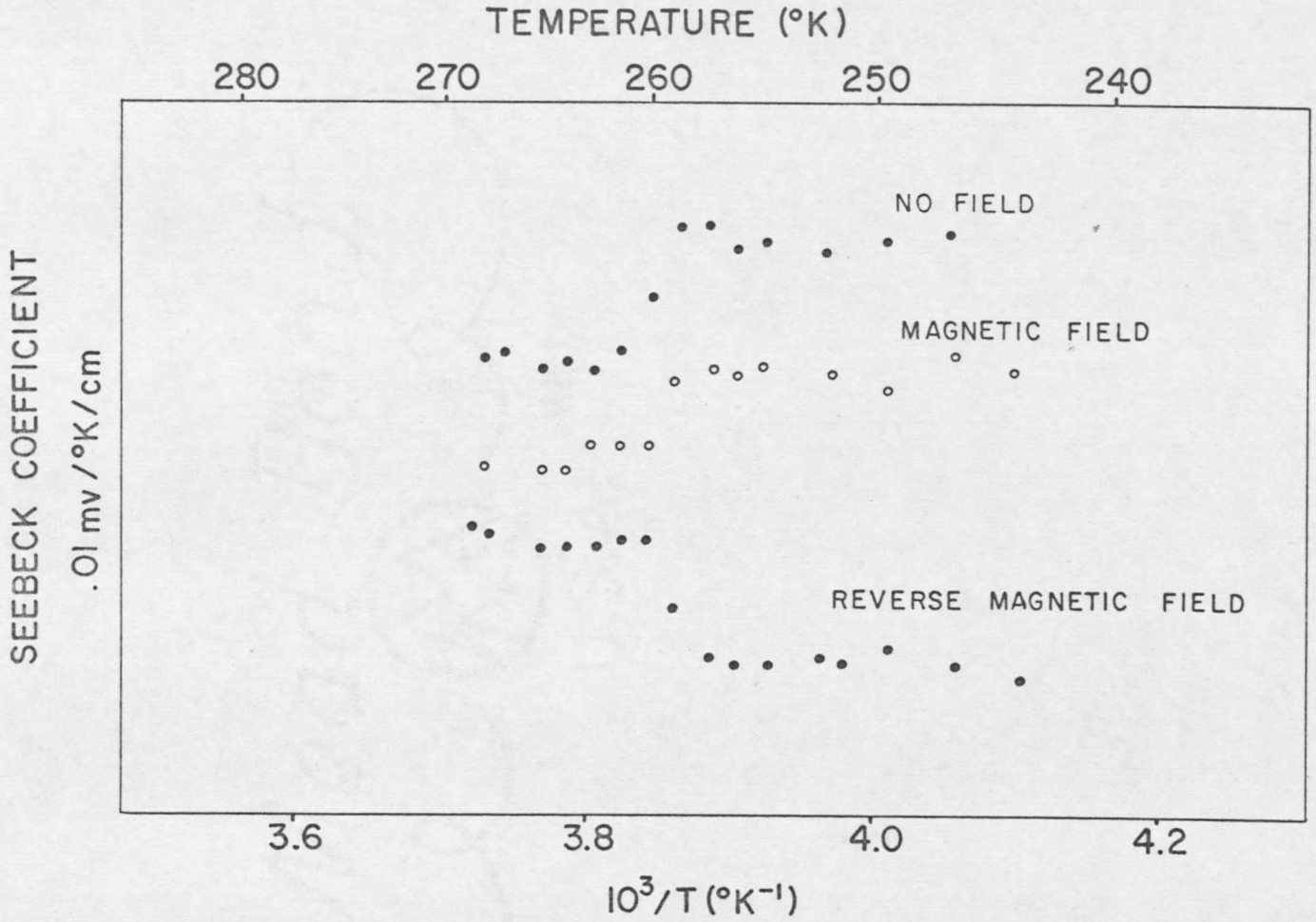


Figure 16. Mg-Doped Sample Along [111] Direction with Applied Magnetic Field.

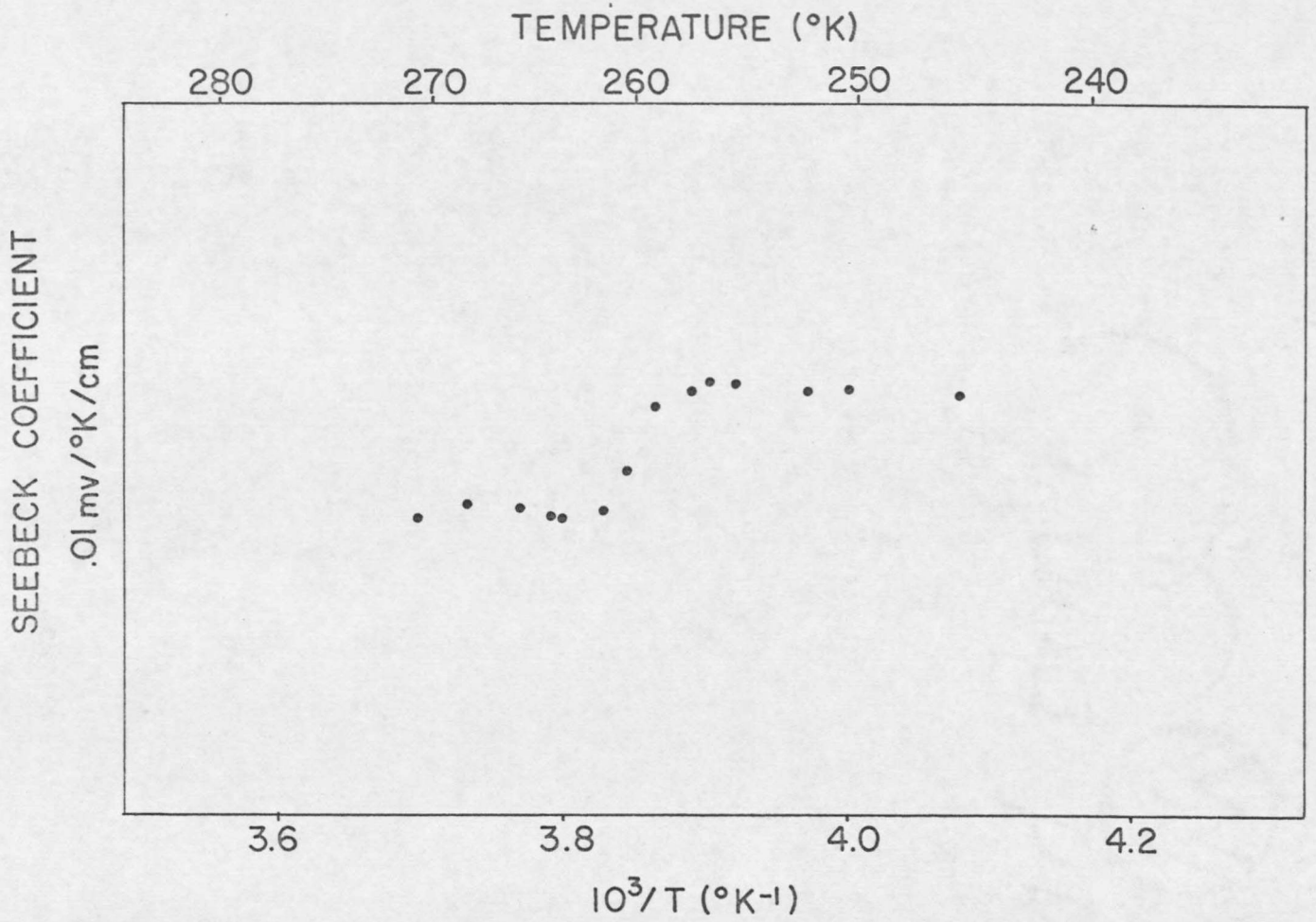


Figure 17. Mg-Doped Sample Along [111] Direction after Removal of Applied Magnetic Field.

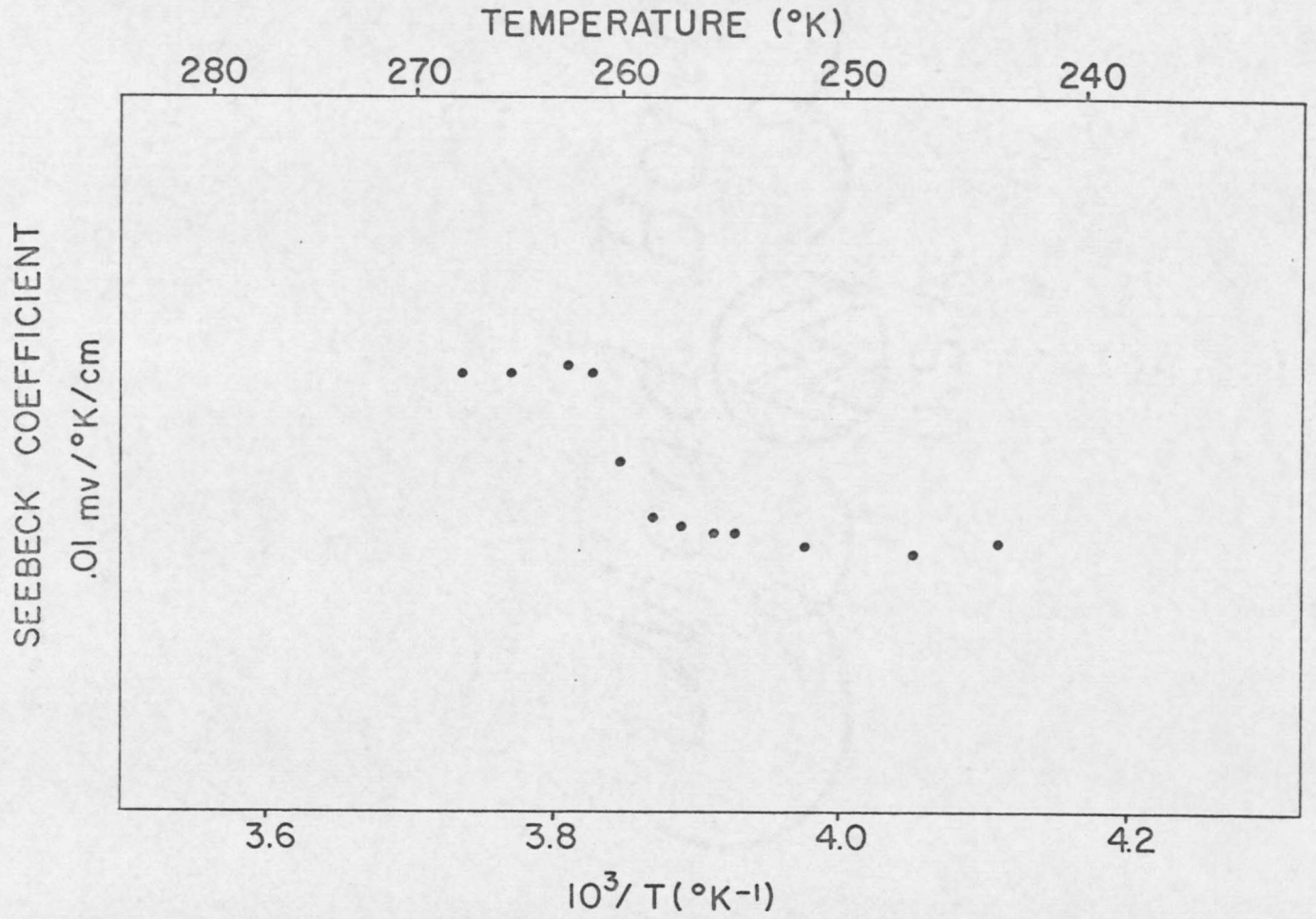


Figure 18. Mg-Doped Sample Along [111] Direction after Removal of Applied Reverse Magnetic Field.

Since a pronounced effect due to magnetic history was seen, choosing between the rise or drop in Seebeck coefficient at T_M proved to be difficult, especially since the first set of Mg-doped samples had been used in Hall-effect measurements and thus had been exposed to a magnetic field. It was felt that magnetic history could be removed by heating the sample above the Néel temperature, which is the magnetic ordering temperature for antiferromagnetic substances. The results reported in figure 13 are for the sample after it had been heated to T_N (this did lead to a reversal of the transition effect from a drop at T_M, which was observed just prior to heating the sample, to a rise at T_M, with no shift in magnitude).

No obervable memory effect was seen in the Ti-doped (111) sample (figure 19). Room temperature magnitudes of the Seebeck coefficient were taken after forward and reverse magnetic fields had been applied and removed, but the magnitudes were not altered.

The Ti-doped [111] sample was observed to have a memory effect associated with applied magnetic fields, although a complete reversal of the transition effect was not seen (figure 20). These same results show that the broad transition has washed out the shift in T_M due to the applied magnetic field.

The Seebeck coefficient near the Morin transition for the Mg-doped (111) sample was not affected by the applied magnetic fields.

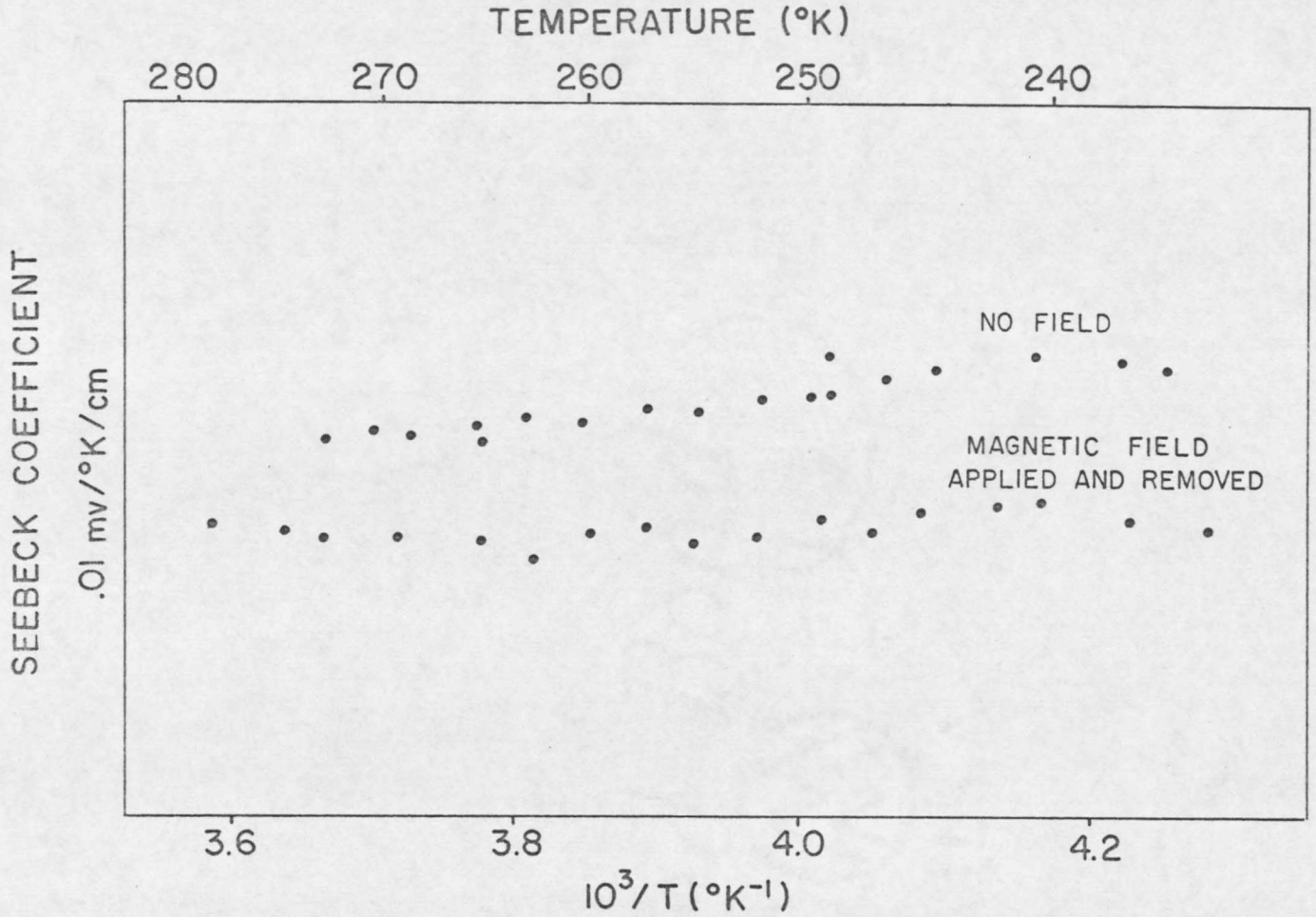


Figure 19. Ti-Doped Sample in (111) Plane Before and After Applying and Removing Magnetic Field.

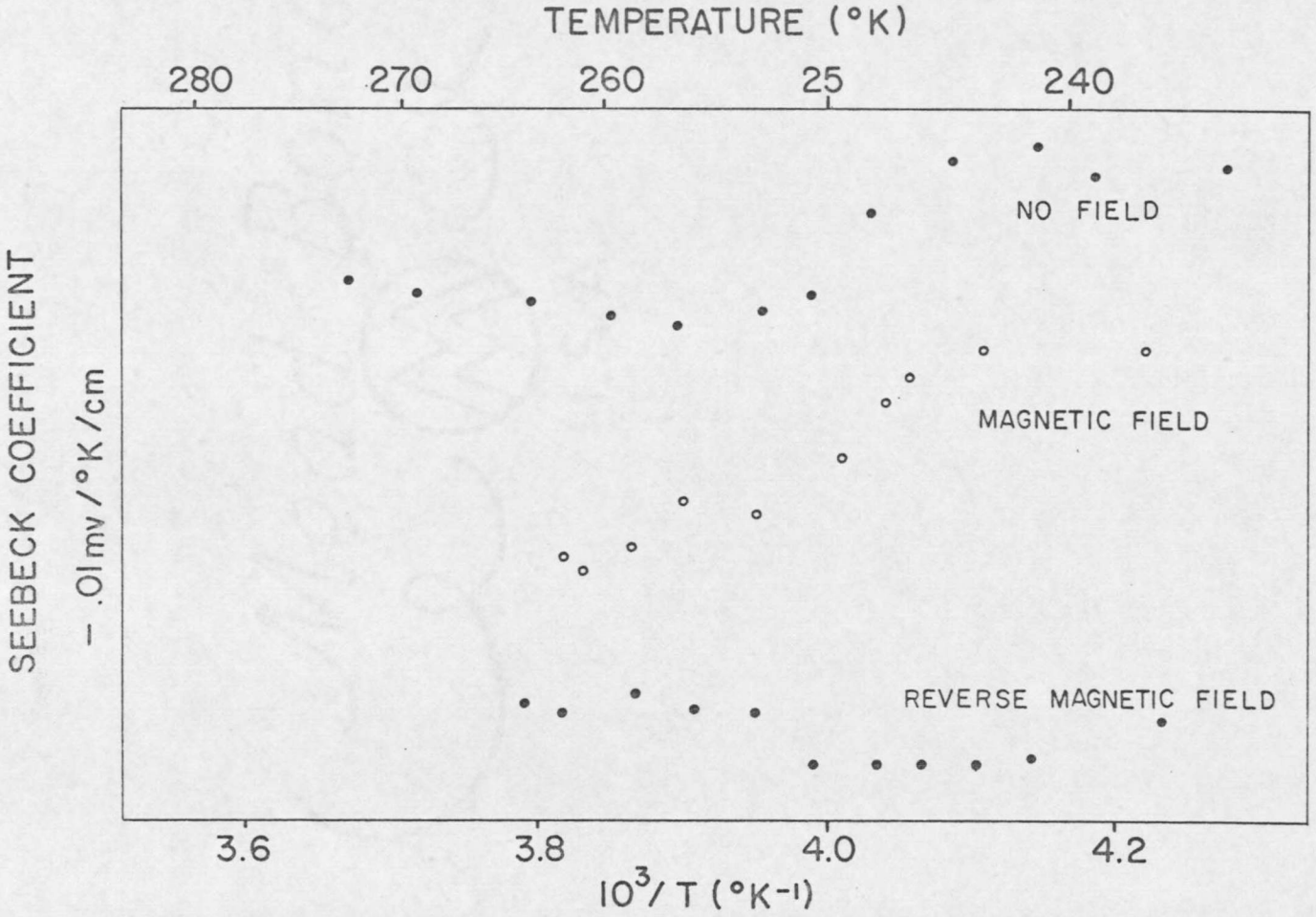


Figure 20. Ti-Doped Sample Along [111] Direction with Applied Magnetic Field.

Again, no transition effect was observed for these samples (figure 21).

Finally, samples for each dopant (Mg and Ti) and orientation were heated to 750°C for ten minutes and then the data were repeated. The results are presented in figures 22-25.

B. Discussion of Results

The previous section was devoted to a presentation of the experimental results with brief comments about important features of the data. In the present section, a critical discussion of these results is presented, and explanations consistent with the results are presented within the framework of the existing theoretical models. Qualitative arguments are presented, and these are followed by treatments of the quantitative aspects of the data. Finally, a possible explanation for the memory phenomenon is discussed.

The data on the Mg-doped samples (figures 9 and 10) agree qualitatively with those reported by Ransom[44] on the Hall effect near the Morin transition (T_M); i.e., a change was seen at T_M for transport along the [111] direction, but no change was seen for transport in the (111) plane. The temperature at which this change took place was lowered slightly when an external magnetic field was applied, which again agrees with Ransom's findings. This happens be-

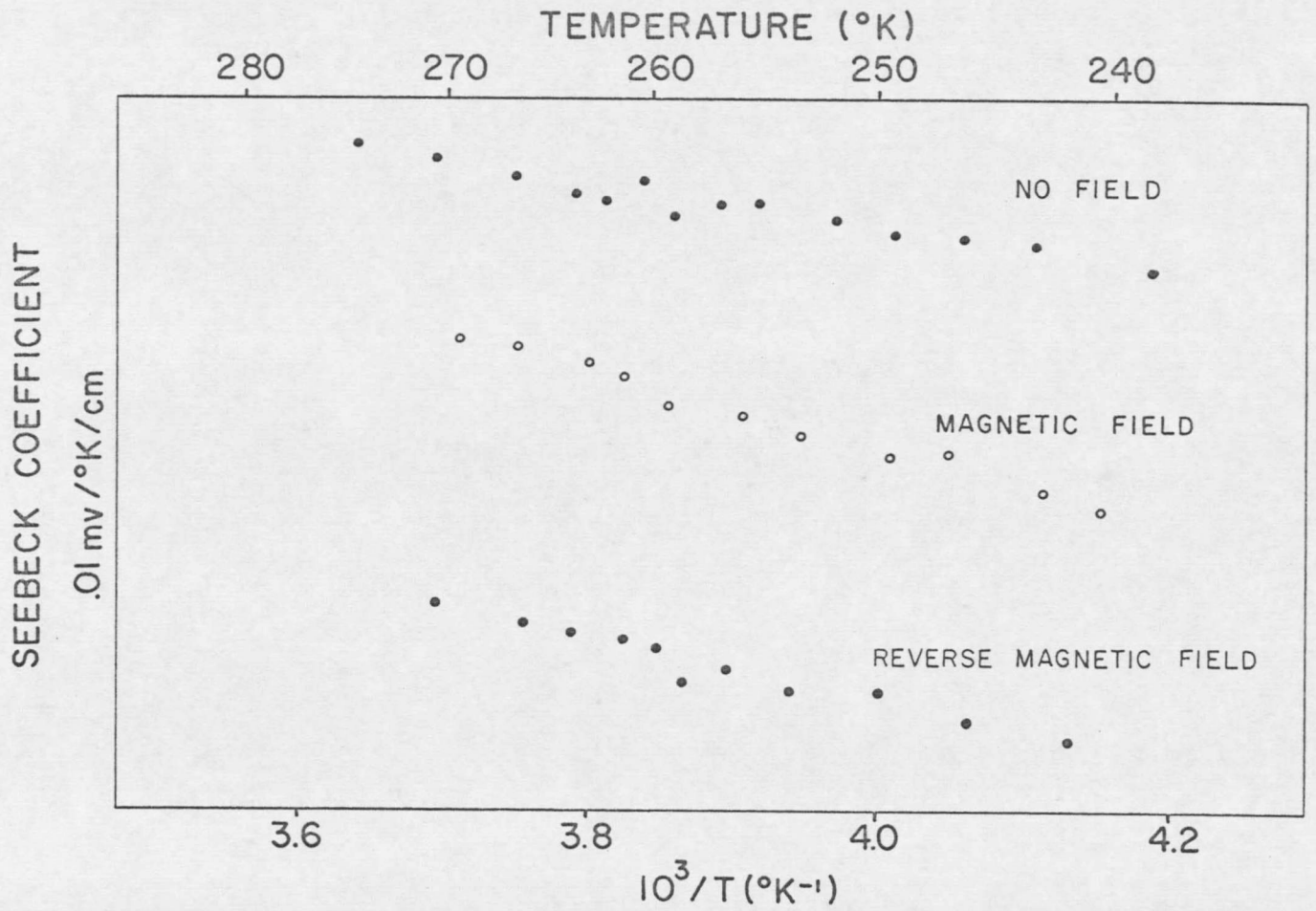


Figure 21. Mg-Doped Sample in (111) Plane with Applied Magnetic Field.

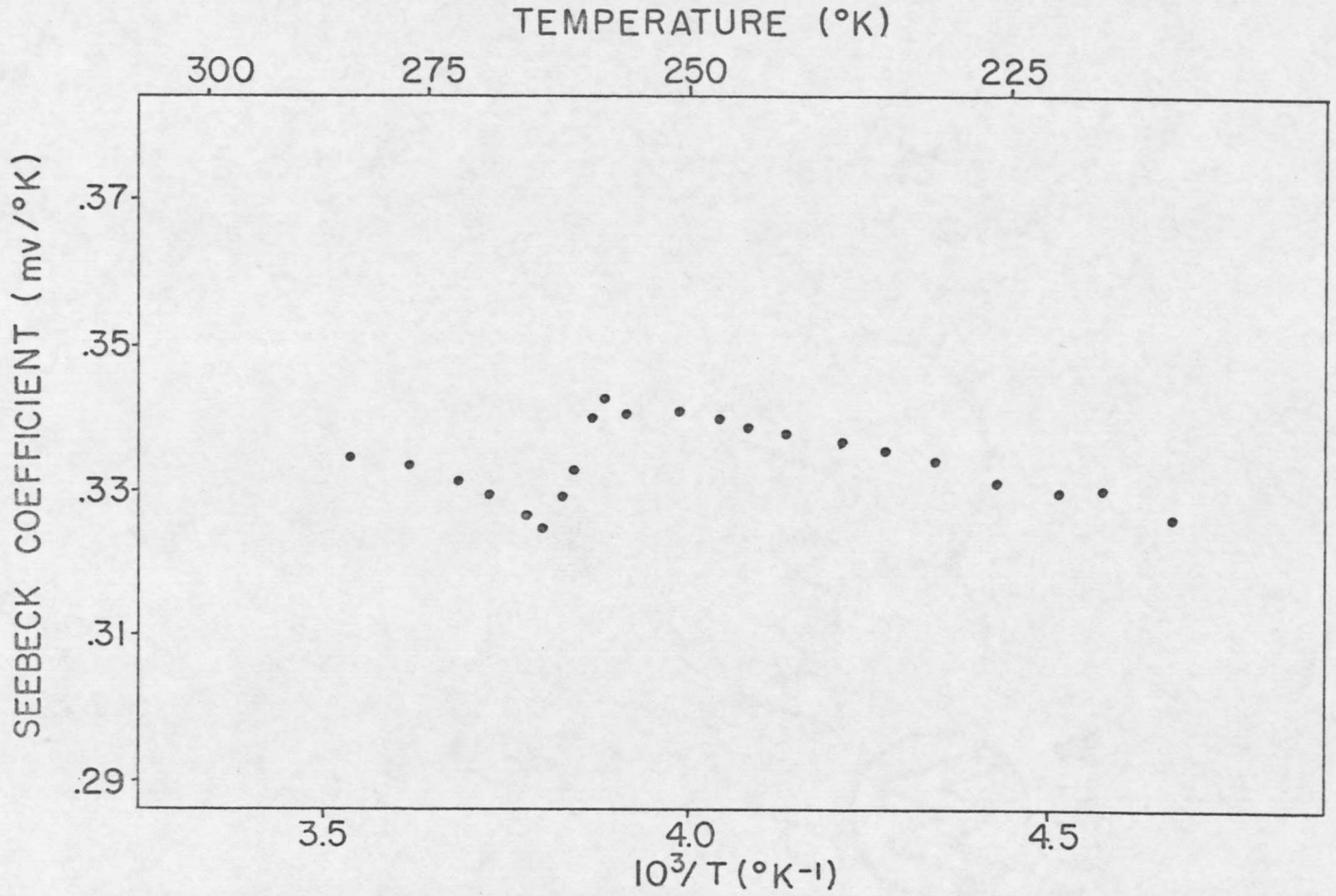


Figure 22. Mg-Doped Sample Along [111] Direction after Heating to T_N.

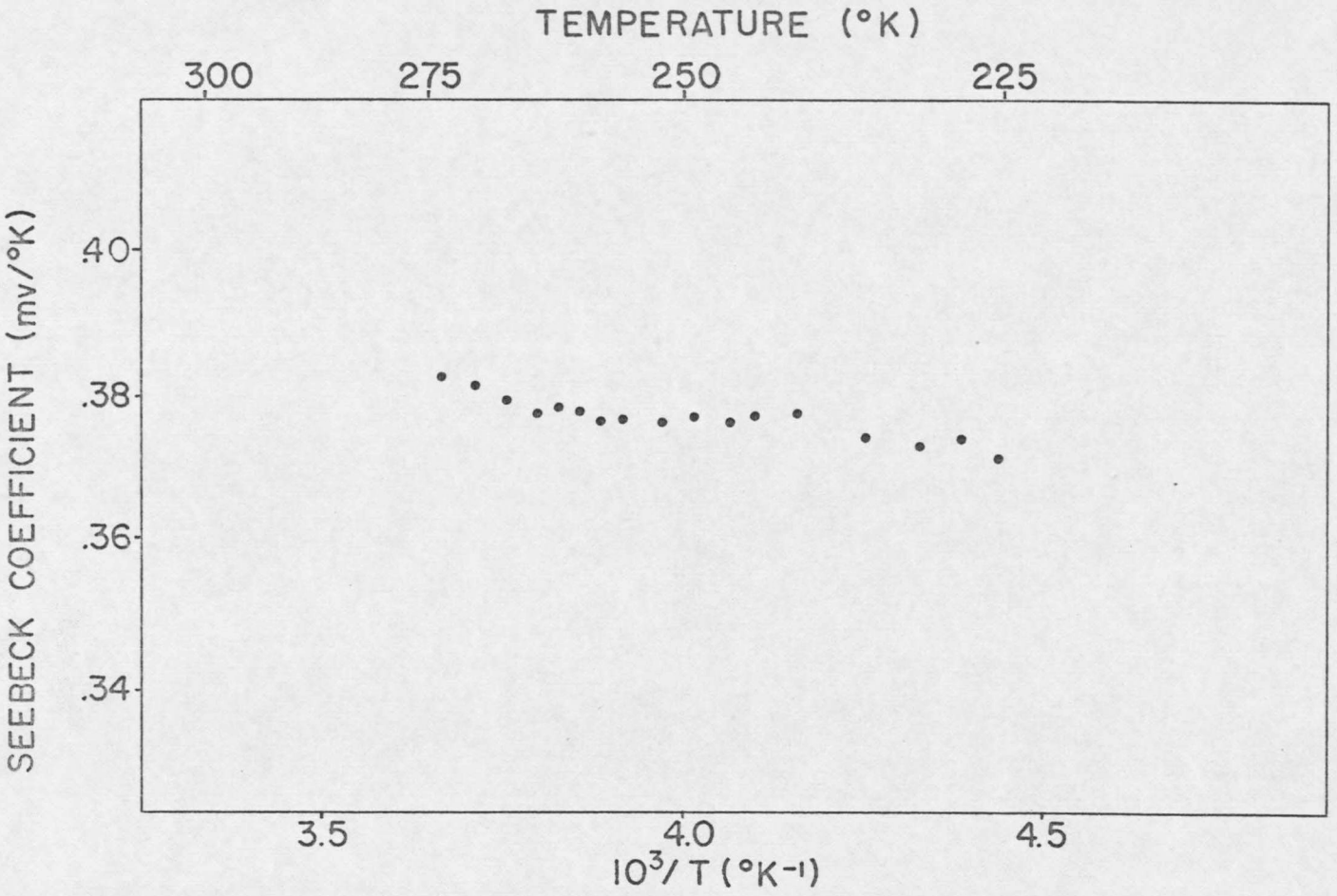


Figure 23. Mg-Doped Sample in (111) Plane after Heating to T_N.

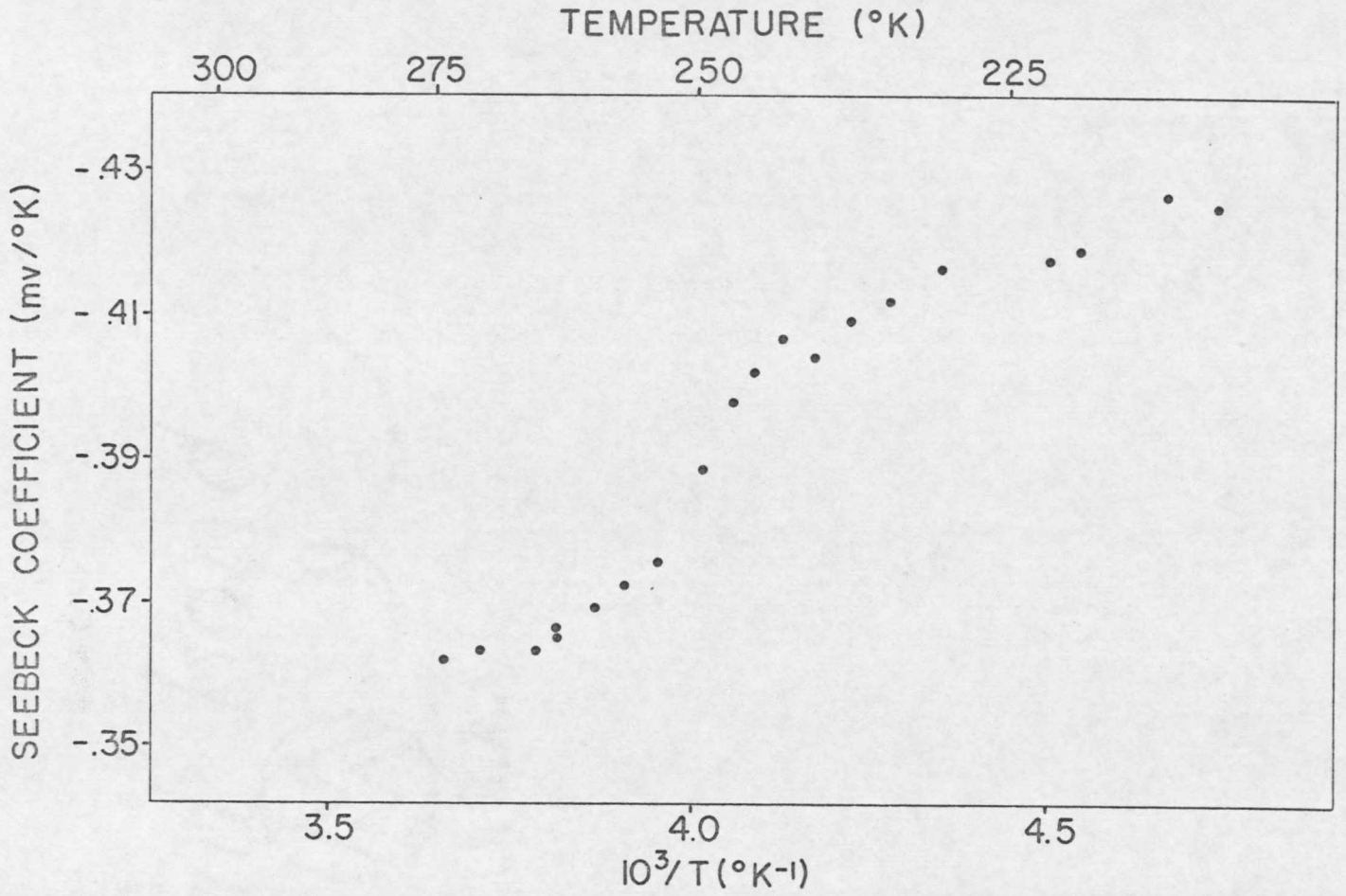


Figure 24. Ti-Doped Sample Along [111] Direction after Heating to T_N.

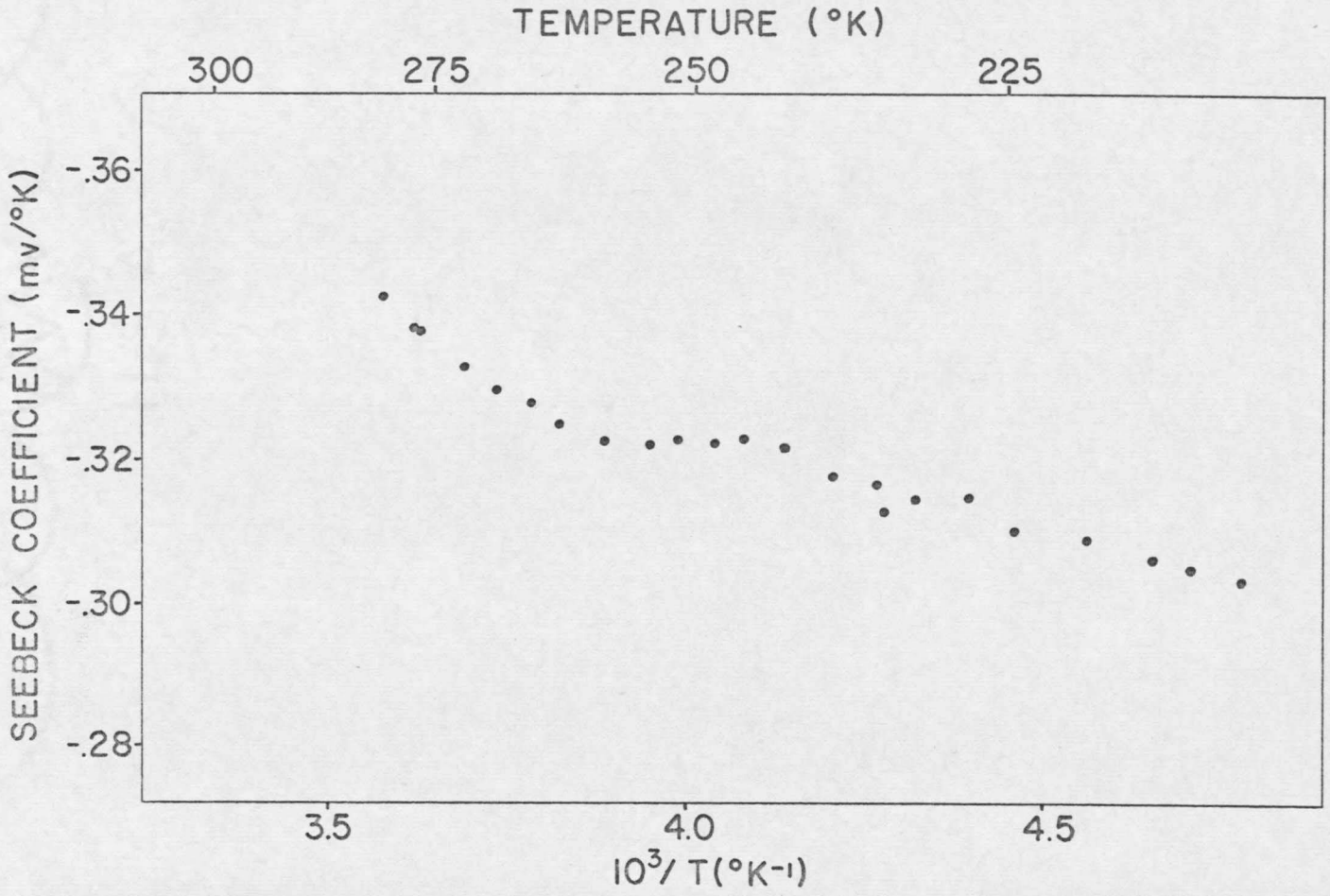


Figure 25. Ti-Doped Sample in (111) Plane after Heating to T_N.

cause a magnetic field applied parallel to the (111) plane introduces an energy term which favors magnetization in the (111) plane along the field direction. The spin reorientation (Morin transition) takes place when the total energy of the system favors magnetization in the (111) plane. Thus, the applied field lowers the temperature at which the transition takes place.

The observed orientation dependence is predicted by double exchange. In section B.3 of Chapter II, an analysis of large polarons indicated that because the large polaron does extend over many lattice spacings, there would not be a strong spin-ordering term associated with the polaron state. Thus, large polarons would not lead to the observed data at T_M. Small polarons are localized at one atomic site, and a spin correlation is a larger effect in this case. The spin interaction is largest for the extreme case of small-polaron hopping because of the complete localization of the carrier between hops. In fact, the orientation dependence in hematite predicted by double exchange is based on the hopping model in which the carrier must satisfy Hund's rules at each site because of the localization. The observed orientation dependence of the Seebeck coefficient at T_M combined with the arguments presented by Bosman and Van Daal[37] on the temperature at which small-polaron hopping becomes important (B.6 of Chapter II) favor the thermally activated small-polaron model for the Mg-doped samples.

In the Ti-doped samples (figures 11 and 12), a transition effect is seen at T_M for transport along the [111] direction, but a smaller effect is also observed for transport in the (111) plane. This effect in the (111) plane was repeated in a fresh sample with the same doping and orientation, although the change in the Seebeck coefficient at T_M was not as abrupt in the fresh sample and the percentage change was reduced (figure 15). The term "fresh" means that the samples were cut from a crystal which had no magnetic history. This result for transport in the (111) plane cannot be explained by the usual double exchange argument. However, since the reorientation of spins at T_M is still felt by the carriers, spin interactions between the carriers and the ions must still be important, which again rules out large polarons in favor of small polarons, and, using the arguments presented for the Mg-doped samples, small-polaron hopping is more appropriate than small-polaron band motion.

Two things should be noticed about the anomalous effect for transport in the (111) plane. First, the percentage change in the magnitude at T_M is small (5 percent in one sample (figure 12) and 2 percent in the other (figure 15)). Second, there is a rise in the Seebeck coefficient versus decreasing temperature at about 250°K, which is the same region where the transition effect is seen for the sample oriented along the [111] direction, but there is also a drop

at temperatures in the neighborhood of 235°K. The Seebeck coefficient roughly fits a straight line with a small hump superimposed on the line for 235°K < T < 250°K. It would be helpful to have results at temperatures well below 235°K to study this apparent magnitude shift in more detail. Unfortunately, the low temperature limit with the present equipment is about 215°K, because of the limits of the refrigeration chamber used to cool the blocks.

According to Flanders and Remeika,[16] for 0.05 percent Ti doping, T_M is about 253°K and the transition occurs over a range of about fifteen degrees. Thus, it appears that the magnitude shifts seen in the Ti-doped samples from 245°K to 260°K are due to the Morin transition. The apparent shift at 235°K is outside this range, and its origin is uncertain. However, a larger titanium concentration than the expected amount would result in a transition effect at temperatures below 250°K.

In one of the few reports of optical data on hematite crystals, Morin observed an absorption peak at 0.7eV which became stronger with increased titanium content in polycrystalline samples. This was interpreted to be the ionization energy of the titanium impurity in the Fe_2O_3 structure, and such a large ionization energy would result in nonionized impurities at temperatures below room temperature. From conductivity measurements, Bosman and Van Daal[37]

estimated the ionization energy for the titanium impurities to be 0.18eV. The results reported by Bosman and Van Daal on the Seebeck coefficient in samples doped with Nb, Zr, or Ti were interpreted as evidence of impurity conduction, with a very pronounced reduction in the expected magnitude below 200°K and extending to 300°K with decreasing effect. With their impurity concentrations of 0.1 atomic percent, this impurity conduction was conjectured to take place via thermally activated hopping from one impurity site to another, provided partial compensation was present. A point they failed to treat in their analysis of the Seebeck coefficient was the effect of grain boundaries in the polycrystalline samples. In conductivity results reported in the same paper, AC methods were necessary to eliminate grain-boundary effects below 170°K. The Seebeck coefficient cannot be taken by the same AC methods so the grain-boundary effects will appear in the Seebeck data, especially below 170°K. The high-impedance grain boundaries would cause a reduction similar to that reported on the Seebeck coefficient at low temperatures by Bosman and Van Daal.

In section C of Chapter II, it was argued that the impurities would likely assume a net spin and become aligned with the appropriate sublattice magnetization, with the result that the inter-impurity hopping would have a spin-dependent term associated with

the transfer probability, similar to the double exchange referred to above. This factor has the form $\cos \theta/2$,[67] where θ is the relative orientation of the spins at the two impurity sites.

Magnetically ordered impurity hopping becomes quite complicated because one has to consider which of the possible lattice sites become impurity sites. For the Ti-doped samples which have been considered in the present work, there is, on the average, one titanium ion for every two thousand iron ions. Since hopping conduction necessarily takes account of the atomicity of the lattice, the placement of these titanium ions in the spin-ordered iron lattice sites becomes a critical parameter. To see this, consider the spin structures shown in figures 26 and 27. The arrows indicate the spin directions at each cation lattice site within each (111) plane. The fact that double exchange predicts no change in transport properties at T_M for transport in the (111) plane is based on the large number of spin states in that plane that are both near to and parallel to the spin state where the carrier is found. Transfers to adjacent planes, although having nonzero probability above T_M ($\cos \theta/2 \neq 0$), contribute a small percentage of the total transport ($\cos \theta/2 = \sin \alpha << 1$, where α is the canting angle).

In the discussion that follows, it will be helpful to have some knowledge of the form of the transfer probability between two

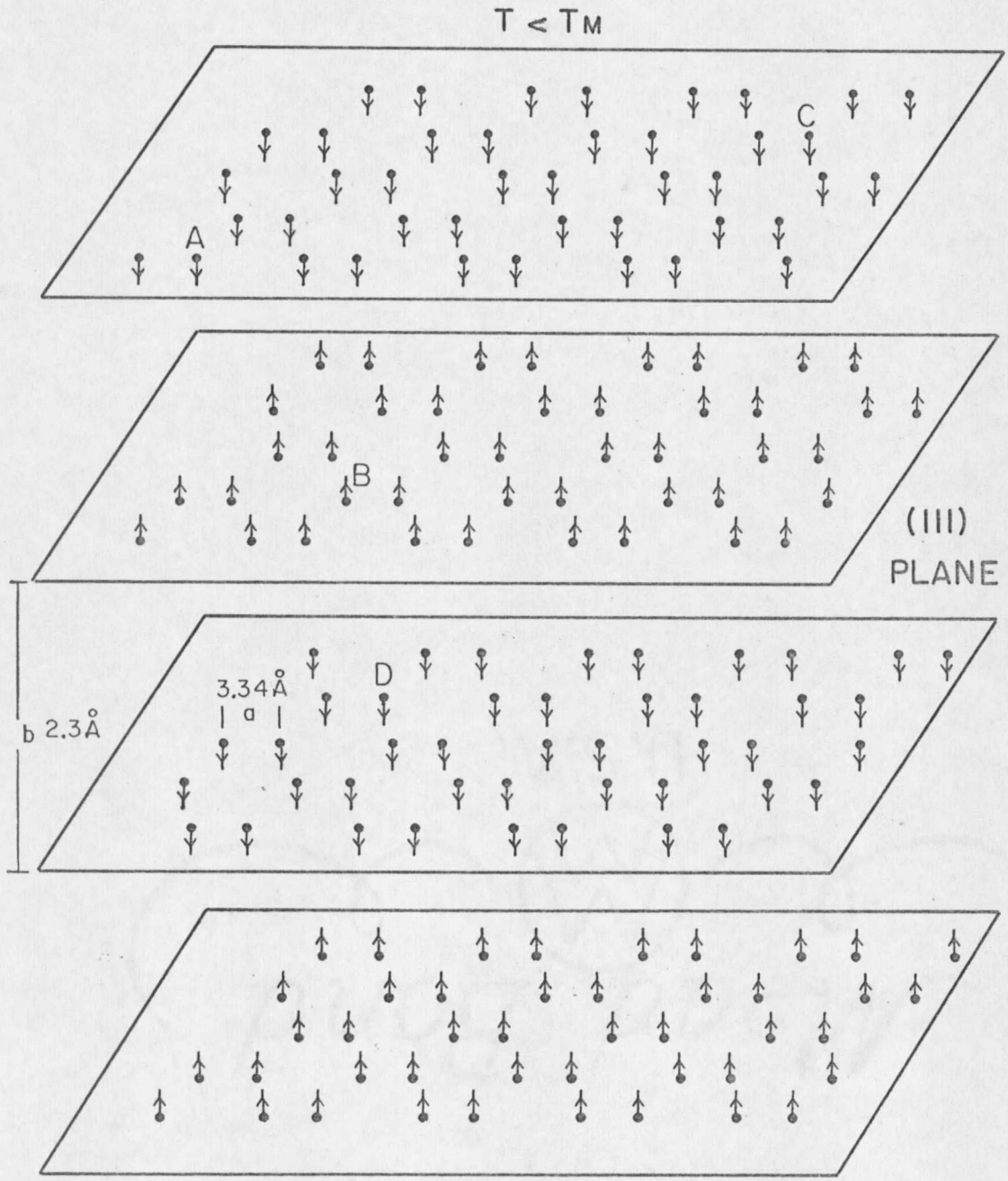


Figure 26. Iron Placement and Spin Structure for $T < T_M$.

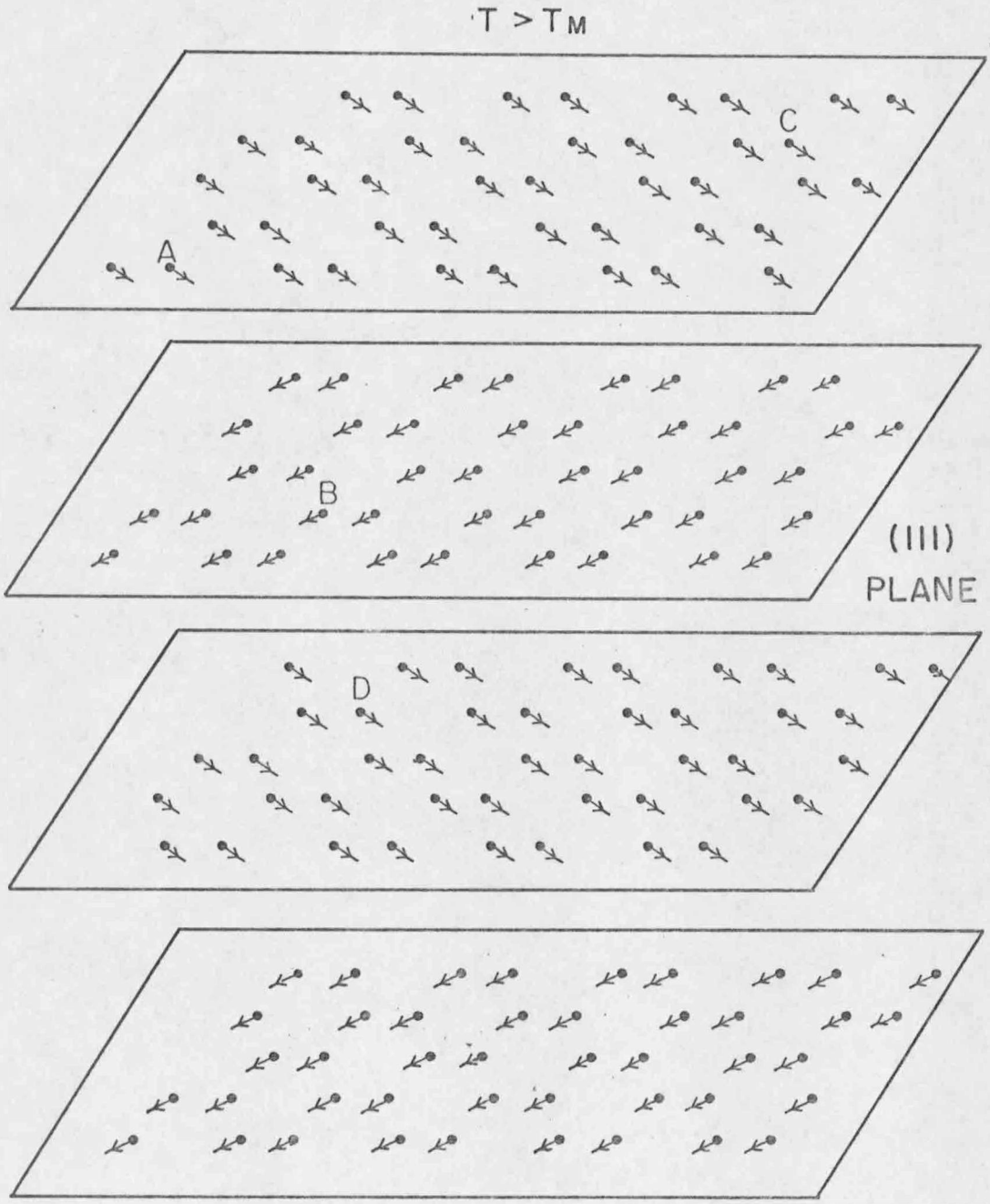


Figure 27. Iron Placement and Spin Structure for $T > T_M$.

sites, i and j. In general terms, the transfer probability Ω_{ij} is

$$\Omega_{ij} \alpha \langle j | V | i \rangle \cos \theta_{ij}/2 ,$$

where $\langle j | V | i \rangle$ is the matrix element related to the exchange interaction between states i and j ignoring spin. For simplicity, this will be abbreviated b_{ij}. This contains the wave functions associated with the initial and final states, and these functions can become quite complicated in a solid. For simplicity of argument, consider the hydrogenic wave functions. The radial part is of interest here, and the general form is

$$\phi(r) \alpha f(r) \exp (-\beta r/r_o) ,$$

where $f(r)$ is a polynomial expression and r_o is a characteristic length, on the order of a lattice spacing. At distances large compared to r_o, the exponential term dominates. The perturbing potential, V, is generally taken as the Coulomb potential, which has a radial dependence $1/r$. This does not alter the exponential dependence at large distances compared to r_o, so the form of b_{ij} will be a complicated product of polynomials and exponentials in r, which reduces to a decreasing exponential at large distances:

$$\Omega_{ij} \alpha \exp (-\beta' r/r_o) \cos \theta_{ij}/2 .$$

If a dilute impurity concentration is substituted at random lattice sites, impurity ions could be found at sites A, B, and C in figure 26. Below T_M, the transfer A $\rightarrow$ B has zero probability because of the antiparallel spins ($\cos \pi/2 = 0$) and the carrier at site A has to look to site C to find an available site for hopping. Above T_M, there is a small but nonzero probability ($\Omega \alpha \exp(-\beta' r_{AB}/r_o) \sin \alpha$) that the transfer A $\rightarrow$ B would take place. The transfer A $\rightarrow$ C is still more favorable from spin arguments ($\Omega \alpha \exp(-\beta' r_{AC}/r_o) \cdot 1$), but the much shorter distance to site B versus that to site C increases the relative probability that the transfer A $\rightarrow$ B will occur rather than the transfer A $\rightarrow$ C ($r_{AB} << r_{AC}$). Thus, inter-impurity hopping could lead to a change in the transport properties at T_M for transport in the (111) plane, still based on double exchange. This effect would likely be small since it relies on non-uniform placement of the impurities throughout the lattice, and the degree of non-uniformity could cause a difference from sample to sample.

One could argue that a random placement of the impurity ions in the lattice would still lead to the same results that double exchange predicts for normal hopping conduction among iron ions in hematite. However, this would require a uniform placement of impurities and it is doubtful that in a random placement, situations

such as the unusually long or short distances hypothesized above can be avoided.

Since reported values for the ionization energy of the titanium impurity indicate that impurity conduction is important at the temperatures of interest here ($T < 300°K$),[37] the foregoing arguments on inter-impurity hopping afford an explanation for the anomalous results for transport in the (111) plane for the Ti-doped samples.

No experimental results are known to exist for the ionization energy of the magnesium impurity in hematite, so it is not known if Mg-doped samples exhibit impurity conduction at higher or lower temperatures than Ti-doped samples. However, the same arguments about impurity conduction which explained the transition effect in the (111) plane for Ti-doped samples limits impurity conduction to a negligible effect for the Mg-doped samples, since no appreciable transition effect was seen for the latter samples in the (111) plane.

Upon checking the repeatability of the first sets of data (figures 9-12) by considering freshly cut samples (no magnetic history) with the same doping and orientation (figures 13-15), good qualitative agreement was seen between similar samples, but the magnitude of the Seebeck coefficient was seen to vary from one

sample to another. A partial explanation of this is obtained from possible variations in impurity concentration. To see how this arises, recall that the Seebeck coefficient has a logarithmic dependence on carrier concentration:

$$S \alpha \ln(1/n) .$$

If the impurity concentration (donors or acceptors) changes by a factor of ten, say from $10^{19}/cm^3$ to $10^{18}/cm^3$, then the carrier concentration also changes by roughly a factor of ten. However, for the Seebeck coefficient, this results in comparing numbers like ln 10 and 19 ln 10 for the percentage change. This results in a percentage change of about five percent. If the impurities are only partially ionized, the numbers would be ln 10 and p ln 10, where p is less than 19. This would give a percentage higher than five.

Morrish and Eaton[15] reported findings on Rh-doped crystals grown by the same technique as the crystals used in this dissertation, in which electron-microprobe analysis revealed a variation of dopant concentration of as much as a factor of five, which makes it conceivable that two samples cut from crystals grown from one melt could have nearly an order of magnitude difference in impurity concentration.

The percentage differences in magnitudes of the Seebeck coefficient for two similar samples were observed to be much greater (25-50%) than those allowed due to variations in the impurity concentrations. This is especially exemplified by the Mg-doped (111) samples, in which a magnitude difference between the two samples of about fifty percent was observed. Another significant difference between these two samples is that the sample with the smaller magnitude was a short portion of an originally full-sized sample which had been broken. The remaining piece was slightly more than half the original length. The difference in sample lengths was originally ignored, since the Seebeck coefficient depends only on the temperature difference across a sample and not on its length. However, in all three cases where early results were checked for repeatability on similar, freshly cut crystals, a magnitude decrease in the Seebeck coefficient between two samples was associated with a decrease in sample length (see figures 9-15 and the tabulated lengths following figure 15). This consistency led to a more thorough investigation of a low-temperature correction to the Seebeck effect due to phonon drag which introduces a dependence on the sample size. To understand the origin of this correction, a consideration of phonon interactions follows.

In collisions between electrons and phonons, the electron either gains or loses energy, and phonons are either destroyed or created. The electron has initial and final wave vectors k and k', respectively, while the phonon has wave vector q. Conservation of energy must always hold, so

$$h\nu - h\nu' = \pm h\nu_q ,$$

where the ν's are the corresponding frequencies. However, conservation of momentum does not have to hold. There are two possibilities, depending on whether conservation of momentum does or does not hold. In normal (N) processes, momentum is conserved, and

$$\hbar k - \hbar k' = \pm \hbar q .$$

In Umklapp (U) processes, momentum is not conserved, and

$$\hbar k - \hbar k' = \pm \hbar q + \hbar g ,$$

where g is a reciprocal lattice vector, which translates a point in one Brillouin zone to an equivalent point in an adjacent Brillouin zone. The momentum associated with the term h g is transferred to the center of mass of the lattice. Since the Umklapp processes include the translation to adjacent Brillouin zones, they only appear at energies greater than or comparable to the Debye energy. The

distribution function contains an energy relative to the Debye energy, so that these processes fall off rapidly below Θ_D.

Since the U processes do not conserve momentum, these processes dissipate phonon momentum, while the N processes conserve it. If a temperature gradient is present across a sample, the phonon system will be disturbed and a phonon gradient results. The flow of phonons down this gradient will attempt to set up an equilibrium state. If Umklapp processes are present, this phonon momentum from hot end to cold end can be dissipated, but as the temperature is lowered, U processes are frozen out and the N processes do not reduce the phonon momentum toward the cold end. In collisions with the carriers, the phonons impart a net momentum to the carriers in the direction of decreasing temperature. Thus, the phonon drift from the hot end to the cold end drags the carriers along. An additional electric field must be set up to balance the flow of these carriers, since the carriers now see a force due to the temperature gradient and the phonon drift.(76)

The effect of phonon drag in the Seebeck data is to cause an increase in the Seebeck voltage as temperature is decreased. This increase does not go on indefinitely, however, since at sufficiently low temperatures the mean free path of the long-wavelength phonons becomes comparable to the sample dimensions. This results in bound-

ary scattering which reduces the phonon drag.[76] The boundary scattering can thus introduce a size dependence into the Seebeck coefficient. Impurity concentration also influences phonon drag, because the impurity sites act as additional scattering centers which dissipate phonon momentum.

To get a feeling for what temperatures are actually involved, an analogy is made between hematite and germanium, for which phonon drag has been reported to temperatures above 200°K.[77] Germanium has a Debye temperature of 360°K, compared with 570°K for hematite. Since the populations of various phonon modes are related to their energies relative to the Debye energy, the populations of the higher energy modes capable of U processes will be less in hematite than in germanium at a given temperature. Thus, at 200°K, there are less U processes in hematite than in germanium, or, equivalently, the phonon drag is more significant at 200°K in hematite than in germanium. This means that phonon drag is likely at temperatures above 200°K in hematite.

Another point which supports a phonon-drag contribution at higher temperatures in hematite than in germanium is that only phonons with wavelength of the carrier contribute strongly to the scattering which causes phonon drag, and since this carrier wavelength depends inversely on the mass, higher energy (shorter wavelength)

phonons contribute in a low mobility semiconductor with its large effective mass.

Two portions of the data from the present work support the phonon-drag model. The strongest evidence is the dependence of the Seebeck coefficient on sample length. The only known explanation for this is the boundary scattering which reduces the phonon-drag contribution to the Seebeck coefficient as the length of the sample is reduced. Additional supporting data is found in the slopes of the Seebeck data presented in this dissertation (figures 9-12). Impurity conduction as presented by Bosman and Van Daal[37] results in a decreasing magnitude in the Seebeck coefficient with decreasing temperature in the impurity-conduction regime. For the results on Mg- and Ti-doped samples of hematite, the Ti-doped samples showed an increasing magnitude with decreasing temperature (figures 11 and 12), while the Mg-doped samples showed a decreasing magnitude with decreasing temperature (figures 9 and 10). This would indicate that impurity conduction is stronger in the Mg-doped samples, but the arguments on double exchange presented earlier in this discussion indicate that the opposite is true; i.e., impurity conduction is strongest for the Ti-doped samples. These slopes can be explained in another way by noting that impurity scattering reduces the phonon-drag contribution. In fact, the results reported by

Geballe[77] on germanium indicated that the type of curve observed for phonon drag in an impure sample is the same as the curve reported by Bosman and Van Daal[37] for impurity conduction; i.e., the magnitude of the Seebeck coefficient increases with decreasing temperature to a point, and then a reversal takes place and the magnitude begins to decrease with decreasing temperature. The temperature at which the slope reversal takes place increases with increasing impurity content. No reported results on similar effects have been found on hematite, but Herring[81] has reported a phonon-drag effect on ZnO data for temperatures below 350°K.

For the present data, the Mg-doped samples have 0.5 percent doping, while the Ti-doped samples have a 0.05 percent doping. Thus, the impurity scattering is more pronounced in the Mg-doped samples, and at a given temperature, the Mg-doped samples can be in the portion of the curve where the magnitude has begun to decrease with decreasing temperature, while the Ti-doped samples are in the portion of the curve where the magnitude is increasing with decreasing temperature.

The observed magnetic memory represents an interesting phenomenon which has potential use in memory devices. The weak ferromagnetic moment above T_M leads to a domain structure similar to that observed in ferromagnetic materials.[78,79,80] This domain structure

results from an energy term due to magnetic poles being set up if complete ordering is present. This domain structure is altered when a magnetic field is applied. To see how domains could influence the change in the magnitude of the Seebeck coefficient near T_M, figures 26 and 27 in conjunction with a double-exchange argument will again be considered. For $T < T_M$ (figure 26) and for transport along the [111] direction, a carrier at site A cannot hop to a site in the plane of site B, but must instead hop to a site in the plane of D. (Recall that the hopping probability $\Omega_{ij} \alpha \exp(-\beta' r/r_o) \cos \theta_{ij}/2$ and for $A \rightarrow B$, $\cos \theta_{AB}/2 = 0$, while for $A \rightarrow D$, $\cos \theta_{AD}/2 = 1$.) The hopping probability for $A \rightarrow D$ depends on the distance between the two sites, about 4.6 angstroms. For $T > T_M$ (figure 27) and for transport along the [111] direction, the carrier at site A has the same probability for hopping to a site in the plane of D as it did for $T < T_M$, but in addition, it now has a non-zero probability of hopping to a site in the plane of B. This probability is reduced from the $A \rightarrow D$ probability by the factor $\cos \theta_{AB}/2 = \sin \alpha$, where α is the canting angle, but it is in turn increased due to the reduced distance which must be traversed (r = 2.3 angstroms). This probability for the $A \rightarrow B$ transition for $T > T_M$ leads to a total hopping probability which is larger for $T > T_M$ than for $T < T_M$. The increased probability for a hop to occur leads to a higher Seebeck

voltage for a given temperature difference. Double exchange accordingly predicts a rise in the magnitude of the Seebeck coefficient with increasing temperature at T_M.

If the regular array of ion spins is disturbed because of domain structure, the double-exchange results will be altered. It is generally accepted[78,79,80] that the domain structure exists for $T > T_M$, but the domains disappear for $T < T_M$. Thus, below T_M, the double-exchange arguments are not altered, but above T_M, regions exist (domains) where the regular spin array holds, but now a domain wall connects this region to another section of the crystal which also has a regular spin array. The spin arrays in these two orientations may be at arbitrary orientations with respect to each other, and the domain wall then acts as a transition region between the two arrays.

The structure of the domain walls has a marked influence on double exchange, since these walls are disruptions in the normal spin configurations. For example, consider the two types of domain walls shown in figure 28. In both of these walls the regular spin structure is altered and in the wall itself double exchange is disturbed since the spins of sites on neighboring or next nearest (111) planes are no longer related by the angles $180° - 2\alpha$ and $0°$, respectively. In fact, there may not be a nearby site in a neighboring

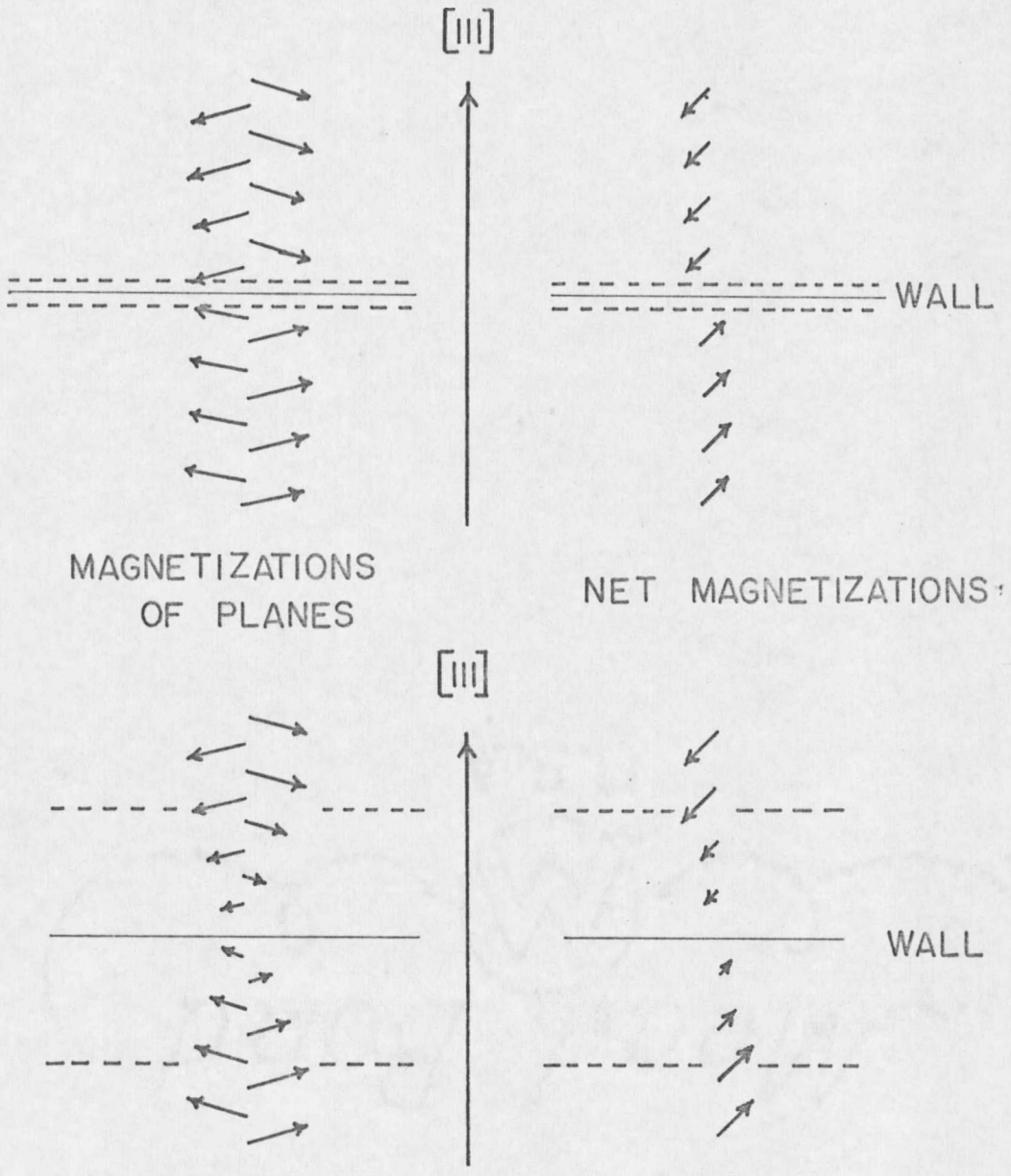


Figure 28. Two Types of 180-Degree Domain Walls.

plane with spin parallel to the spin of the carrier's host ion, so that the hopping probability is reduced by the factor cos $\theta/2$ for hopping motion through this wall. Depending on the form of the domain wall, the entire hopping probability can be reduced from the single domain value for $T > T_M$ when the domain walls are present. This can lead to a drop in the Seebeck coefficient at T_M with increasing temperature, instead of the predicted rise for single domains.

The type of domain structure depicted above has been reported for hematite by Eaton and Morrish[80] with domain walls parallel to the (111) plane. However, those authors were unable to define the structure of the domain wall. In impure hematite samples, a memory effect was seen in which the domain walls moved to nucleating points (usually impurity sites) as the sample was cooled to T_M (and the domain structure disappeared). When the sample was reheated past T_M, the previous domain structure reappeared. This was attributed to the presence of impurity sites which were not altered by the stresses associated with the Morin transition.[79]

For pure samples, the domain structure could be removed with applied fields of about 25 oersteds (gauss = oersteds in cgs units since B = H).[80] This amounted to forcing all the domains to line up in an effectively single domain configuration (saturation). For

impure samples including natural single crystals, the domain structure was harder to remove because of the presence of strains and/or impurities.[79,80] Eaton and Morrish[80] found that in doped samples, the observed domain structure was irregular and sometimes nonexistent. Ransom[44] reported results on the anisotropy of the Hall voltage within a plane containing the [111] axis in which he found that the Hall voltage exhibited a sharp drop in magnitude when the external field became parallel to the [111] direction, and the amount of change increased with increased magnetic field strength up to about 10 kilogauss, which Ransom interpreted as increasing alignment of the domain structure with increased magnetic field strength. The results indicated that in the Mg-doped samples which were studied, saturation of the domain structure did not occur for fields below 10 kilogauss.

The magnetic field (~1500 gauss) which was applied to the doped crystals in the present investigation is much weaker than the saturation field reported by Ransom. The present data support this since if saturation was taking place with the applied field, there would be no reason for different results when the direction of the field was reversed; in both cases of applied-field direction, saturation would result in an equivalent magnetic moment perpendicular to the transport direction. In the present data, reversing the

field direction is accompanied by a reversal of the change in magnitude of the Seebeck coefficient at T_M for samples doped with both Mg and Ti and oriented along the [111] direction.

Since the applied magnetic field did not alter the effect (if any) at T_M for transport within the (111) plane, this is taken as evidence supporting the domain model reported by Eaton and Morrish[80], in which the material was similar to a single domain within a (111) plane.

CHAPTER V

CONCLUSIONS

The present data on the Seebeck coefficient in Ti- and Mg-doped single crystals of hematite support the idea that electronic transport processes in these magnetic semiconductors are influenced by the magnetic state. In particular, at the low-temperature magnetic transition (the Morin transition), the reorientation of the magnetic moments produced a change in the Seebeck coefficient for samples of both dopings aligned along the $[111]$ direction, while no change was observed for the Mg-doped samples in the (111) plane, and a small change (2-5 percent) was seen for the similarly oriented Ti-doped samples. These data are consistent with double exchange which involves localization of the carrier at an atomic site and thermally activated hopping between sites, except for those data on the Ti-doped (111) samples, which can be explained by including a contribution due to inter-impurity hopping.

In comparing the results on two samples with the same doping and orientation, the qualitative features of the Seebeck coefficient versus $1/T$ were repeated, but the magnitudes for the two samples were different. This magnitude difference was observed to be directly related to differences in the sample lengths. This length dependence is not predicted by the usual Seebeck effect, but appears

in the correction due to phonon drag. Phonon drag also provides an explanation for the differences in the slopes of the Seebeck curves for Mg and Ti dopings. This is due to the increased impurity scattering in the Mg-doped samples, which have an order of magnitude more impurity concentration than do the Ti-doped samples. The impurity scattering reduces the contribution to the Seebeck coefficient due to phonon drag.

An interesting memory effect was observed, in which the change in the Seebeck coefficient at T_M was altered with an applied magnetic field, and the data showed a memory of the magnetic field after the field had been removed. This is explained in terms of a domain structure which is not saturated with the applied field strength.

The data presented in this dissertation indicate additional experiments which would be appropriate. The contributions due to impurity conduction and phonon drag would be more distinct if data were available on a spectrum of impurity concentrations and to lower temperatures. Investigations of additional types of impurities in single crystals would be helpful; specifically, Nb and Zr impurities are both n-type dopants, and Seebeck data reported on these dopants in polycrystalline samples have indicated significant impurity conduction at temperatures below room temperature.[37] Data on additional impurities leading to p-type dopings would also be of interest.

The phonon drag depends on the phonon dispersion in the hematite structure, so data on the phonon dispersion in this crystal structure would be helpful.

A better understanding of the memory phenomenon would result from data at various magnetic field strengths.

Since there is confusion in the literature regarding the basic transport mechanism, a thorough investigation of conductivity in single crystals of hematite would seem appropriate.

Finally, a more thorough investigation of the relationship between length of the samples and magnitude of the Seebeck coefficient would be helpful.

APPENDICES

Appendix I

Holstein[56] formulated the one-dimensional small-polaron problem in terms of the tight-binding approximation. The details of that method are summarized here.

There are two assumption basic to the tight-binding method:

1) the total wave function for the system is assumed to be a linear combination of atomic wave functions; i.e.,

$$\Psi(\bar{r},x_1,\ldots, x_n) = \sum_n a_n(x_1,\ldots, x_n)\, \phi_n(\bar{r},x_n) \quad ,$$

2) the potential at a given site is a sum of potentials due to all molecules in the lattice; i.e.,

$$V(\bar{r},x_1,\ldots, x_n) = \sum_{n=1} U(\bar{r} - n\bar{a}, x_n) \quad ,$$

where $\bar{a}$ is the unit lattice vector.

In addition, the molecular potential U is assumed to be short ranged:

$$U(\bar{a}, x_n) \ll U(0, x_n) \quad .$$

Use will be made of this assumption shortly.

Since the ϕ_n's are atomic wave functions, they are solutions of the atomic equation

$$\left[-\frac{\hbar^2}{2m} \nabla^2 + U(\bar{r} - n\bar{a}, x_n) \right] \phi(\bar{r} - n\bar{a}, x_n)$$

$$= E(x_n)\ \phi(\bar{r} - n\bar{a}, x_n) \quad ,$$

where the $E(x_n)$'s are eigenvalues.

To find the expansion coefficients a_n for Ψ, the time-dependent Schroedinger equation of the complete system must be treated. This includes the electronic contribution plus a lattice contribution and has the form

$$i\,h\,\frac{\partial \Psi}{\partial t} = \left[-\frac{\hbar^2}{2m} \nabla^2 + \sum_{n=1}^{n} U(\bar{r} - n\bar{a}, x_n) \right.$$

$$\left. + \sum_{n=1}^{n} \left(-\frac{\hbar^2}{2M} \frac{\partial^2}{\partial x_n^2} + \frac{1}{2} M\omega_o^2 x_n^2 \right) \right] \Psi .$$

A point to note in this expression is that the interaction term between the electron and the vibrating lattice is included through the dependence of the electronic potential on the nuclear coordinate x_n.

If the above expression is now multiplied by the complex conjugate of ϕ, $\phi_n^*(\bar{r}, x_n)$, and an integration is performed ower $\bar{r}$, the electron coordinate, the result is (following Holstein's notation):

$$\sum_m T_{nm}\left[i\hbar\frac{\partial}{\partial t} - \sum_p\left(-\frac{\hbar^2}{2M}\frac{\partial^2}{\partial x_p^2} + \frac{1}{2}M\omega_o^2 x_p^2\right) - E(x_m)\right]$$

$$\cdot a_m(x_1, \ldots, x_p)$$

$$= \sum_{\substack{m \\ p\neq m}} \left[\int \phi^*(\bar{r} - n\bar{a}, x_n)\, U(\bar{r} - p\bar{a}, x_p)\, \phi(\bar{r} - m\bar{a}, x_m)\, dV\right]$$

$$\cdot a_m(x_1, \ldots, x_p) - \frac{\hbar^2}{2M}\sum_m \int \phi^*(\bar{r} - n\bar{a}, x_n)$$

$$\left[2\frac{\partial \phi(\bar{r} - m\bar{a}, x_m)}{\partial x_m}\frac{\partial a_m}{\partial x_m} + a_m\frac{\partial^2 \phi(\bar{r} - m\bar{a}, x_m)}{\partial x_m^2}\right] dV \quad ,$$

where $T_{nm} = \int \phi^*(\bar{r} - n\bar{a}, x_n)\, \phi(\bar{r} - m\bar{a}, x_m)\, dV = \delta_{nm} + S_{nm}$.

If ϕ_n and ϕ_m were orthogonal, $T_{nm} = 0$ unless $n = m$. The S_{nm} term is the non-orthoganality integral. Holstein made the assumption that these were small and existed only for nearest neighbors m and n.

If both sides of the above equation are multiplied by the inverse of T_{nm}, defined by

$$\sum_p \bar{T}_{np} T_{pm} = \delta_{nm} \quad ,$$

and

$$\bar{T}_{nm} = \delta_{nm} - S_{nm} \quad ,$$

the above equation becomes:

$$\left[i\hbar \frac{\partial}{\partial t} - \sum_{p} \left(- \frac{\hbar^2}{2M} \frac{\partial^2}{\partial x_p^2} + \frac{1}{2} M\omega_o^2 x_p^2 \right) - E(x_n) \right] a_n(x_1, \ldots, x_p)$$

$$= \sum_{\substack{l,m \\ p \neq m}} \bar{T}_{nl} \left[\int \phi^*(\bar{r} - l\bar{a}, x_l)\, U(\bar{r} - p\bar{a}, x_p)\, \phi(\bar{r} - m\bar{a}, x_m) dV \right]$$

$$\cdot a_m(x_1, \ldots, x_p) - \frac{\hbar^2}{2M} \sum_{l,m} \bar{T}_{nl} \int \phi^*(\bar{r} - l\bar{a}, x_l)$$

$$\cdot \left[2 \frac{\partial \phi(\bar{r} - m\bar{a}, x_m)}{\partial x_m} \frac{\partial a_m}{\partial x_m} + \frac{\partial^2 \phi(\bar{r} - m\bar{a}, x_m)}{\partial x_m^2} a_m \right] dV \,.$$

The tight-binding method makes it appropriate to consider all overlap integrals as being small. These include the non-orthoganality integrals S_{nm} and other integrals for which $l \neq m$. Since these integrals are small, any terms containing products of two or more such integrals were neglected. In addition, since the potential is small except at the local site under consideration, products containing wave functions and potential localized at different sites were neglected with respect to terms containing two or more of the functions localized at the same site. With these approximations, the first term on the right side of the previous equation becomes:

$$\sum_{m\neq n}\left[\int \phi^{*}(\bar{r}-n\bar{a},\, x_n)\, U(\bar{r}-n\bar{a},\, x_n)\, \phi(\bar{r}-m\bar{a},\, x_m)\,dV\right] a_m(x_1,..,x_p)$$

$$+\left[\int \left|\phi(\bar{r}-n\bar{a},\, x_n)\right|^2 \left(\sum_{p\neq n} U(\bar{r}-p\bar{a},\, x_p)\right) dV\right]$$

$$\cdot\, a_n(x_1,\ldots,\, x_p)\ .$$

Holstein was able to drop the second term on the right side since it contained derivatives of electronic functions with respect to nuclear coordinates. He pointed out that these terms represent the interaction between the nuclear kinetic energy and the electronic wave functions.

Holstein then introduced additional notation:

$$W_n(x_1,\ldots,\, x_n) = \int \left|\phi(\bar{r}-n\bar{a},\, x_n)\right|^2 \left[\sum_{p\neq n} U(\bar{r}-p\bar{a},\, x_p)\right] dV\ ,$$

$$J(x_n,\, x_m) = \int \phi^{*}(\bar{r}-n\bar{a},\, x_n)\, U(\bar{r}-n\bar{a},\, x_n)\, \phi(\bar{r}-m\bar{a})\, dV\ .$$

By assuming that $J(x_n,\, x_m)$ was negligible except for nearest neighbors, his final result was

$$\left[i\,h\frac{\partial}{\partial t} - \sum_p \left(-\frac{h^2}{2M}\frac{\partial^2}{\partial x_p^{\,2}} + \frac{1}{2}M\omega_o^{\,2}\, x_p^{\,2}\right) - E(x_n) - W_n(x_1,\ldots,\, x_n)\right]$$

$$\cdot\, a_n(x_1,\ldots,\, x_n) = \sum_{\pm} J(x_n,\, x_{n\pm 1})\, a_{n\pm 1}(x_1,\ldots,\, x_n).$$

Appendix II

In this section, more details of the experiment are presented through photographs of some of the equipment.

Figure A-1 is a general view of the measuring apparatus, including the combined heat blocks/sample holder which is located in the refrigeration chamber on the right. The equipment on the lower shelf is for the heater circuit, while that on the upper shelf is for temperature difference, ambient temperature, and Seebeck voltage.

Figure A-2 is a close-up of the heat block assembly. The thermocouples can be seen coming out of the blocks horizontally on the left, while the voltage leads appear on diagonals. The connections visible at lower left are for one of the heaters. The block mounts and corner posts were made of aluminum and brass, respectively, so that no interactions were set up when a magnetic field was applied.

Figures A-3 and A-4 are two views of the goniometer mounted on the diamond saw table. An aluminum block was machined to fit the goniometer base, and this block fit the saw table in such a way as to preserve alignment of the crystal for cutting. The vernier was made on the back side of the crystal mount to provide a third rotational axis with known rotation. The mount in the foreground

of figure A-3 was used for dicing samples out of the aligned crystals. It had provisions for a 90° rotation.

The sample generally had to be supported more firmly on the mounting rod for the initial cut, so a shroud of aluminum-oxide cement was used to strengthen the mount.

Figures A-5 and A-6 are x-ray photographs from a Laue back-reflection camera, which were taken on a (110) face and a (111) face, respectively. In his thesis, Besser[72] outlined a method for interpreting the picture of the (110) face (these crystals grow on (110) faces). Two correct rotations of the crystal about separate axes bring the (111) face perpendicular to the x-ray beam. The trigonal symmetry of hematite about the [111] axis is very evident in figure A-6.

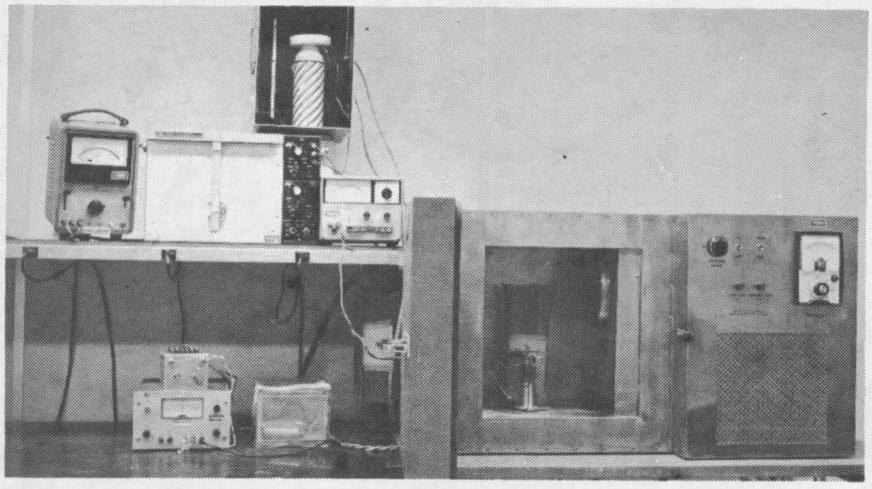


Figure A-1.

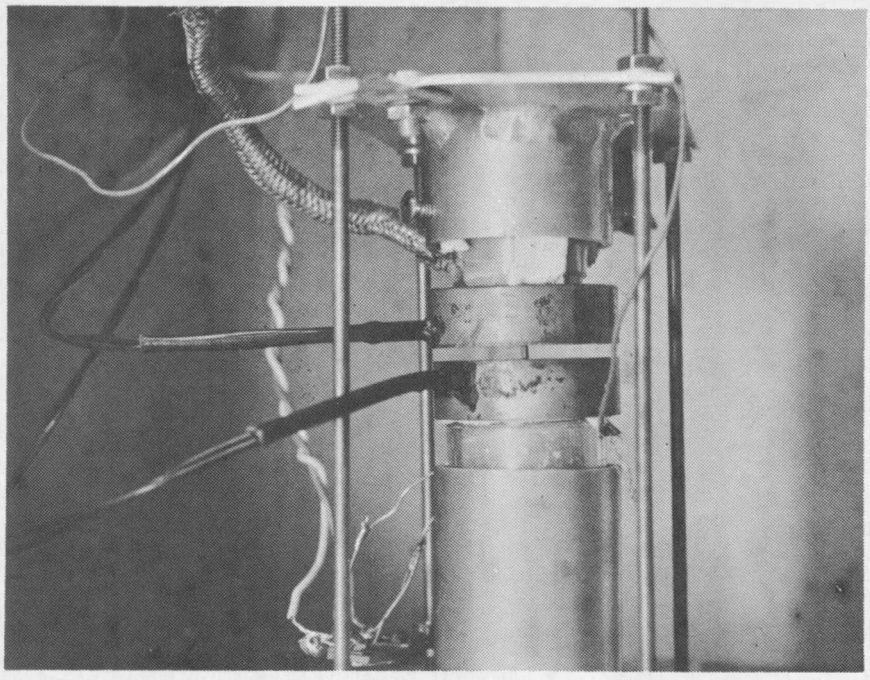


Figure A-2.

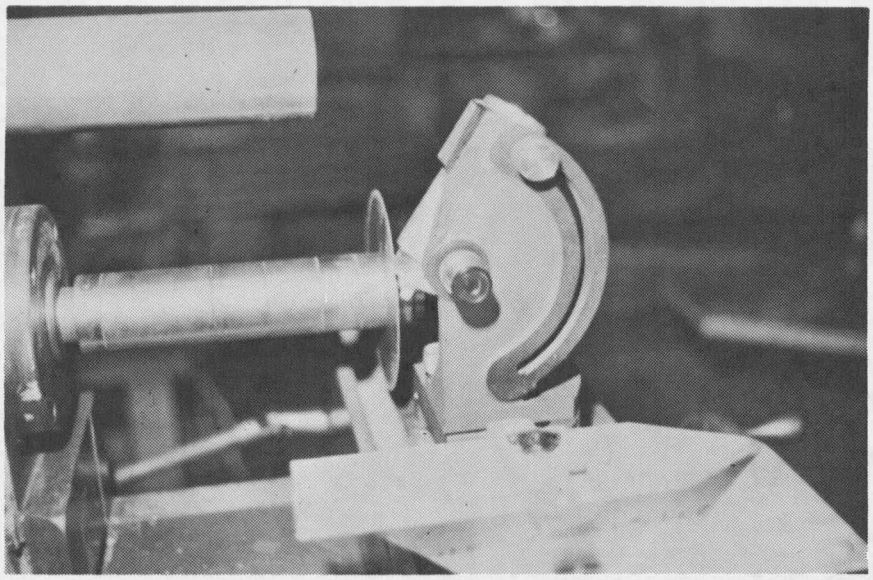


Figure A-3.

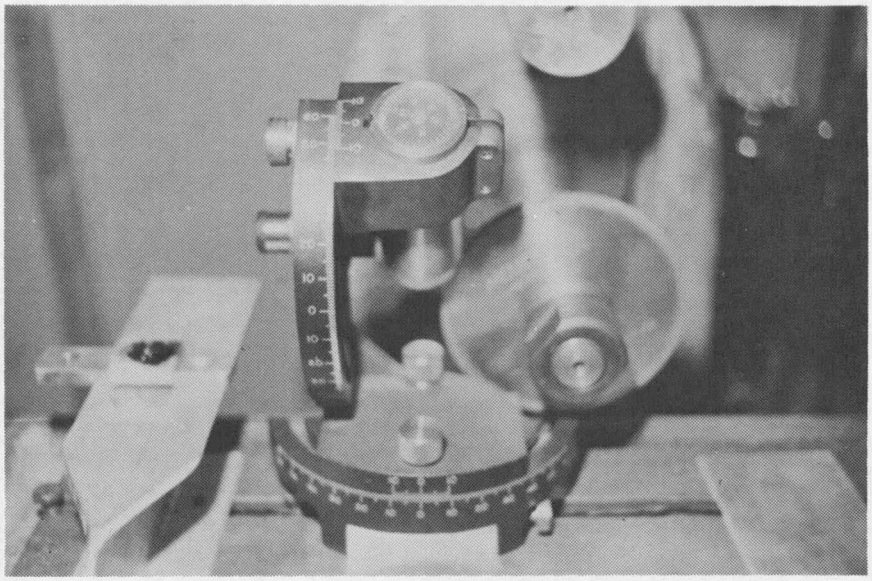


Figure A-4.

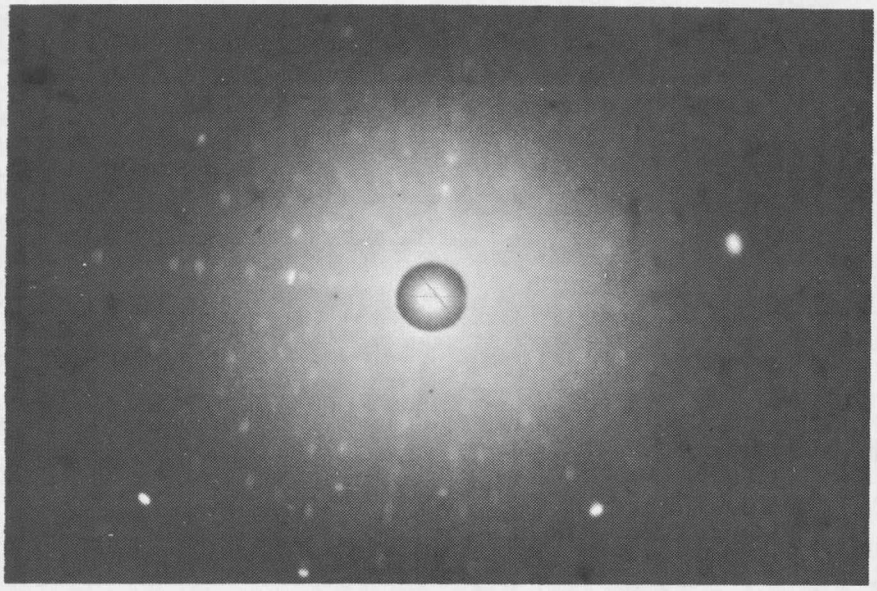


Figure A-5.

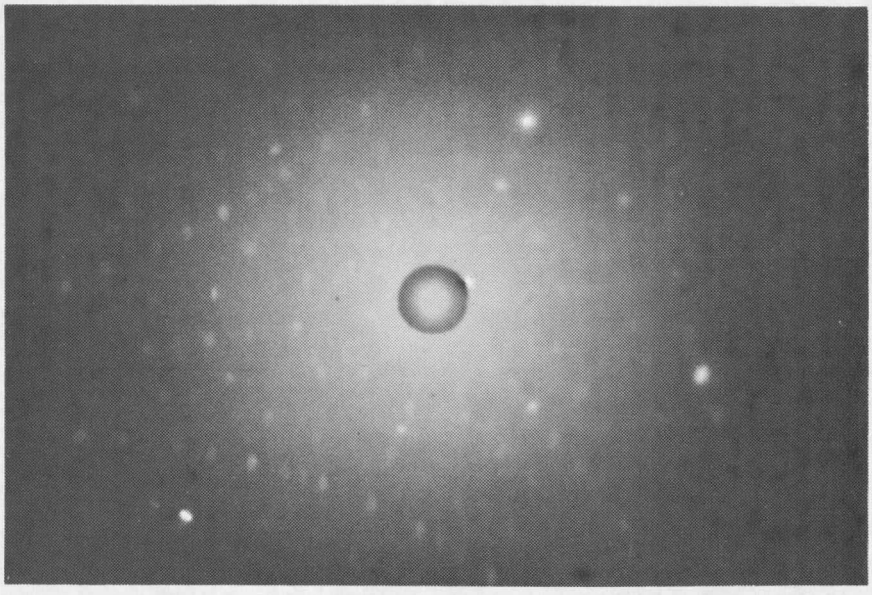


Figure A-6.

BIBLIOGRAPHY

1. Pauling, L., and S.B. Hendriks, J. Am. Chem. Soc. 47, 781 (1925).

2. Morrish, A.H., Physical Principles of Magnetism, New York: John Wiley & Sons, 1965, Chapter 8.

3. Shull, C.G., W.A. Strauser, and E.D. Wollan, Phys. Rev. 83, 333 (1951).

4. Anderson, P.W., Phys. Rev. 115, 2 (1959).

5. Morin, F.J., Phys. Rev. 78, 819 (1950).

6. Néel, L., Rev. Mod. Phys. 25, 58 (1953).

7. Li, Y.Y., Phys. Rev. 101, 1450 (1956).

8. Jacobs, I.S., and C.P. Bean, J. Appl. Phys. 29, 537 (1958).

9. Lin, S.T., J. Appl. Phys. 30, 306S (1959); 31, 273S (1960); 32, 394S (1961).

10. Dzialoshinski, I., J. Phys. Chem. Solids 4, 241 (1958).

11. Moriya, T., Phys. Rev. 120, 91 (1960).

12. Haigh, G., Phil. Mag. 2, 505 (1957).

13. Haigh, G., Phil. Mag. 2, 707 (1957).

14. Kaye, G., Proc. Phys. Soc. 80, 238 (1962).

15. Morrish, A.H., and J.A. Eaton, Presented at 16th Annual Conference on Magnetism and Magnetic Materials, Miami, Fla., Nov. 1970.

16. Flanders, P.J., and J.P. Remeika, Phil. Mag. 11, 1271 (1965).

17. Sunagawa, I., and P.J. Flanders, Phil. Mag. 11, 747 (1965).

18. Flanders, P.J., and N.J. Schuele, Phil. Mag. 9, 485 (1964).

19. Anderson, P.N., F.R. Merrith, J.P. Remeika, and W.A. Yager, Phys. Rev. 93, 717 (1954).

20. Morrish, A.H., and C.W. Searle, Proceedings of the International Conference on Magnetism (Nottingham), 574 (1964).

21. Iida, S., and A. Tasaki, Proceedings of the International Conference on Magnetism (Nottingham), 583 (1964.

22. Gardner, R.F.G, F. Sweett, and D.W. Tanner, J. Phys. Chem. Solids 24, 1175 (1963).

23. Morin, F.J., Phys. Rev. 83, 1005 (1951).

24. Morin, F.J., Phys. Rev. 93, 1195 (1954).

25. Gardner, R.F.G., F. Sweett, and D. W. Tanner, J. Phys. Chem. Solids, 24, 1183 (1963).

26. Appel, J., Solid State Physics 21, 193-391 (1968).

27. Heikes, R.R., and W.D. Johnston, J. Chem. Phys. 26, 582 (1957).

28. Methfessel, S., and D.C. Mattis, "Magnetic Semiconductors" in Encyclopedia of Physics, Vol. 18: 1, Magnetism, eds. S. Flügge and H.P.J. Wijn, New York: Springer-Verlag, 1968, pp. 389-562.

29. Bosman, A.J., and C. Crevecouer, Phys. Rev. 144, 2, 763-70 (15 April 1966).

30. Van Daal, H.J., and A.J. Bosman, Phys. Rev. 158, 3, 736-747 (15 June 1967).

31. Austin, I.G., A.J. Springthorpe, and B.A. Smith, Phys. Lett. 21, 1, 20-22 (15 April 1966).

32. Aiken, J.G., and A.G. Jordan, J. Phys. Chem. Sol. 29, 12, 2153-67 (December 1968).

33. Acket, G.A., and J. Volger, Physica 32, 1543-1550 (1966).

34. Firsov, Yu. A., Sov. Phys. Solid State 10, 10, 2387-2394 (April 1969).

35. Emin, D., and T. Holstein, Ann. Phys. 53, 3, 439-520 (July 1969).

36. Bransky, I., and N.M. Tallan, J. Chem. Phys. 49, 3, 1243-49 (1 Aug. 1968).

37. Bosman, A.J., and H.J. Van Daal, Adv. Phys. 19, 77, 1-112 (1970).

38. Adler, D., and J. Feinleib, J. Appl. Phys. 40, 3, 1586-1588 (Mar. 1969).

39. Adler, D., and J. Feinleib, Phys. Rev. Lett. 21, 14, 1010-12 (30 Sept. 1968).

40. Bosman, A.J., H.J. Van Daal, and G.F. Knuvers, Phys. Lett. 19, 5, 372-3 (15 Nov. 1965).

41. Fröhlich, H., Helv. Phys. Acta 41, 67, 838-9 (1968).

42. Platzmann, P.M., Polarons and Excitons, eds. C.G. Kuper and G.D. Whitfield, New York: Plenum Press, 1963, pp. 123-153.

43. Efros, A.L., Sov. Phys. Solid State 10, 9, 2245-6 (March 1969).

44. Ransom, C.L., Thesis, Montana State University, Bozeman (1968).

45. Zener, C., Physics Rev. 82, 403 (1951).

46. See for example Kittel, C., Introduction to Solid State Physics, New York: John Wiley & Sons, 1966, Chpt. 9.

47. Blatt, Frank J., Physics of Electronic Conduction in Solids, New York: McGraw-Hill, Inc., 1968, p. 109.

48. Reference 47, p. 305.

49. Smith, R.A., Semiconductors, London: Cambridge Univ. Press, 1959, p. 172.

50. Holstein, T., Ann. Phys., 8, 343 (1959).

51. Fröhlich, H., Polarons and Excitons, eds. C.G. Kuper and G.D. Whitfield, New York: Plenum Press, 1963, p. 1.

52. Lee, T.D., and D. Pines, Phys. Rev. 88, 960 (1952).

53. Lee, T.D., F. Low, and D. Pines, Phys. Rev. 90, 297 (1953).

54. Smith, A.C., J.F. Janak, and R.B. Adler, Electronic Conduction in Solids, New York: McGraw-Hill, 1967, p. 176.

55. Pekar, S.I., Fortschr. Physik 1, 367 (1954).

56. Holstein, T., Ann. Phys. 8, 325 (1959).

57. Friedman, L., Phys. Rev. 135, A233 (1964).

58. Kubo, R., J. Phys. Soc. Japan 12, 570 (1957).

59. Ziman, J.M., Principles of the Theory of Solids, Cambridge: Cambridge Univ. Press, 1964, Chapter 7.

60. Madelung, O., Z. Naturforsch. 13a, 22 (1958).

61. Schotte, K., Z. Physik 196, 393 (1966).

62. Kadanoff, L.P., and G. Baym, Quantum Statistical Mechanics, New York: Benjamin, 1962.

63. deWit, H.J., Phil. Res. Repts. 23, 449 (1968).

64. Lang, I.G., and Yu. A. Firsov, Sov. Phys. Solid State 5, 2049 (1964).

65. Yamashita, J., and T. Kurosawa, J. Appl. Phys. Suppl. 32, 2215 (1961).

66. Grønvold, F., and E.F. Westrum, Jr., J. Am. Chem. Soc. 81, 1780 (1959).

67. Heikes, R.R., Transition Metal Compounds, ed. E.R. Schatz, New York: Gordon & Breach, 1964, p. 1.

68. Appel, J., Phys. Rev. 141, 2, 509 (1966).

69. Haubenreisser, W., Phys. Status Solidi 1, 619 (1961).

70. Merzbacher, E., Quantum Mechanics, New York: John Wiley & Sons, 1961, p. 269.

71. The author wishes to thank Calvin Ransom for providing the single crystals from which the samples were cut.

72. Besser, P., Thesis, Univ. of Minnesota, Minneapolis.

73. Baleshta, T.M., and D.W. Carson, J. Sci. Inst. (J. Phys. E.) (G.B.), ser. 2, 1, 469-470 (Apr. 1966).

74. Appreciation is expressed to Craig Zaspel for taking the paramagnetic resonance on the vanadium-doped sample.

75. Appreciation is expressed to Bruce Culver for running the emission spectroscopy on the samples.

76. Johnson, V.A., Progress in Semiconductors, Vol. 1, ed. A.F. Gibson, New York: John Wiley & Sons, 1956, pp. 65-97.

77. Geballe, T.H., Semiconductors, ed. N.B. Hannay, New York: Reinhold, 1959, pp. 371-2.

78. Blackman, M., and B. Gustard, Nature, 193, 4813, 360-1 (27 Jan. 1962).

79. Gustard, B., Proc. Roy. Soc. A297, 1449, 269-74 (1967).

80. Eaton, J.A., and A.H. Morrish, J. Appl. Phys. 40, 8, 3180-5 (July 1969).

81. Herring, C., Semiconductors and Phosphors. New York: Interscience, 1958, 191.

MONTANA STATE UNIVERSITY LIBRARIES
3 1762 10011340 4

D378
St11
cop.2

Staab, Roger Irwin
Effect of the Morin transition on the Seebeck coefficient in single crystals of doped hematite

NAME AND ADDR

D378
St 11
cop. 2